TECHNISCHE UNIVERSITÄT WIEN

VIENNA UNIVERSITY OF TECHNOLOGY

DISSERTATION

Medical Visualization for Orthopedic Applications

ausgeführt zum Zwecke der Erlangung des akademischen Grades eines Doktors
der technischen Wissenschaften

unter Anleitung von
Ao.Univ.Prof. Dipl.-Ing. Dr.techn. Eduard Gröller
Institut für Computergraphik und Algorithmen
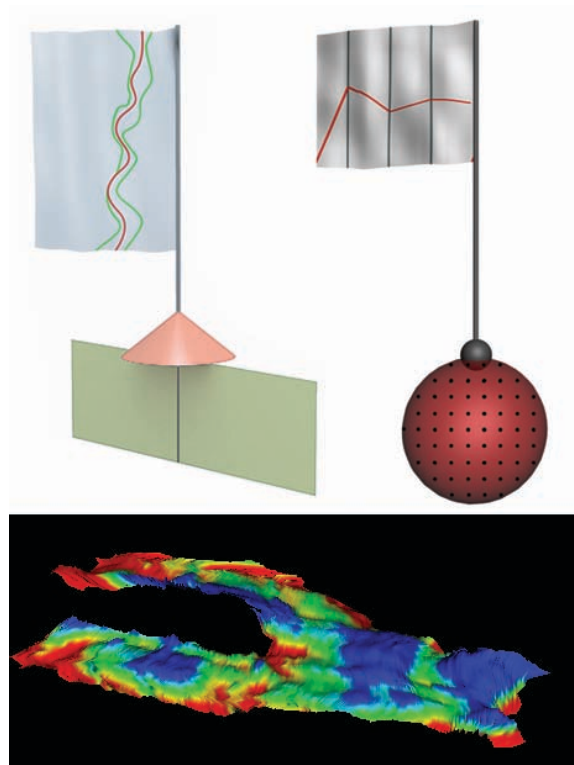der Technischen Universität Wien

eingereicht an der Technischen Universität Wien, Fakultät für Informatik, durch

Dipl.-Ing. Matej Mlejnek
Matrikelnummer: 9726073
Gaullachergasse 33/35
1160 Wien, Österreich
geboren am 21.03.1977

Wien, im Mai 2006

Medical Visualization for Orthopedic Applications

PhD Thesis

Matej Mlejnek

Institute of Computer Graphics and Algorithms
Vienna University of Technology, Austria
mlejnek@cg.tuwien.ac.at

Abstract

This dissertation discusses visualization techniques of articular cartilage for both quantitative and qualitative assessment. Articular cartilage is a very thin structure covering the endings of human bones. Thus, even slight changes in its thickness and inner structure may indicate an occurrence or progress of degeneration. The early detection of these factors is crucial for diagnosis and treatment of cartilage degeneration. Research to find treatments to stop or even reverse these degenerative changes is well in progress.

Magnetic resonance imaging is currently the best and most used non-invasive technique for acquisition of soft tissue structures like articular cartilage. In this work we use two types of data: a high-resolution anatomical scan of the cartilage and a T_2 map, which is computed from a set of sequences with varying parameters. While the thickness of the data can be precisely assessed from the anatomical scan, the T_2 map offers information on the inner structures of the cartilage.

Since the femoral cartilage is a curved thin-wall structure with a relatively small extent in one direction, it is very difficult to estimate its thickness from a stack of slices or even from a three-dimensional reconstruction of its surface. We discuss inspection of the tissue by unfolding and, thus, representing the tissue as a two-dimensional height field. Such a transformation of the object enables the application of 2D geometrical operations in order to observe subtle details in the thickness of the tissue.

Nowadays scanners allow a quality assessment checking disruptions in the pattern of the T_2 map of the patellar cartilage. The T_2 map illustrates the quality of the cartilage and changes in the pattern of T_2 map indicate defects before changes in the thickness itself occur. We propose the Profile Flags - an intuitive interface for probing of the T_2 maps by browsing the reconstructed surface of the cartilage. The Profile Flag is positioned on the reconstructed surface of the tissue, and can be moved along it. The Profile Flags can be applied to annotate local as well as global characteristics of the underlying data in a single still image. Furthermore, we present a set of extensions to Profile Flags for selection, classification and automatic positioning. Profile Flags can also be used to measure time-varying dynamic contrast enhanced magnetic resonance imaging data.

Kurzfassung

Die vorliegende Dissertation behandelt Visualisierungstechniken zur quantitativen und qualitativen Beurteilung des Zustandes von Gelenksknorpelgewebe. Es handelt sich dabei um dünne Knorpelstrukturen, die Gelenksköpfe im menschlichen Körper bedecken. Selbst geringe Änderungen in ihrer Dicke und Strutur können auf eine Degeneration hindeuten. Die Früherkennung solcher Veränderungen ist von großer Bedeutung sowohl für die Diagnose und Behandlung der auslösenden Krankheiten als auch für die Erforschung ihrer Ursachen.

Die Magnetresonanztomographie ist derzeit eines der am meisten verbreiteten bildgebenden Verfahren zur Untersuchung von Weichteilgewebe. Im Rahmen dieser Arbeit kommen zwei Typen von MR Daten zur Anwendung: ein hochaufläsender anatomischer Scan des Knorpelgewebes und eine sogenannte T_2-Map, welche aus Sequenzen mit variirenden Parametern berechnet werden kann. Während die Dicke des Gelenksknorpels mit Hilfe des anatomischen Scans mit hoher Präzision bestimmt werden kann, kann aus der T_2-Map Information über seine Struktur gewonnen werden.

Insbesondere die Untersuchung des femoralen Gelenksknorpels (Knorpelgewebe, welches den Oberschenkelkopf bedeckt) ist schwierig: Bedingt durch seine gewundene Struktur sind konventionelle Methoden basierend auf Schichtbildsequenzen oder dreidimensionaler Rekonstruktion zumeist ungeeignet. Aus diesem Grund wird in der vorliegenden Arbeit eine Technik zur Auffaltung des Gewebes behandelt. Die so gewonnene Repräsentation als zweidimensionales Höhenfeld erlaubt die Anwendung von geometrischen Operationen, um eine verbesserte Darstellung von selbst geringen Annomalien zu ermöglichen.

Durch Untersuchung der T_2-Map können darüberhinaus Veränderungen in der Struktur des Knorpelgewebes der Patella (Kniescheibe) erkannt werden bevor permanente Schäden entstehen. In dieser Arbeit wird die Profilflaggen-Metapher vorgestellt, welche eine einfache Sondierung von T_2-Maps erlaubt. Eine Profilflagge wird auf der rekonstruierten Oberfläche des Knorpelgewebes platziert und kann darauf bewegt werden. Profilflaggen bieten eine einfache Schnittstelle zur Interaktion und Dastellung der zugrundeliegenden Daten und sind somit zur Untersuchung und Annotierung von lokalen und globalen Charakteristika des Gewebes geeignet. Neben dem grundlegenden Konzept werden zahlreiche Erweiterungen vorgestellt, die sich mit Selektion, Klassifikation und automatisierter Positionierung der Profilflaggen beschäftigen. Auch eine Anwendung zur Untersuchung von mit dynamischer kontrastmittelunterstützter Magnetresonanztomographie (DCE-MRI) gewonnenen Daten wird behandelt.

Acknowledgments

Contents

Chapter 1

Introduction

Though the history of magnetic resonance imaging (MRI) has started in the late fourtees, it has been originally used only for chemical and physical analysis. The first demonstrations in medicine can be dated to the seventees, when it has been used for the first time on a human body. Since that time, the cross-sectional magnetic resonance technology is developing fast, increasing both, in spatial resolution and signal-to-noise ratio [33].

An ideal screening technique should have the following properties: lack of harmful side-effects, high patient acceptance, high diagnostic reliability, low costs of the inspection practice, and availability of efficient therapies to the alleviation of the investigated disease [27]. Magnetic resonance imaging satisfies the first two attributes by the lack of ionizing radiation and is thus useful for an effective population screening. MRI is employed in early diagnoses of diseases and also in the evaluation of disease progress. The third criteria is primarily dependent on the technical degree of both software and hardware components used in the approach. MRI has a high potential in various areas of medical imaging. In the following sections, we discuss the recent research and technical advances of MRI for orthopedics.

1.1 Magnetic Resonance Imaging (MRI)

Magnetic resonance imaging is a noninvasive procedure, which is based on nuclear magnetic resonance. In contrast to radiography (X-rays) and computed tomography, MRI is based on the absorption and emission of energy in form of radio waves. It does not involve harmful ionizing radiation. To obtain images, a patient is positioned within a constant magnetic field B_0. Since certain nuclei, e.g., hydrogen nuclei, exhibit magnetic properties, they act like magnets in the magnetic field and spin align with an outside magnetic field. If a radio frequency (RF) pulse is applied to the scanned tissue in B_0, the nuclei absorb energy and get excited. This disrupts the alignment until the RF transmitter is switched off. The re-emitted energy is

picked up by the receiver coil and the signal is reconstructed. Different image types can be created by varying the sequence of the RF pulse [53, 29].

The primary obstacles in achieving good image quality with MRI are the high noise and bias. Since the commonly used low pass filtering can remove small features, several sophisticated approaches have been proposed for denoising and bias correction of magnetic resonance data [22, 79, 56, 5, 57]. Sophisticated filters are usually very time-consuming and may require up to several hours of processing time. Motion artifacts are another problem of MRI which is due to the rather long scanning times. Examples of such artifacts include patient breathing or colon peristalsis during the scanning procedure [63].

Due to the high patient acceptance and the lack of harmful ionizing radiation MRI is applied in many research areas: neurology, angiography, cardiac MRI, etc. [27]

1.2 Knee Cartilage

MRI is also a promising tool for in-vivo studies in orthopedics. This is due to the ability to easily differentiate between different types of soft tissues. MRI is currently the most accurate non-invasive technique for diagnosing cartilage lesions. An accurate assessment of cartilage thickness and quality is necessary for the early detection of joint degeneration.

1.2.1 Anatomy of Articular Cartilage

Joint surfaces are formed by articular cartilage, usually called also hyaline cartilage. The anatomy of articular cartilage is very complex with a well hydrated and pressurized structure. It consists of chondrocytes and a large extracellular matrix composed of water (75-80%), collagen II fibrils (20%), and aggregates of proteoglycans (5%) [75]. The cartilage does not possess a uniform thickness. It is influenced by different factors, e.g., size of bone, pressure, stress, age [49].

Hyaline cartilage consists of three histologic layers based on the orientation of the collagen fibers (Figure 1.1):

- The outer layer (superficial zone) consists of collagen fibers aligned tangentially to the surface of the cartilage. It makes up approximately 10% of the thickness of the cartilage. The water content in this layer is the highest and decreases towards the bone.

- The transitional layer makes up approximately 40% of the cartilage thickness with collagen fibers oriented arch-like and directed towards the surface. In
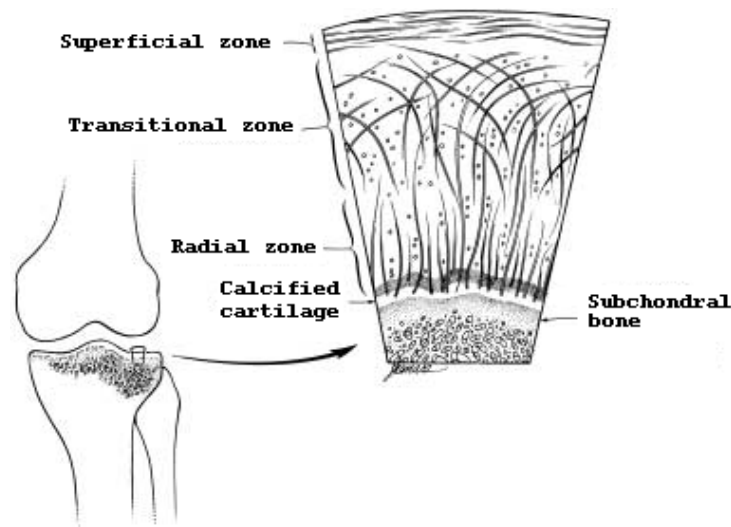
Figure 1.1: *Sketch of the layers of hyaline cartilage with orientation of collagen fibers (figure taken from Disler et al. [18])*

this layer the collagen fibers are thicker than in the superficial zone, but thinner than in the radial zone.

- In the radial zone the collagen fibers are oriented perpendicularly to the cartilage surface. In this layer, the number of chondrocytes is the highest in comparison to the other layers of hyaline cartilage. The collagen fibers of this layer are rooted in the calcified cartilage, which is the connection between cartilage surface and subchondral bone. The radial zone and the calcified cartilage constitute approximately 50% of the articular cartilage. These layers also possess a higher concentration of proteoglycans.

In the human knee joint, three touching bones, namely femur, patella and tibia are covered by articular cartilage at the contact areas. Figure 1.2 shows a sagittal slice through a human knee with annotated bones. The femur is covered by femoral cartilage, the patella by patellar cartilage, while the end of the tibia is formed by tibial cartilage.

1.2.2   Functions of Articular Cartilage

The hyaline cartilage supports certain very important functions, e.g., distribution of weight, maintenance of low contact stress, frictionless motion, shock absorbtion, and allows the diffusion of nutrients to its cells. The orientation of collagen fibers in different layers is crucial for protecting against shear and tensile forces and shocks. The main protection against pressure is provided by the swelling ability
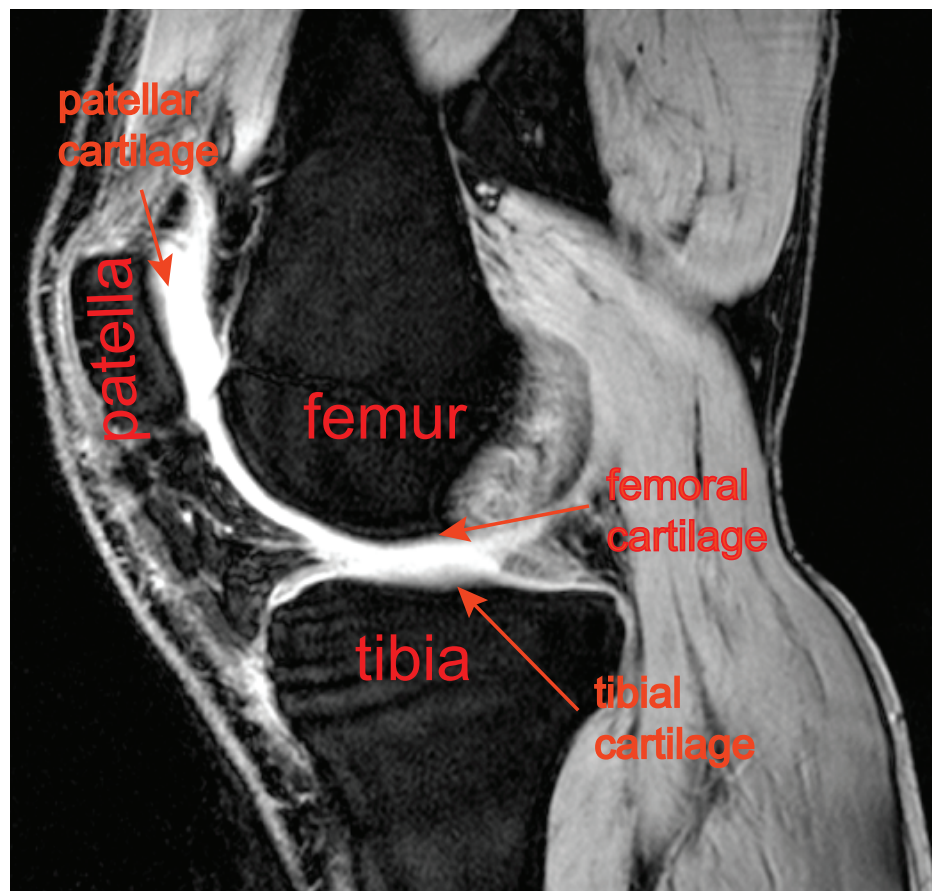
Figure 1.2: *Sagittal slice of the knee with annotated bones and three types of cartilage, i.e., femoral, patellar and tibial cartilage.*

of the proteoglycans. Together with water, proteoglycans provide mechanical resistance. Water is serving as a lubricant, in case compressive forces are executed on the surface of the articular cartilage.

1.2.3 Pathological Changes in Articular Cartilage

Damage to the cartilage can be either post-traumatic or degenerative, both may lead to osteoarthritis. In osteoarthritis, softening of the cartilage is observed, causing the tissue to be less resistant to load bearing. Ulceration and thinning of the cartilage occurs in the next stage of osteoarthritis, leading to exposure of the bear bone in the course of several years. Clinically, this is accompanied by pain, stiffness and progressive loss of function. Research to find treatments to stop or even reverse these degenerative changes are well in progress. Essential to a treatment at an early stage of osteoarthritis is early detection of cartilage degeneration [18, 35, 26]

grade	Outerbridge [54]
1	softening, swelling, fibrillation
2	fragmentation and fissuring ≤ 1.5 inch in diameter
3	fragmentation and fissuring > 1.5 inch in diameter
4	erosion of cartilage down to subchondral bone
grade	Shahriaree [67]
1	softening
2	swelling, blistering
3	surface irregularity, thinning
4	ulceration with exposure of subchondral bone

Table 1.1: *Classification of pathologic changes in articular cartilage.*

Osteoarthritis is most frequently found by adults as well as young people involved in sports [26]. It is difficult to detect osteoarthritis in an early stage. The common symptoms are pain, stiffness, and limitation of a joint's function. As the disease progresses, the symptoms become worse.

The early stage of osteoarthritis can be described by a decomposition of the collagen framework of the hyaline cartilage, decreased content of proteoglycans and increased water content. This results in swelling and softening. The body responds with an increased anabolic and catabolic activity, as well as proliferation of chondrocytes. This activity may lead to a thickening of articular cartilage and can last for several years. As the healing attempt of the body fails, the result is fibrillation, fissures, erosion and cracking of the cartilage. Due to the impossibility of cartilage regeneration, this is an irreversible process [26].

Until now there is no agreement on a unified classification system of pathologic changes in articular cartilage. However, two systems are most widely used as described by Outerbridge [54] and Shahriaree [67]. Both systems recognize four grades of pathologic changes, starting with softening through fissuring and blistering to exposure of subchondral bone (see Table 1.1).

1.2.4 MRI of Articular Cartilage

Radiographic methods, such as X-rays, offer an effective and fast tool for assessing the progress of osteoarthritis. Unfortunately, detection is possible only when a significant part of the cartilage is affected. It is important to develop methods that detect earlier stages of the disease to be able to stop the deterioration of the hyaline cartilage. Magnetic resonance imaging has the potential to improve the visualization of articular cartilage, and localize and quantify pathological changes of hyaline

cartilage. With the advent of recent MRI sequences, which exhibit a high soft tissue contrast, it is possible to delineate articular cartilage disorders with high spatial resolution and satisfactory signal-to-noise ratio. These considerations are important for an accurate segmentation of cartilage from adjacent tissues. Moreover, MRI of the knee is beneficial due to the absence of ionizing radiation, although to some extend slower than other scanning modalities. Verstraete el al. [75] consider that an MR sequence for accurate detection of cartilage degeneration should be able to:

- detect changes in the subchondral plate

- delineate bone marrow oedema, subchondral cysts, and granulation tissue

- detect changes in the internal structure and composition of articular cartilage

- show superficial and deep defects

- display cartilage with an optimal contrast and high spatial resolution

Due to the complex composition of cartilage collagen fibers, several typical MRI artifacts can occur:

- Truncation artifacts [26] are most evident as signal fluctuation parallel to thin structures with sharp borders. They are caused by band-limited sampling (see Figure 1.3 a).

- The magic angle effect [50] imitates cartilage defects due to increased signal intensity in anisotropic structures, which are oriented at about a $55°$ angle to the main magnetic field B_0; (see Figure 1.3 b)

- The partial volume effect [4] is caused by the large size of a voxel. It is apparent on boundaries with high signal intensity variation (see Figure 1.3 c) and leads to blurred or bumpy material interfaces.

- The chemical shift [74, 53] leads to a misregistration between fat and water contained in the hyaline cartilage. This is caused by the different Larmor frequency of fat and water (see Figure 1.3 d).

Two factors in the quantitative and qualitative characterization of cartilage degeneration are the thickness of the layer and the tissue quality, respectively. Since the cartilage is only few millimeters thick, even a subtle change in thickness and quality can indicate the progress of the disease. The classification of changes in these two important factors is essential for diagnosis and for estimating the progress of the degeneration process.
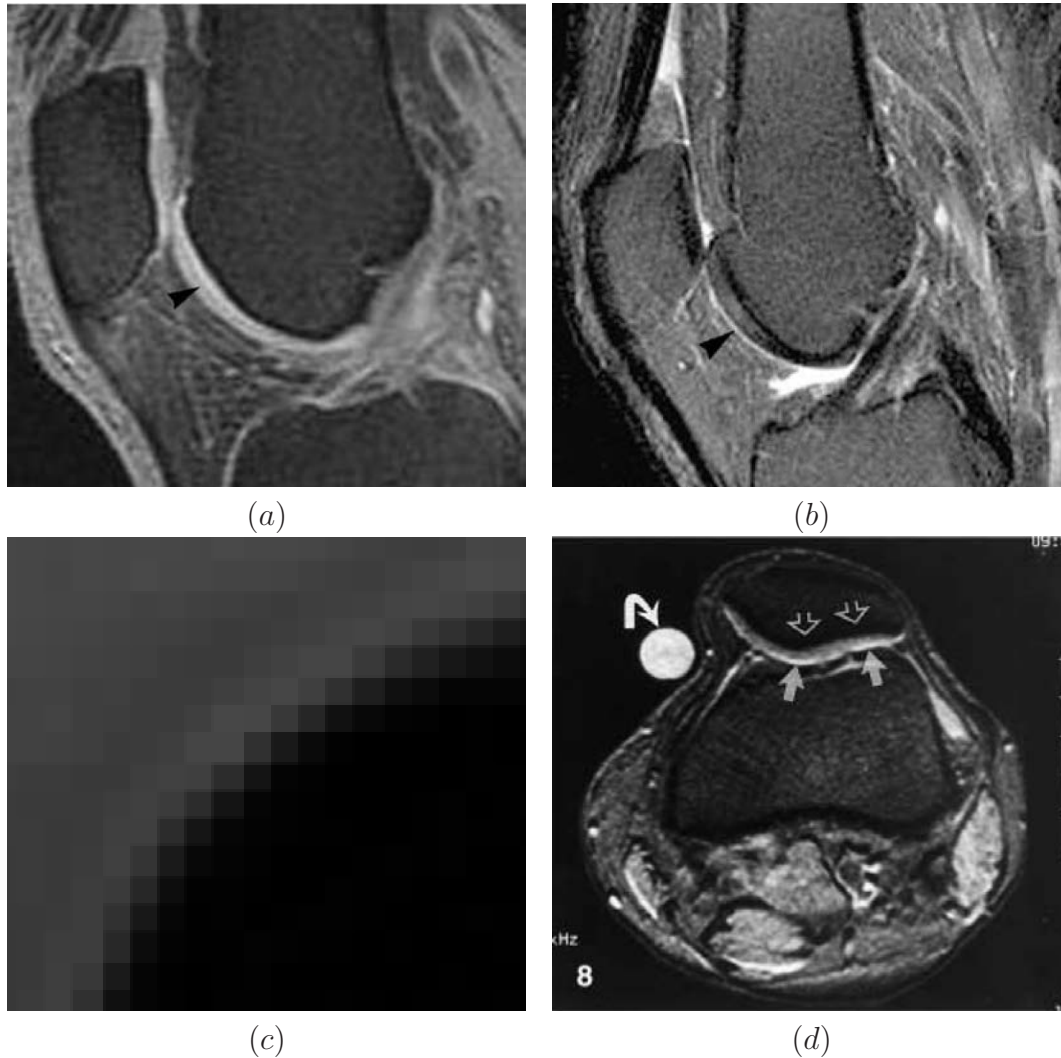
Figure 1.3: *MRI artifacts: a) truncation artifact, b) magic angle effect (figure taken from Guermazi et al. [26]), c) partial volume effect (figure taken from Lakare et al. [40]), d) chemical shift artifact - band of bright (solid arrows) and dark (open arrows) signal at the fat-fluid interface (figure taken from Disler et al. [18]).*

For screening of the knee cartilage, two magnetic resonance imaging (MRI) sequences are used: a high-resolution anatomical scan for the examination of the thickness and a T_2 map for the evaluation of the tissue quality. In the latter sequence the damage is represented by a disruption in the typical pattern of T_2 values. In a clinical environment these two scans are usually studied on two linked screens

7

in a slice-by-slice manner. This is a time-consuming process with reduced spatial perception, which may lead to false diagnosis. Furthermore, the communication between the radiologist and the orthopedist performing the surgery is not a trivial task, since they operate with different types of data. While the radiologist is performing the diagnosis on a stack of 2D slices, the orthopedist would need to access the 3D volumetric information during the surgical procedures.

Two metrics, volume and thickness of the cartilage, are used for a quantitative characterization of the cartilage. Cartilage volume correlates with the progression of the disease and can be used for the evaluation of the response to therapies. Segmentation of the hyaline cartilage plays a crucial role influencing the quality of the results.

As stated above, two MR acquisition sequences are used for the quantitative and qualitative measurements, respectively. The surface of the articular cartilage is generated from the anatomical scan, while the T_2 map is calculated from a sequence of spin-echo images. The T_2 map represents the tissue quality. A set of spin-echo images M_i is acquired by varying the echo time t_i. Then, the T_2 map is calculated by fitting a non-linear mono-exponential curve on a voxel-by-voxel basis. The signal intensity of each voxel $V(j)$ of an image M_i can be approximated by $V(j) \approx V_0(j) \cdot exp(\frac{-t_i}{T_2(j)})$, where $V_0(j)$ is the intensity of the voxel at echo time $t_i = 0$ and $T_2(j)$ is the relaxation time constant. We are fitting a curve through a weighted least squares approach. This is done by minimizing the sums of the squares of deviations between measured and expected values over all sequences: $min \sum_{i=0}^{N}(ln(V(j)) - ln(V_0(j)) + \frac{t_i}{T_2(j)})^2 w_i$. $N+1$ is the number of sequences and the w_i are the weighting constants determining how strong the image M_i affects the curve. This approach is chosen because of its high accuracy/computational cost ratio [46].

The disruptions of typical patterns in the T_2 map can be validated by so called T_2 profiles [68, 62]. A T_2 profile is a curve of varying T_2 values along a line that is perpendicular to the subchondral bone and ends at the surface of the cartilage (see Figure 1.4). Due to the arrangement of T_2 values in layers parallel to the underlying subchondral bone, the T_2 profiles have a typical shape for healthy cartilage. T_2 profiles in areas with damaged cartilage significantly differ from these shapes. For comparison of different regions within the cartilage, multiple T_2 profiles are computed and compared. A normalized T_2 profile is computed in order to enable the comparison of two T_2 profiles with different lengths. A normalized T_2 profile is a curve which returns T_2 values for the normalized distance in the interval between the subchondral bone (distance 0.0) and the articular surface (distance 1.0).
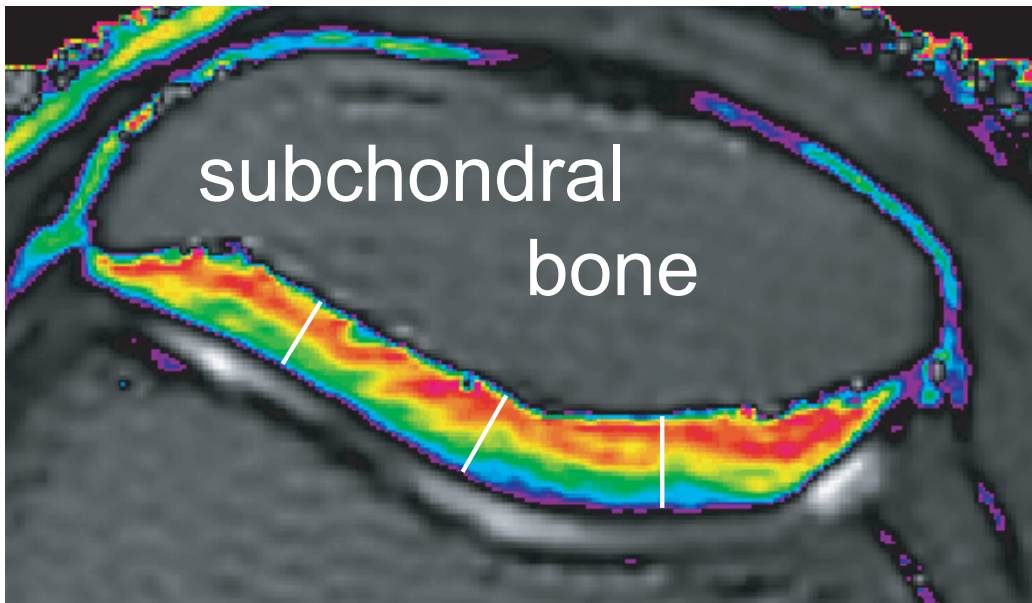
Figure 1.4: *Color-coded T_2 map of the articular cartilage with three locations of T_2 profiles (white lines).*

1.2.5 Cartilage Segmentation

There are several approaches to cartilage segmentation. Three classes of methods to cartilage segmentation can be identified: manual segmentation, semi-automatic (data-driven, hybrid) segmentation, and model-driven segmentation based on shape modelling. If slice-by-slice segmentation is applied, it is usually carried out in sagittal slices. Along this axis, the topology of extracted cartilage contours do not radically change in adjacent slices. Since the scanned MRI data are generally anisotropic, i.e. the in-plane voxel distance is smaller than the slice thickness, additional linearly interpolated contour slices can be inserted between adjacent slices.

Manual segmentation is usually time-consuming and requires an experienced user in order to obtain satisfactory results. The second group, hybrid methods, use thresholding, region growing or edge detection filters for navigating the user through the segmentation steps. These methods are in general faster, even though they are applied to individual 2D slices. This requires the processing of a stack of parallel 2D slices. Brett et al. [8] use a semi-automatic region growing algorithm for segmentation of the femoral cartilage. The algorithm is repeated slice by slice for the entire dataset. Cohen et al. [13] apply a semi-automatic segmentation technique based on B-spline interpolation. The initial curve is coarsely defined along each cartilage boundary. Then the B-spline curve is registered according to the gradient vector evaluated along the curve. Finally the curve is resampled at more precise
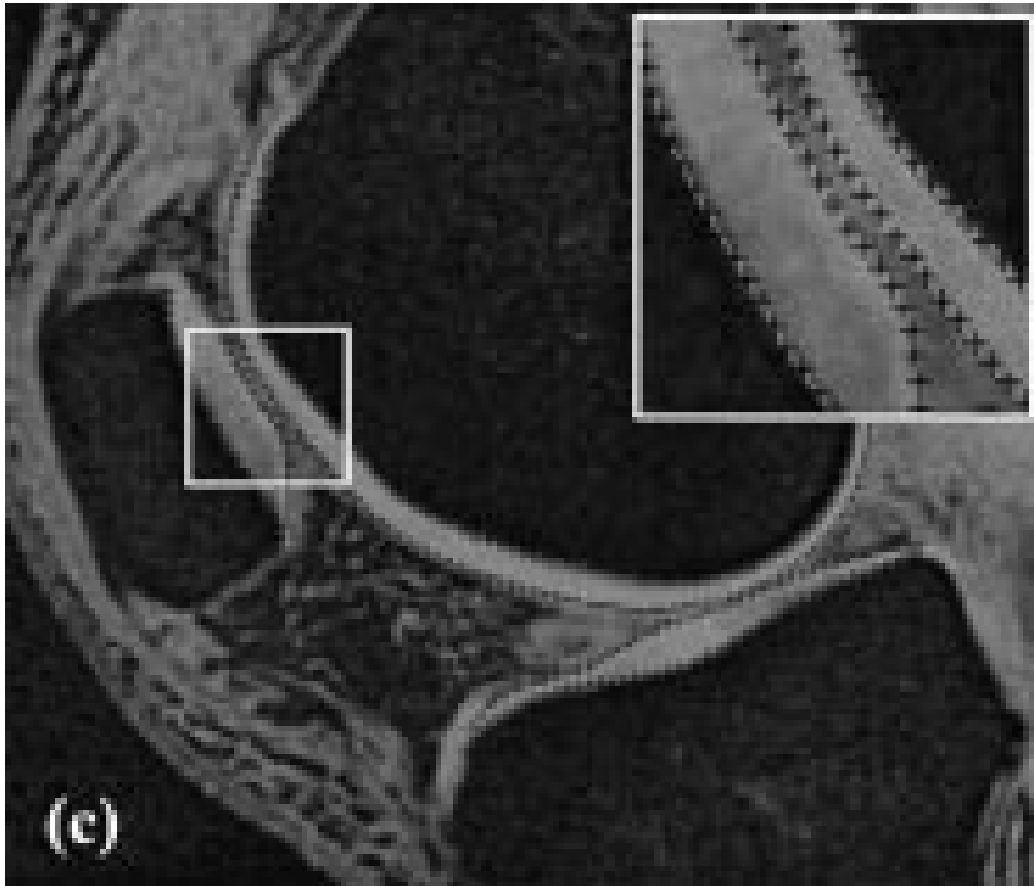
Figure 1.5: *Semi-automated segmentation of hyaline cartilage (figure taken from Cohen et al. [13]).*

intervals and the boundaries are detected by projecting the image gradient along the edge (see Figure 1.5). Lynch et al. [45, 44] propose a similar approach based on cubic splines. Their main goal is to reduce the human interaction time and improve the measurement reliability. In the first step, the user has to mark the ends of the cartilage and six control points in each slice, defining a cubic spline within the articular cartilage. This is usually done in one of the central slices of the scan. Then the spline is interpolated across sagittal slices and both the inner and the outer cartilage boundaries are detected by the Canny filter [10]. Schnier [66] discusses the application of the region-growing algorithm for the segmentation of cartilage in his PhD-thesis. The seed point as well as the contact areas have to be corrected by the user (see Figure 1.6). Alexander et al. [1] propose a method based on the 3D Euclidean distance transformation. For each point, the distance to the nearest point on the underlaying bone is computed.

In order to perform a comparison of two or more measurements over time, and,

Figure 1.6: *Three-dimensional rendering of knee cartilage (figure taken from Schnier [66]).*

thus, to determine the rate of the cartilage loss [82], it is necessary to determine rigid body transformations that align one surface with another one (see Figure 1.7). Solloway et al. [70, 69] describe a model-driven approach to cartilage segmentation based on Active Shape Models (ASM). First, a database, including segmentation templates, has to be built up slice-by-slice. For each slice an experienced radiologist marks twenty equally spaced points along the cartilage boundary, which are joined by two spline curves (inner and outer boundary). Then the marked points are statistically evaluated and the resulting model represents the set of possible cartilage shapes and grey-level variations. The fitting and the deformation of model to a specific data set is computed iteratively by comparing the grey-level values close to the model's landmark points and the data. Williams [81] propose a unit sphere as a reference for the registration of the subchondral bone. This reduces the number of points to be registered to two spherical mappings. Then the algorithm is searching for correspondences based on a statistical shape model. Another reference model has been proposed by Cohen et al. [15]. An anatomical coordinate system based on the subchondral bone topology is designed from a set of healthy specimens, which were scaled and aligned with each other. Pirnog [58] discusses various semi-automatic methods for cartilage segmentation and implements a framework which includes a large set of the above discussed methods.

The main challenges of cartilage segmentation include: accurate determination
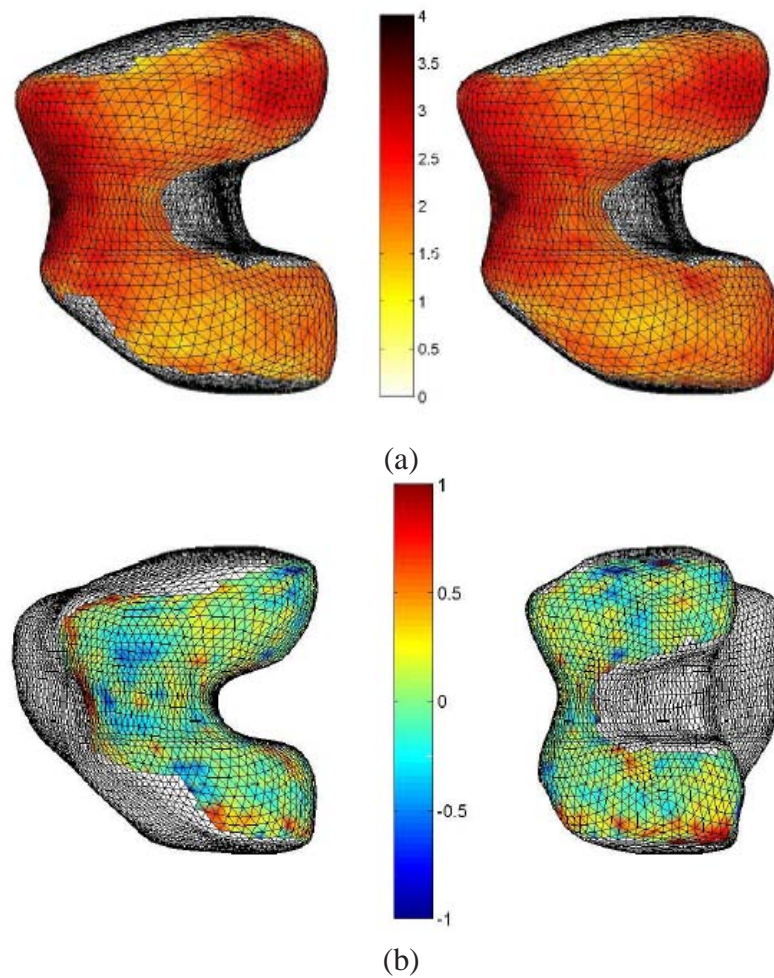
Figure 1.7: *a) Cartilage thickness maps in two time-steps (0 and 6 months) and b) the difference between the maps (from two different angles)(figures taken from Williams et al. [81]).*

of the cartilage boundary, time to segment cartilage from adjacent soft tissue, and the precision of the thickness and volume measurement.

1.2.6 Cartilage Thickness Mapping and Volume Computation

From the surface geometries of the outer articular cartilage and the underlying subchondral bone, commonly two quantities are measured: cartilage thickness and cartilage volume. Hohe et al. [32] discussed the curvature of the cartilage

Figure 1.8: *Three different approaches to compute cartilage thickness: vertical distance (left), proximity method (middle), and normal distance (right). A_{TC} stands for the outer cartilage boundary and A_{TB} denotes the subchondral bone (figure taken from Heuer et al. [31]).*

surface as a potential risk factor for osteoarthritis.

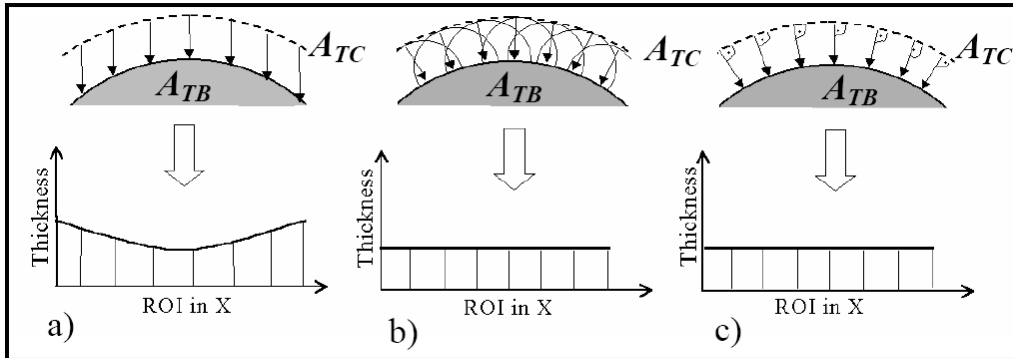Heuer et al. [31] compared three commonly used approaches to measure the thickness of articular cartilage on a synthetic dataset (see Figure 1.8). The first method just measures the vertical distance between points on the bone surface and cartilage surface. The proximity method uses the distance transform and calculates the length of the normal vector connecting the two surfaces. The most accurate results are produced with normal distances, however the error in thickness estimation strongly depends on the underlying data.

Alexander et al. [1], Faber et al. [21], Schnier [66] and Cohen at al. [13] measure the distance of each point on the outer boundary of the cartilage to the bone along the surface normal. Eckstein et al. [19] and Williams et al. [81] compute the distance from the bone to the outer boundary of the cartilage, since the bone shape is more stable over time than the shape of the cartilage. Muensterer et al. [51] calculate the thickness of the cartilage along rays perpendicular to the central axis, which is defined as the maximal signal intensity within the cartilage. Since the rays are not perpendicular to the boundary of the cartilage, the overestimation of cartilage thickness is corrected by trigonometric operations on the raw thickness. The correction is done for each intersection ray not perpendicular to the cartilage boundary. Athesian et al. [3] calculated in an early study the thickness maps and other corresponding quantities as the length of vectors between two bicubic patches representing the inner and the outer cartilage surface, respectively. Solloway et al. [70, 69] and Brett et al. [8] constructed the medial axis of two splines, which specify the inner and outer cartilage boundary, respectively. Then, they calculate the thickness as the length of the vector normal to the medial axis, which intersects both, the inner and the outer surface. The computed thickness map is usually
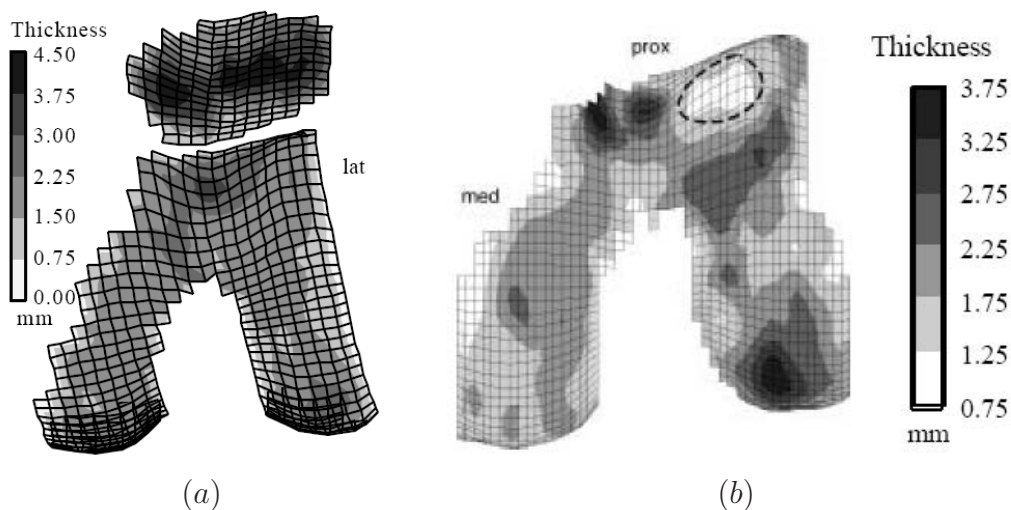
Figure 1.9: *Cartilage thickness map a) with healthy thickness distribution, b) with lesion (dashed circle) (figure taken from Cohen et al. [14]).*

displayed as a contour map or using color coding of the thickness information (see Figure 1.9).

1.3   The Scope of this Work

In this work we present two approaches to visualize both qualitative and quantitative pathological changes in articular cartilage.

In chapter 2, we describe a method to visualize the thickness of femoral cartilage. Given the MRI volume data of articular cartilage, medical doctors investigate pathological changes of the thickness. Since the femoral cartilage is very thin, it is impossible to reliably map the thickness information by direct volume rendering. Our idea is based on unfolding such a structure while preserving thickness. This allows to perform anisotropic geometrical operations (e.g., scaling the thickness). However, flattening of a curved structure implies a distortion of its surface. The distortion problem is alleviated through a focus-and-context minimization approach. Distortion is smallest close to a focal point which can be interactively selected by the user.

Chapter 3 introduces Profile Flags, a tool for the visualization of T_2 maps of patellar cartilage. Given the anatomical scan and the T_2 map of the cartilage, we combine the information on the shape and the quality of the cartilage in a single

image. The Profile Flag is an intuitive 3D glyph for probing and annotating of the underlying data. It comprises a bulletin board pin-like shape with a small flag on top of it. While moving the glyph along the reconstructed surface of an object, the curve data measured along the pin's needle and in its neighborhood are shown on the flag. The application area of Profile Flags is manifold, enabling the visualization of profile data of dense but inhomogeneous objects. Furthermore, it extracts the essential part of the data without removing or even reducing the context information. By sticking Profile Flags into the cartilage, one or more significant locations can be annotated by showing the local characteristics of the data at that locations.

In chapter 4, we discuss several extensions of the basic concept of Profile Flags. It includes a new interface for thickness visualization, selection of a set of profiles based on spatial as well as curve differences and automatic positioning of Profile Flags. Moreover, we show an adaptation of Profile Flags for measuring of time-signal profiles in a set of time-dependent MR volumes. Additionally, we shortly discuss the evaluation of the used methods by our medical partners. This dissertation concludes with Chapter 5, which summarizes the presented topics and achievements.

Chapter 2

Interactive Thickness Visualization of Articular Cartilage

2.1 Introduction

Nowadays MR scanners and pulse sequences are very well capable of imaging cartilage and allow the assessment of its quality. Spatial perception is considerably reduced when viewing the MR volume just slice by slice or by a multi-planar reconstruction In practice a data resolution of 512x512x50 is used. This makes reading of the data by the radiologist unnecessarily difficult and prolongs the examination time. Moreover, the femoral cartilage is a curved structure. Thereby, reading of the thickness changes from a direct volume rendered or a reconstructed surface model is quite difficult (see Figure 2.1 (a)). Until now, the default technique for visualizing cartilage thickness has been color mapping. Williams et al. [81] visualized the cartilage thickness on the surface of the underlying bone.

Our approach to femoral cartilage visualization deals with unfolding of the cartilage and depicting it as a height field (see Figure 2.1 (b)). In comparison to direct volume rendering or surface reconstruction methods, the height field representation of the cartilage eliminates the complexity of the 3D shape of the femoral cartilage. This allows the user to concentrate solely on the inspection of the cartilage thickness. The height field representation of the cartilage offers several visualization modes for representing the thickness information: color mapping, scaling, glyphs, iso-lines, etc. The entire femoral cartilage is depicted at once, thus, giving an overview of the global thickness.

Curved surfaces cannot be flattened without some amount of distortion. The distortion can be reduced, or in some cases (e.g., developable surfaces) even eliminated by introducing cuts and seams. Such operations split the surface and introduce discontinuities, thus, losing spatial coherence [55].

17
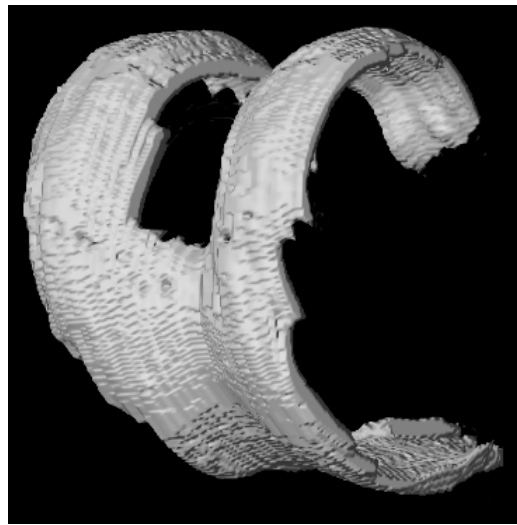
(a)
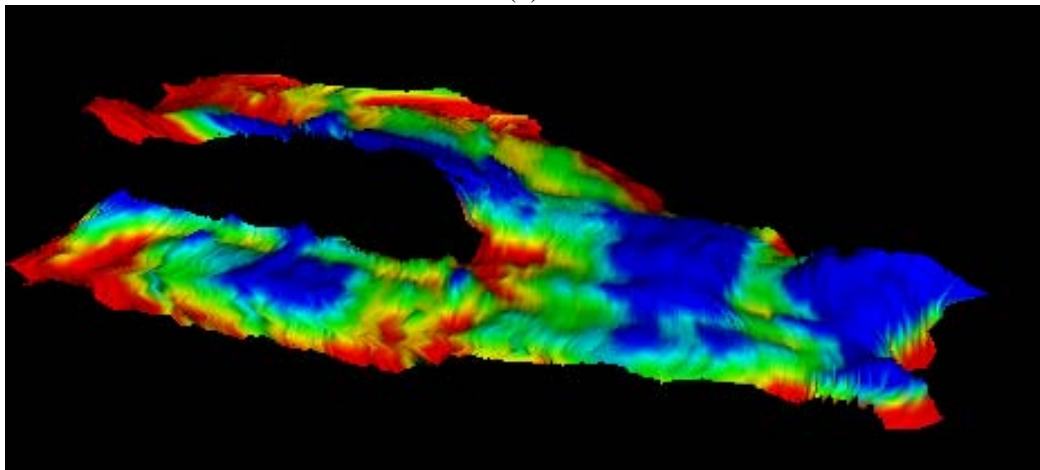
(b)

Figure 2.1: *Surface reconstruction of femoral cartilage from an MRI scan (a), and thickness height-field of the unfolded tissue (b).*

In our approach we locally minimize the distortion, in a user-defined area of interest (focus). The remaining part of the cartilage (context) is depicted in order to give an overview of the thickness of the entire cartilage. Since the overall thickness of the cartilage is different for each patient (according to the patient's body mass, age, sex, etc.), it is necessary to see the entire surface at once while inspecting it. The focal point on the surface of the cartilage can be interactively selected by the user.

The main contribution of this chapter is the handling and processing of articular cartilage as a typical thin-wall object. Another example of thin-wall objectswould
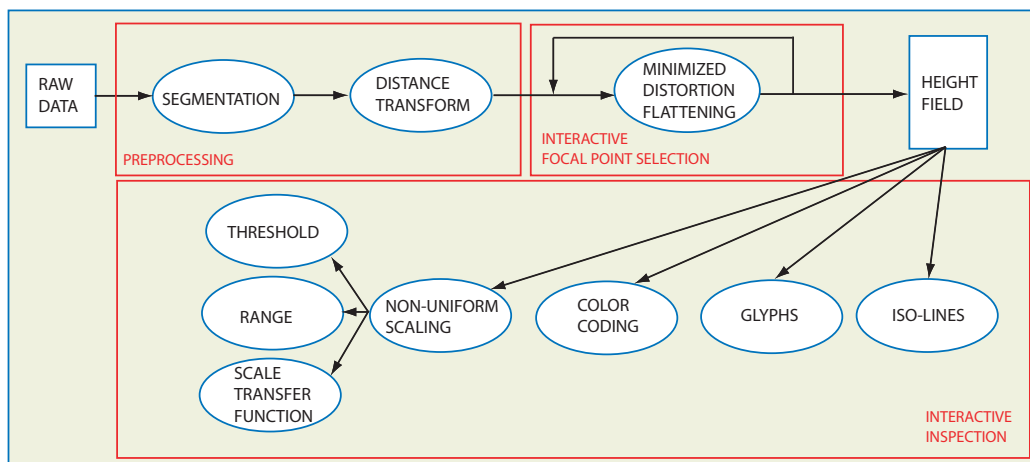
Figure 2.2: *Pipeline for thickness visualization.*

be colon walls. These objects have two dimensions with significant extent, whereas the third dimension (the thickness) is considerably smaller. The substantial difference in size requires the application of anisotropic operations (e.g., non-uniform scaling in the thickness direction). We investigate surface flattening and discuss visualization techniques, which can be applied to the flattened surface.

Flattening requires the parameterization of the surface. In this respect a large body of work has been done for texture mapping purposes. The unfolding of anatomical structures has been discussed as an investigation tool in several areas of medical imaging, e.g., colon unfolding [76, 28], curved planar reformation [36], or flattening of the brain surface [2, 23]. For these applications, the primary goal of the parameterization is usually the minimization of the global distortion over the entire surface. This process is time consuming and does not allow an interactive input from the user. In many medical applications, recent research has concentrated on detecting and investigating relatively small features. Therefore, we make use of local minimization of the distortion, preserving the shape and size of the area of interest, which can be interactively changed.

The chapter is structured as follows. In section 2.2, the visualization pipeline for thickness visualization will be sketched, describing the sequential stages in detail. Afterwards, an overview of operations on the resulting height field will be given in section 2.3. Finally, we summarize and conclude the work in section 2.4.

2.2   Pipeline for Thickness Visualization

The proposed pipeline for thickness visualization consists of the following steps (see Figure 2.2). First, the raw volumetric data are semi-automatically segmented

to identify the cartilage regions. In the second step, the distance between the inner and outer cartilage boundary is computed using a distance transform. Finally, the outer surface of the pre-segmented cartilage is triangulated using the minimum edge criterion [20]. All these operations are done in the preprocessing step. The following steps are guided by the user who is provided with an immediate visual feedback. The flattening of the triangular mesh proposed in this chapter is based on similar principles as the work by Sorkine et al. [71]. We however use different criteria for grading of the free vertices. We enable the user to interactively select a focal point, where the thickness shall be examined locally. The flattened mesh with assigned per-vertex thickness values corresponds to a height field with a triangulated base that consists of about 20K triangles. Thus, the operations on the height field can be performed in real-time on commodity hardware. In the following, we will describe the pipeline steps in detail. The segmentation procedure is shortly described in section 2.2.1. Section 2.2.2 discusses the measurement of cartilage thickness, while in section 2.2.3 we explain the flattening of the surface.

2.2.1 Cartilage Segmentation

In order to describe the entire visualization pipeline, the segmentation process is only shortly sketched in this section. In the literature, several approaches to cartilage segmentation have been discussed (see section 1.2.5). Two main classes of segmentation methods are usually applied: manual segmentation and semi-automatic segmentation. If slice-by-slice segmentation is applied, it is usually carried out on sagittal slices. Along this direction, the topology of extracted cartilage contours does not radically change between the adjacent slices. Since the scanned MRI data are generally anisotropic, i.e., the in-plane voxel distance is smaller than the slice thickness, additional linearly interpolated contour slices are usually inserted between the adjacent slices.

To segment the femoral cartilage from the MRI volume, we use an active contour model (snake) controlled by forces proposed by Lobregt et al. [43]. A snake, initially introduced by Kass et al. [37], is a parametric deformable contour. It is controlled by internal and external forces, which are usually defined in energy terms. The internal forces keep the snake smooth, while the external forces attract it to features, such as object boundaries.

The outcome of the segmentation is the contour of the cartilage in a slice. Due to our interest in the thickness of the tissue on the outer surface, the contour is split into two parts (see Figure 2.3). The first part is the inner boundary (green line) which is adjacent to the underlying bone. The second part of the contour is the outer boundary (red line) of the cartilage (blue). In the next step, we calculate the thickness from the outer to the inner boundary.
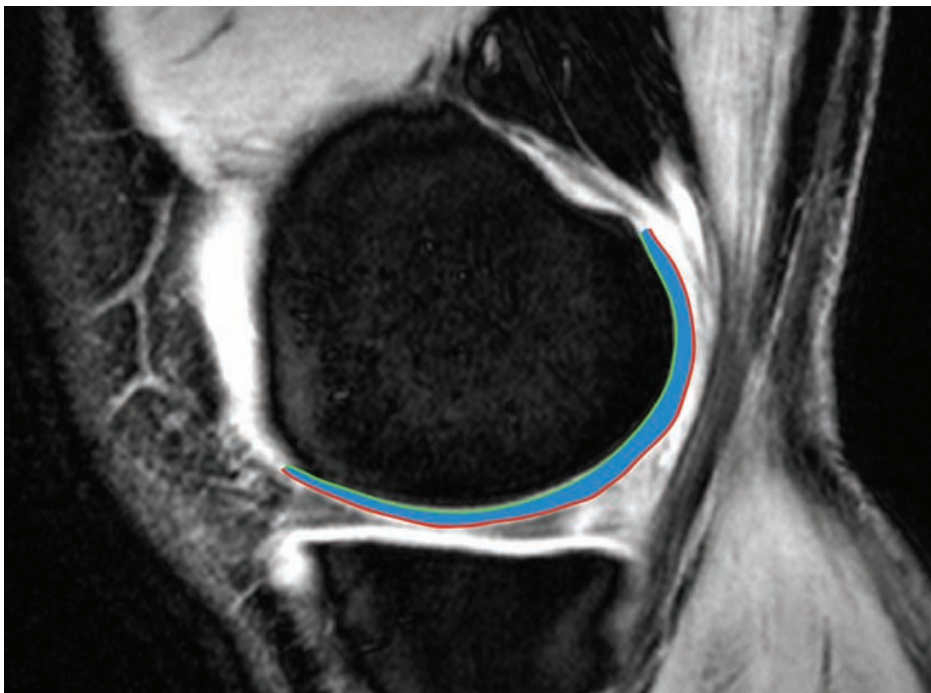
Figure 2.3: *Sagittal slice of an MR scan of the knee joint. The femoral cartilage is marked in blue with the inner boundary represented by the green line and the outer boundary shown by the red line.*

2.2.2 Thickness Measurement

There are several possibilities to calculate the thickness of a thin tissue (see section 1.2.6). Heuer et al. [31] summarize three possibilities to measure cartilage thickness: vertical distance, proximity method (closest neighbor on the opposite surface), and normal distance (distance along the normal vector). For curved surfaces, the vertical distance metric is not appropriate since the computation of the distance is performed always along a constant (vertical) direction.

Applying the proximity method, we are looking for the Euclidean distance $D_E()$ between a point p belonging to the outer boundary of the cartilage and the nearest point r belonging to the inner boundary I.

$$D_E(p) = min(\sqrt{(p_x - r_x)^2 + (p_y - r_y)^2 + (p_z - r_z)^2}); \quad r \in I$$

The distance computation can be efficiently approximated by the calculation of a distance field starting from the underlying bone. Recently, many optimizations of distance transforms have been discussed in the literature. They can be grouped into two categories: chamfer distance transforms and vector distance transforms [65]. The chamfer distance transform propagates the local distance by adding the neighborhood values, thus, propagating also the errors. On the other hand, the vector

distance transform, introduced by Danielsson [17], propagates the distance vector to the nearest sample point of the object surface, thus, minimizing the average error. Vector distance transforms are in general slower than chamfer distance transforms. We are computing the distance field only for a thin cartilage layer close to the bone surface. Since we need an accurate measurement of the thickness, we use the computational more expensive, but more accurate vector distance transform by Mullikin [52].

2.2.3   Flattening of Articular Cartilage

In order to perform unfolding of the cartilage, it is necessary to parameterize the outer boundary of the cartilage. Parameterizations of surfaces are often used in the area of texture mapping. In order to measure the precision and faithfulness of the parameterization, several different metrics, e.g., based on preservation of lengths, angles, or areas, can be applied [7, 42, 64, 24]. There are several parameters which can be adjusted in order to determine the trade-off between the different types of distortions and interactivity. The setting of the parameters depends on the specific application.

For the purpose of flattening the curved surface of the cartilage into the corresponding 2D plane, the parameterization should fulfill the following criteria:

- We are interested not only in the thickness of the inspected part of the cartilage, but also in its size. Therefore, we need a parameterization, which minimizes area distortion. The ideal solution is an equiareal mapping.

- Local as well as global self-intersections have to be avoided - this is a common problem in the area on surface parameterization.

- We do not allow multiple patches - the entire cartilage is rendered as one height field in order to preserve spatial coherence.

- Since the distortion cannot be fully eliminated for the entire patch, we allow an interactive selection of an area of interest, where the distortion is primarily minimized.

- The parameterization has to be fast in order to allow interactive feedback.

As mentioned above, our parameterization technique has been inspired by the method presented by Sorkine et al. [71]. Since the cartilage contours are organized in planar slices, we need to prevent intersections of the contours also in parametric space. We deal with this problem in the following way. In order to efficiently prevent local as well as global intersections, we align all points belonging
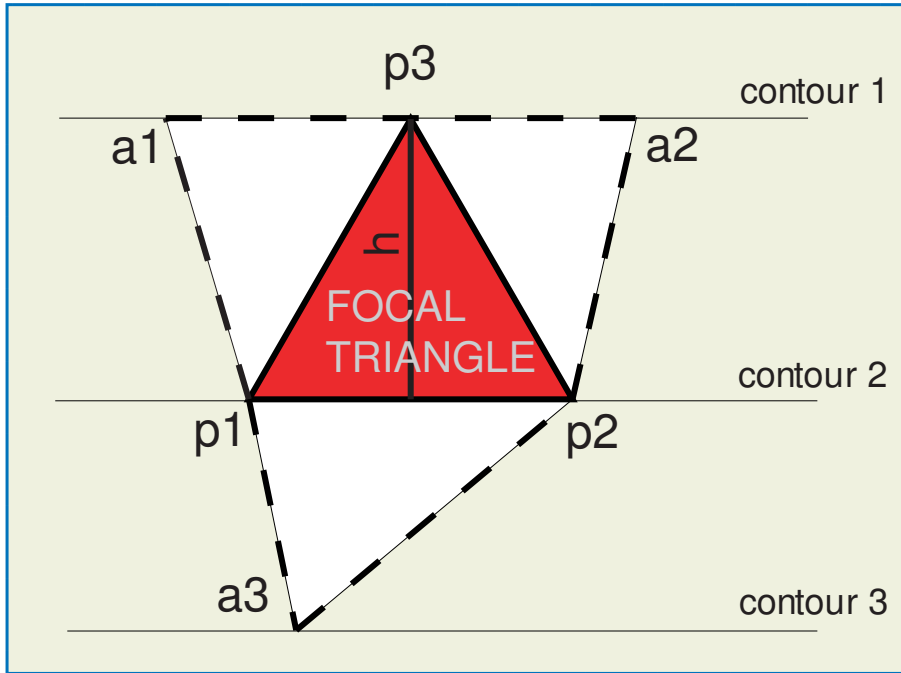
22

Figure 2.4: *Surface flattening: The focal triangle $(p1, p2, p3)$ is rigidly transformed to the patch. In the next step one point from the active set $\{a1, a2, a3\}$ is chosen and added with the corresponding triangle to the mesh. This process is continued iteratively until all triangles are added to the 2D plane.*

to one contour onto a line. This reduces the distortion minimization issue to a one dimensional optimization problem, thus, enabling reasonable frame rates.

In order to meet all of the above mentioned constraints we grow a planar patch around the selected focus triangle in the following manner (see Figure 2.4). First, the focal triangle, the one which includes the focal point, is rigidly transformed into the 2D plane. Since the triangle vertices are arranged in planar contours, each triangle consists of two points $(p1, p2)$ belonging to one contour and a third one $(p3)$ belonging to the neighboring contour. The distance between these two slices is defined by the height of the focal triangle ($height = \frac{2 \cdot area}{|p2 - p1|}$) (see Figure 2.4). Moreover, we define as an active set those points which have not been added to the patch yet but are forming a triangle with two points on the boundary of the patch. In the next step the patch is iteratively flattened by adding active points a_i to the patch. Positions of a_i are selected on the line corresponding to a contour so that, for example, the area of the currently flattened triangle is preserved. In this way, in each step a triangle nearest to the focal point is newly added to the patch. Note that arrangement of the points in the contours prevents local as well as global intersections. Any other surface parameterization method, based on
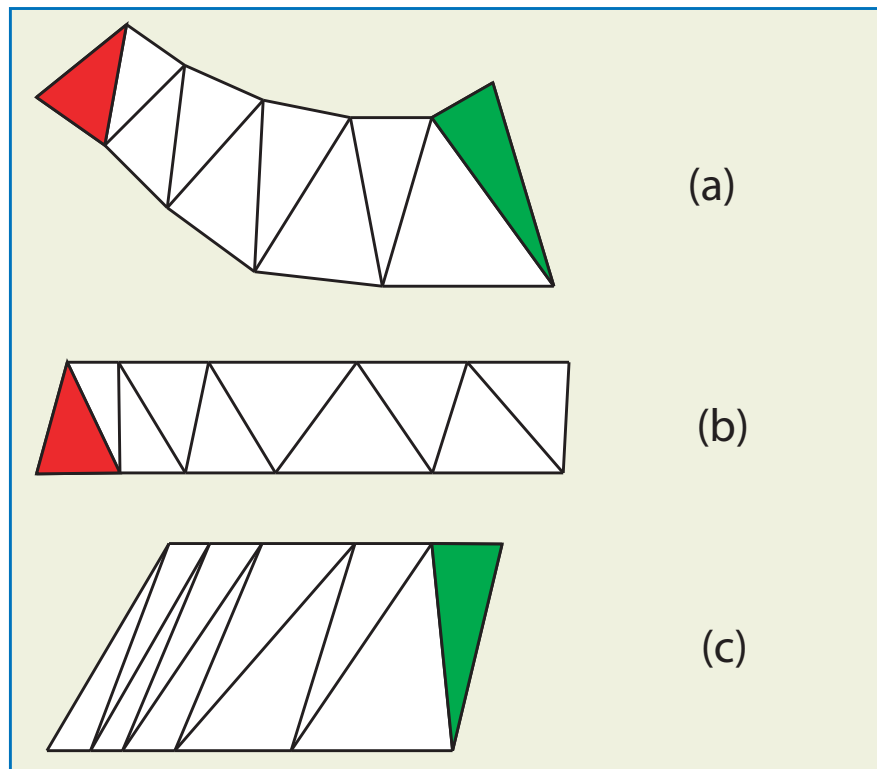
Figure 2.5: *Surface flattening: curved mesh in 3D (a). Depending on the choice of the focal triangle, i.e., red triangle, or green triangle, the patch is growing by aligning of the points in contours along lines and by minimizing the area distortion (b),(c).*

different constrains, can be performed in a similar way. The selection of the focal triangle is performed during cartilage inspection by a mouse click on the surface of the height field. Notice, that, due to the above mentioned alignment of the processed points, the distortion minimization for a new focal triangle yields an interactive feedback. Thus, the user is able to investigate all suspicious areas of the cartilage within several seconds.

For the sake of clarity, we illustrate the method on a simple example. Assume, we want to minimize the area distortion. Figure 2.5 demonstrates the difference in result when selecting two different focal triangles (red or green, see Figure 2.5 (a)). The selected focus triangle is rigidly transformed to the patch and determines the distance between the transformed contours (see Figure 2.5 (b),(c)). The further added triangles preserve their area by changing their location inside the contour.
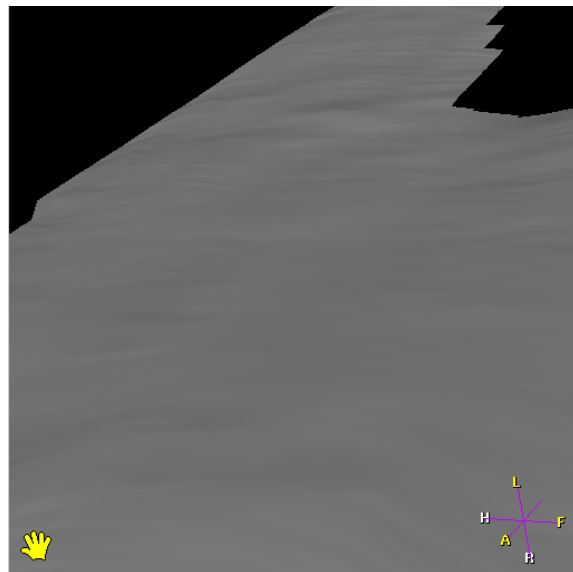
(a)
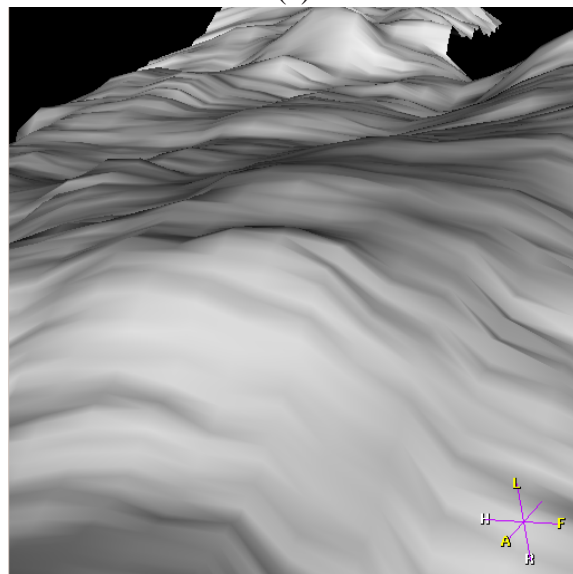
(b)

Figure 2.6: *A detailed cartilage surface without (a) and with (b) non-linear scaling. The roughness of the surface is hardly noticeable without scaling.*

2.3   Operations on the Height Field

The planar representation of the curved cartilage surface enables an effective visualization of its thickness. Slight changes in the thickness on the reconstructed surface may, however, not be noticeable (see Figure 2.6 (a)). Uniform scaling as

25
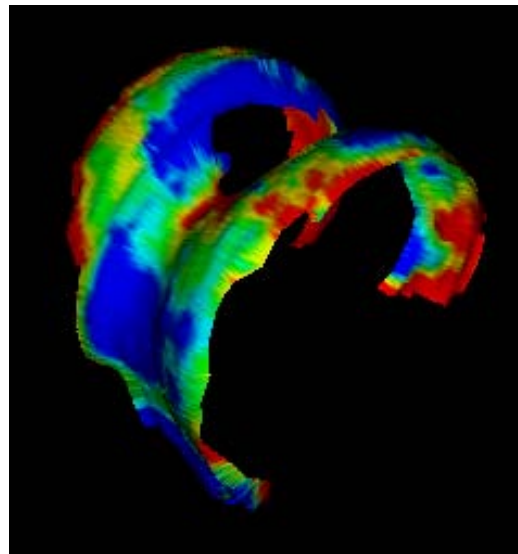
(a)
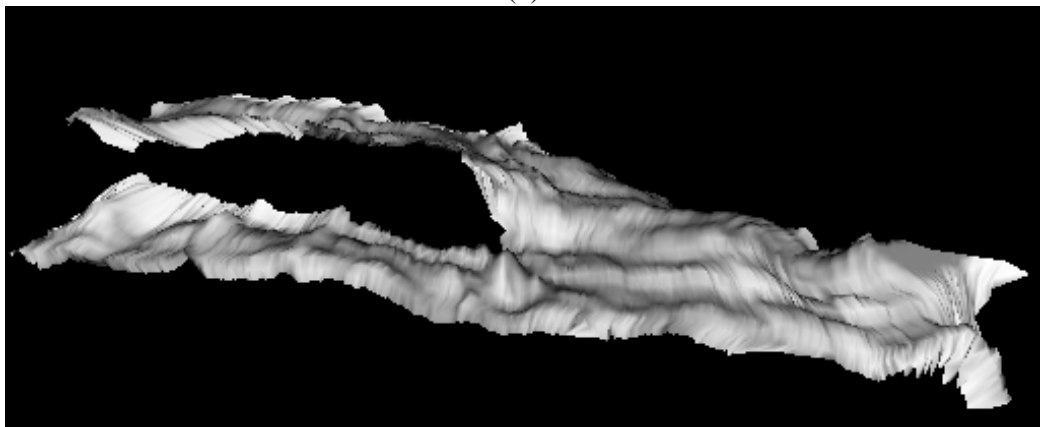
(b)

Figure 2.7: *Color coded thickness on the reconstructed surface (a) and the height field representation with scale factor 3.0 (b). The "plastic" view of the cartilage offers an intuitive information about its thickness.*

an initial guess of improvement will not be of much help. Since we would like to enhance the thickness information, we propose a non-uniform scaling by applying scaling only in the height direction (see Figure 2.6 (b)). This has already been done for earth visualizations to emphasize topographic variations like mountains and valleys. Note, that the below described non-uniform scaling may lead to self-intersections for non-convex surfaces. The height field representation of cartilage thickness does not have to deal with this problem. The triangulated surface is flattened into the 2D plane and the thickness is mapped to the third coordinate.

26
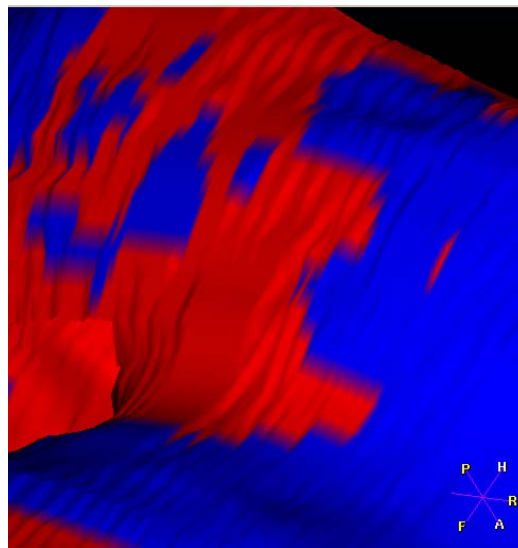
(a)
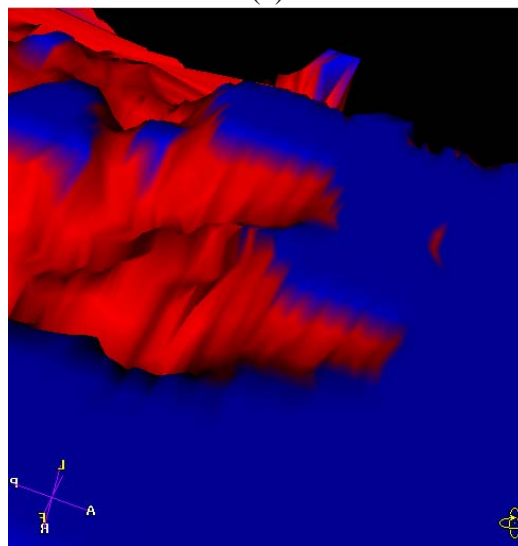
(b)

Figure 2.8: *Thresholded non-linear scaling: the color map on the reconstructed surface depicts areas on the cartilage surface with thickness below a certain threshold (red), while the remaining part is mapped to blue (a). The non-linear scaling enables a more detailed view of the thickness changes in the thin area (b).*

Thus, the height field can be scaled in the thickness direction without distorting the thickness values (see Figure 2.7).

Similarly, a wide range of two-dimensional techniques can be applied in order to visualize scalar or vector values on the curved surface. To illustrate the breadth

27
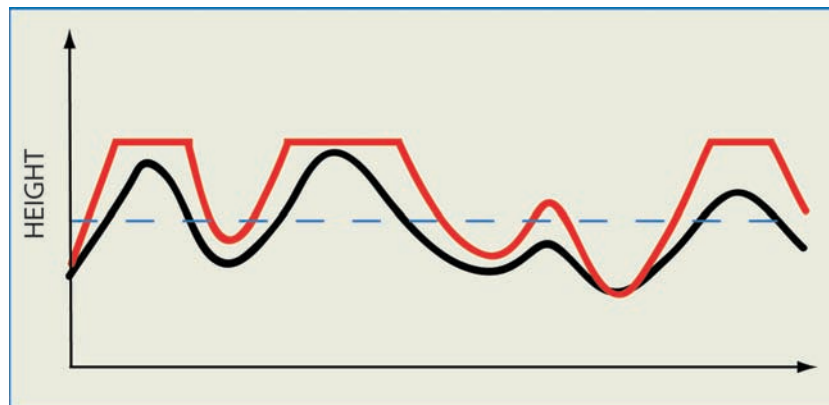
(a)
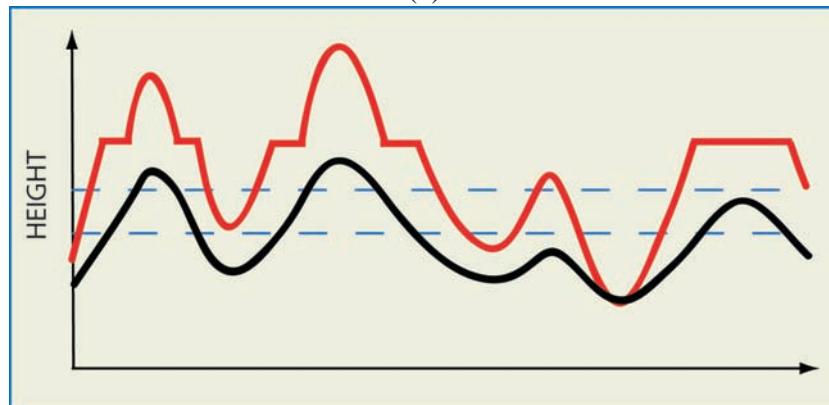
(b)

Figure 2.9: *Sketch of the thresholded non-linear scaling (a), and the non-linear scaling on an interval (b). The original function is depicted in black, while the scaled function is depicted in red. The blue dotted lines represent the thresholds.*

of the application area we discuss several visualization techniques for height fields, which exploit the flattening of a curved surface.

2.3.1 Thresholded Non-linear Scaling

In the case of cartilage visualization, we are interested in areas where the cartilage is thinning. Therefore, we want to inspect those areas, where the thickness is below a certain threshold. When scaling the entire height field, the enhancement of already thick areas, which are of less or no interest, may disturb the inspection, or hide the parts of the height field where the thickness is rather low. This is especially true if the variation of the thickness, which is of interest, is relatively small as compared to the overall thickness range. Therefore, in addition to the non-uniform scaling
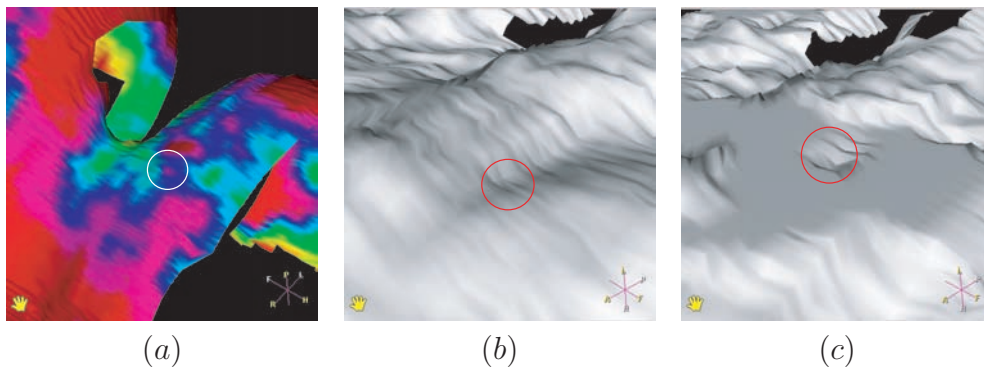
(a)	*(b)*	*(c)*

Figure 2.10: *Thresholded non-linear scaling: The scaling factor can be set independently for each thickness interval. This allows to flatten the values which have no importance for the inspection, while scaling only the values below and above the value range, respectively: reconstructed surface (a), non-uniformly scaled surface (b), thresholded scaling with three intervals (low, middle, high) (c). Flattening of the middle values, allows the user to concentrate on the areas with the suspicious values (circle).*

thickness versus spatial extent, we propose a thresholded non-linear scaling along the thickness dimension (see Figure 2.8). Thresholded non-linear scaling clips all thickness values above the threshold and linearly scales all thickness values below the threshold. Figure 2.9 (a) illustrates this concept.

2.3.2 Non-linear Scaling on an Interval

A natural extension to thresholded non-linear scaling is the scaling on a certain range interval of thickness values. An arbitrary number of value ranges can be defined in order to perform custom scaling for each interval. Figure 2.10 illustrates a case with three height intervals. Let us assume, we are interested only in the pathologic cases, i.e., where the thickness is below one threshold or above another threshold. Three intervals are defined for low, middle and high thickness values. A linear scaling can be defined for each interval, respectively. Setting the scaling factor to zero for the values in the range between the two thresholds, allows the user to concentrate on the areas with the suspicious/specific low and high values (see circle in Figure 2.10 (c)). The idea is sketched in Figure 2.9 (b).

2.3.3 Scale Transfer Function

As mentioned above the overall thickness of the cartilage varies from patient to patient. Thus, we need a tool which enables the detection of subtle thickness changes on each range of the thickness values. Using the basic non-linear scaling approach, interesting features may be occluded by other scaled areas, which are not
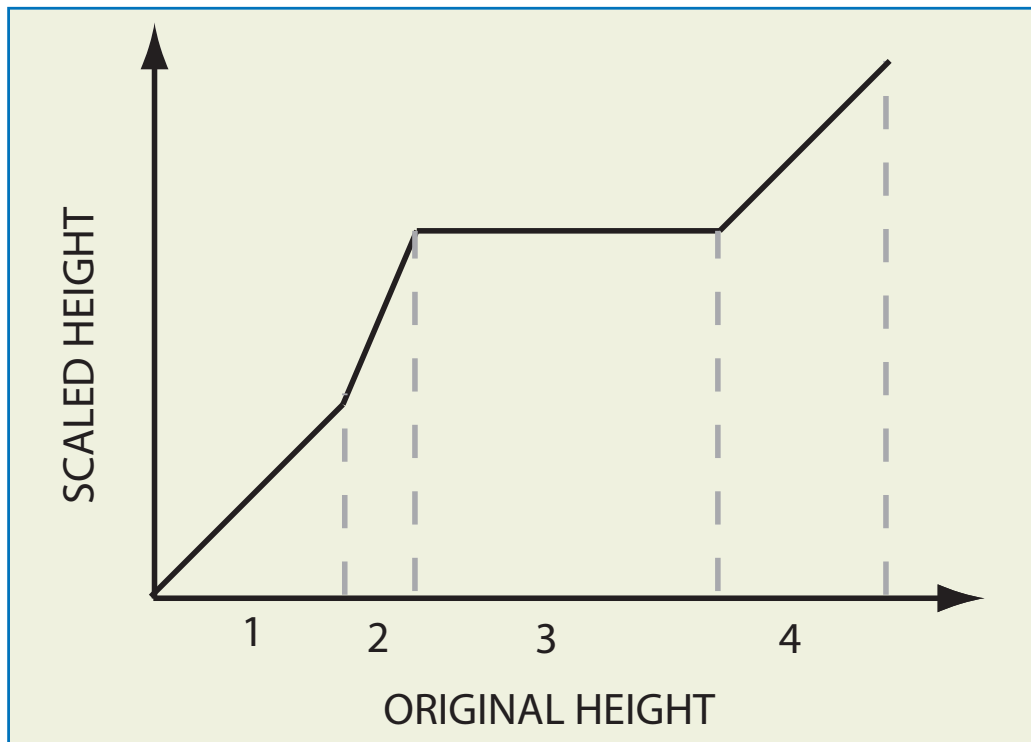
Figure 2.11: *An example of a simple scale transfer function. The scaling is performed on interval 2, while the values in the intervals 1 and 4 are preserved. The constant mapping of the values belonging to interval 3 flattens the surface in this area.*

of interest. This drawback can be overcome by generalizing thresholded non-linear scaling. We define a continuous piecewise linear scaling transfer function [11], which maps the original thickness values in the height field representation to the scaled values (see Figure 2.11). Note, that constant region correspond to flattening of the field (see Figure 2.11, interval 3). Thickness preservation is achieved in intervals, where $\triangle x = \triangle y$ (see Figure 2.11, interval 1 and 4).

2.4   Conclusions

We have presented a method to visualize the thickness of curved thin objects. The approach has been illustrated on the visualization of articular cartilage. This is a structure where the detection of slight thickness changes is vital for diagnosis. Unfolding of anatomic organs is promising since it enables the application of 2D visualization methods. A direct application of these methods is not possible on the curved reconstructed surfaces. The following examples show the extraction of the thickness information enhanced by iso-lines (see Figure 2.12), by color
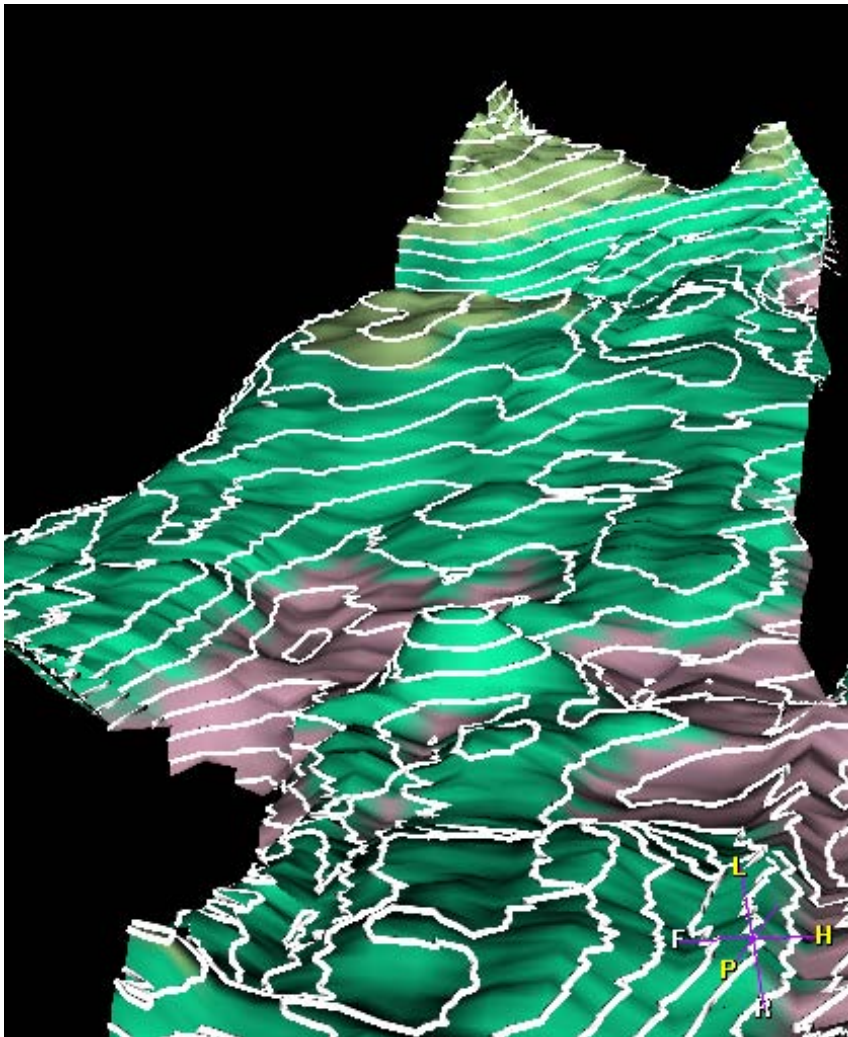
Figure 2.12: *Height field representation of the cartilage thickness enhanced by iso-lines.*

coding (see Figure 2.13), and by glyphs (see Figure 2.14). These representations of the unfolded cartilage provide additional information to the visualization, e.g., absolute thickness, or thickness gradient magnitude.

The above described techniques have been implemented as part of a framework for cartilage visualization. It includes several linked views, which allow inspection of the articular cartilage with links to views on the reconstructed surface as well as on the original slices.
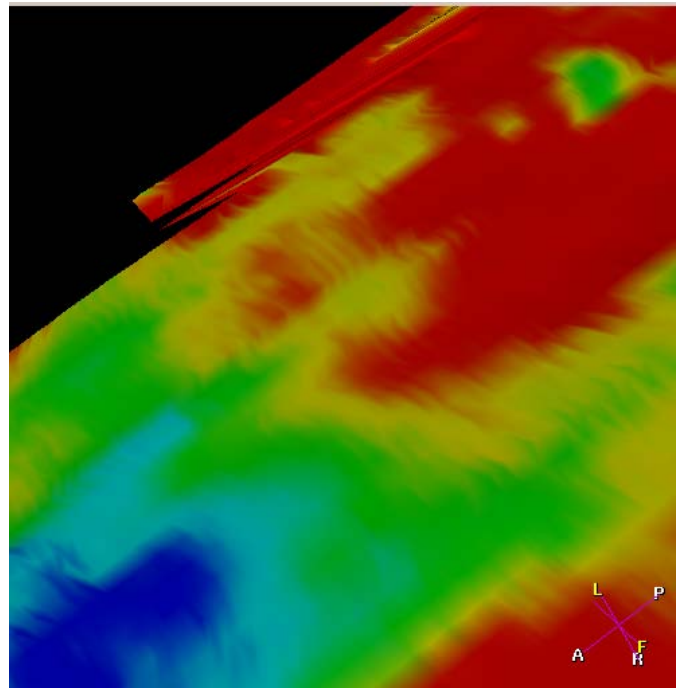
(a)
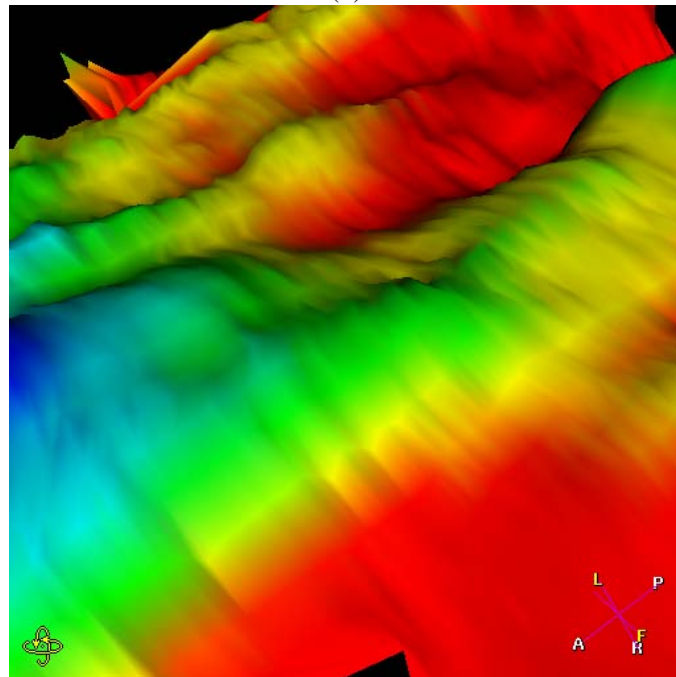
(b)

Figure 2.13: *Surface of the cartilage without (a) and with non-linear scaling (b). By increasing the scale factor it is possible to inspect also tiny changes in the thickness of the tissue.*

32
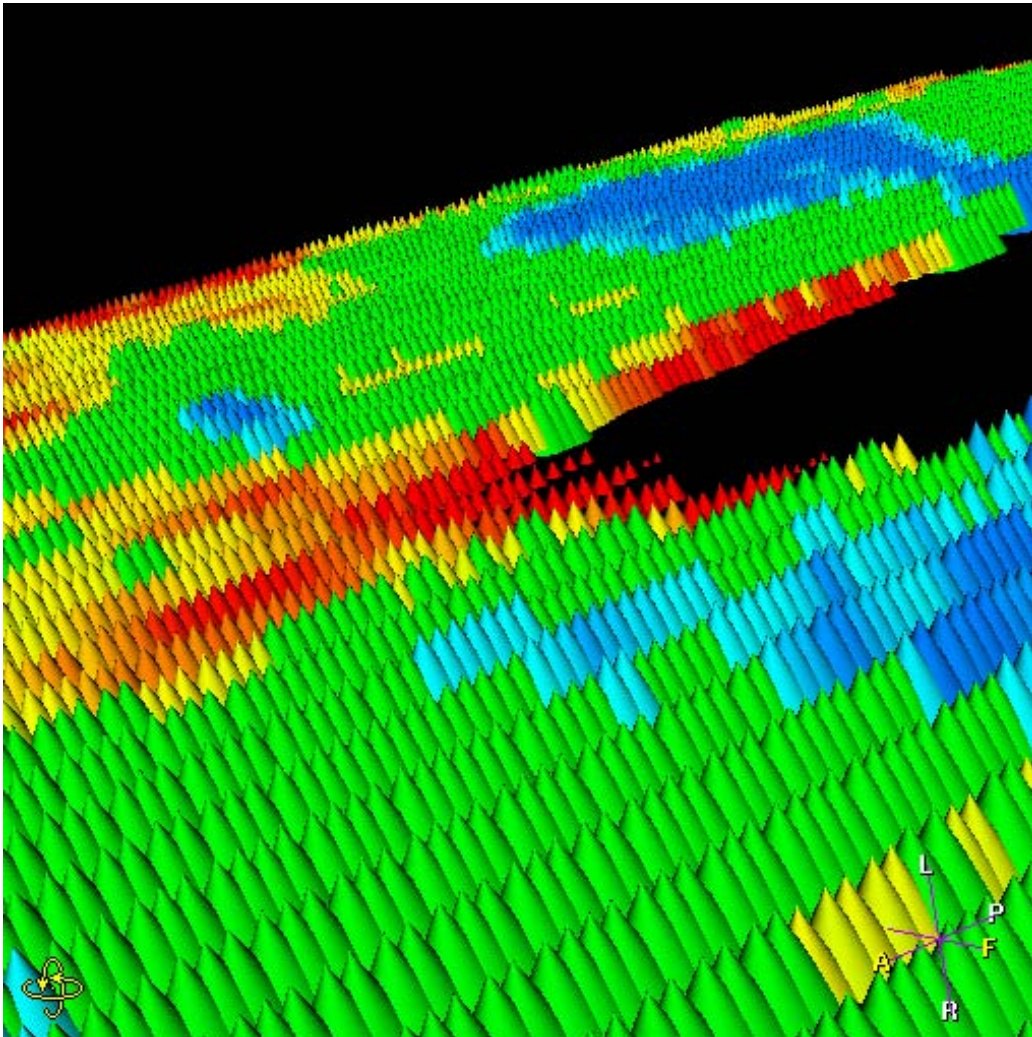
Figure 2.14: *Glyph representation of the surface thickness: the size of the glyphs increase with the thickness value.*

33

Chapter 3

Profile Flags: a Novel Metaphor for Probing of T_2 Maps

3.1 Introduction

Current MR cartilage-imaging techniques allow a detailed examination of the joint cartilage, including both thickness and quality of the tissue. In general, two types of MR sequences are used: a high-resolution anatomical scan (e.g., a 3D water suppressed sequence or proton density weighted sequence) and a T_2 map, representing the tissue quality. The computation of T_2 maps from spin-echo images is discussed in section 1.2.4. Figures 3.1(a) and (b) show one slice of the anatomical scan and the T_2 map of the patellar cartilage, respectively. The anatomical scan gives the information about the shape and thickness of the cartilage. In T_2 maps the radiologists are searching for disruptions of typical T_2 patterns. Therefore, these two scans are usually studied on two linked screens in a slice-by-slice manner or by multi-planar reconstruction for radiological assessment. This considerably reduces the spatial perception and prolongs the examination time. A 3D representation of the cartilage anatomy is a valuable tool for radiologists, giving added 3D information for a better localization of lesions. For a better communication with the orthopedists diagnostic information is illustrated in one single image with anatomic correlation. This allows an easy access to this information, for example during surgical procedures. Integration of qualitative information as provided by the T_2 map into the 3D representation gives an even more valuable inspection tool.

Our approach deals with combining the anatomical information with the quality information of the cartilage. Although the knee is fixed during the acquisition, these two sequences have to be registered by an affine transformation. Registration is based on local correlations [80] to compensate slight patient's movements. Then, the surface of the articular cartilage is reconstructed from the high-resolution anatomical scan. In order to obtain the T_2 map limited to the interior of the cartilage, the previously computed segmentation mask is applied to the T_2 map.
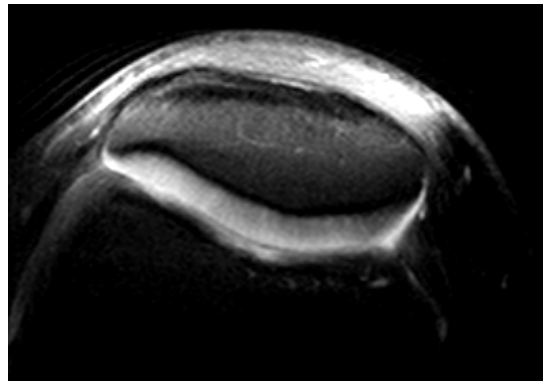
(a)
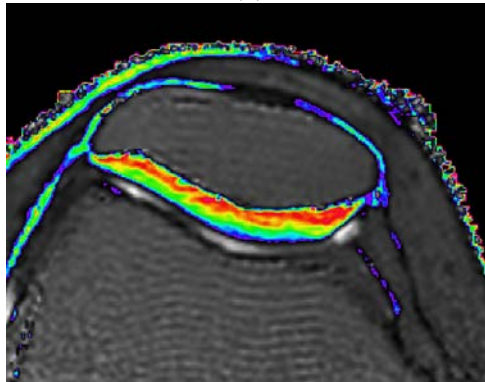
(b)
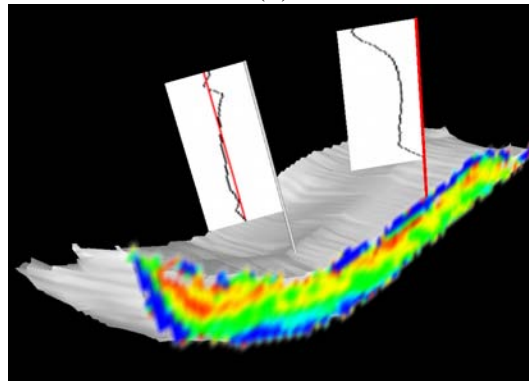
(c)

Figure 3.1: *One slice of an anatomical scan of a patella (a) and the corresponding T_2 map (b) of articular cartilage investigated with Profile Flags (c).*

Recently, the spatial distribution of the T_2 relaxation times within the cartilage has been widely discussed in medical literature [49, 50, 62, 48]. For the validation of the quality of the cartilage by means of disruptions in the T_2 map, so called T_2 profiles are calculated. A T_2 profile is the curve of varying T_2 values along a

line that is perpendicular to the subchondral bone and that ends at the surface of the cartilage (see Figure 1.4). For healthy cartilage the T_2 profiles have a typical characteristic shape. This is due to the fact that for healthy cartilage the T_2 values are arranged in layers parallel to the subchondral bone. The T_2 profiles in lesion areas significantly deviate from these characteristic shapes. Multiple T_2 profiles can be generated in order to obtain local characteristics for comparison of different regions of the cartilage and comparison between specimens. Since several factors, e.g., the age or the physical proportions of the patients, are significant for the thickness and the T_2 relaxation times, a normalized profile can be computed. It yields the T_2 times for the normalized distances between the subchondral surface (distance 0.0) and the articular surface (distance 1.0). This enables a comparison of spatial variation of two profiles with different lengths.

The main contribution discussed in this chapter is the introduction of the Profile Flag, a novel user interface for investigating T_2 maps (see Figure 3.1(c)). This glyph enables probing of the T_2 maps within the articular cartilage. It provides information about the thickness as well as the quality of the cartilage. The Profile Flag improves on two ineffective steps in the workflow of articular-cartilage inspection in clinical practice. Firstly, by browsing the T_2 profiles on a reconstructed surface of the cartilage, the radiologist does not need to switch between two screens in order to observe both, the thickness changes and the quality within the cartilage. Moreover, by using multiple Profile Flags, the disruptions in the structure of the T_2 map and thus the deviation from a "healthy" profile can be visualized in an intuitive way. Secondly, the commonly used procedure of communication between the radiologist and the orthopedist involves marking and printing out all slices including the identified lesion. Using the Profile Flag, the investigating radiologist can simply annotate the affected regions on a reconstructed surface by showing the local characteristics of the cartilage in one single image.

The chapter is structured as follows. Related work on volumetric data interaction and annotation is reviewed in section 3.2. Then, the necessary environment for the visualization of the T_2 maps is sketched in chapter 3.3. In the central section 3.4 of the chapter, we discuss the different setups of the Profile Flag. Results are shown in section 3.5. In chapter 3.6 we discuss possible extensions to the Profile Flag. Finally, we summarize and conclude the chapter in section 3.7.

3.2 Related Work

There is a large body of work discussing the annotation of volumetric data. Every feature can be annotated by a rectangular caption, which is located outside the volume in image space. Each caption is assigned to one pre-defined feature in the data. Usually, the main issue of papers from this track is the arrangement of the

rectangles with the purpose of avoiding overlap in image space [30]. Bell et al. [6] address the above mentioned issues in a virtual 3D environment. Several groups are discussing glyphs with picking and manipulating capabilities in virtual environments [73].

Recently, the use of advanced interaction tools is gaining popularity beyond what is already available in medical workstations. Besides the commonly used cutting planes (or even, arbitrary cutting objects), McGuffin et al. [47] presented an interactive tool for investigation of volumetric data based on different kinds of deformations and layerings of the objects. More application-specific glyphs have been presented by Huitema and van Liere [34] for molecular data, comprising translation and measurement capabilities. In Preim et al. [59], measurements like distances or angles, can be determined by an intuitive interface.

In flow visualization, de Leeuw and van Wijk [41] present a glyph for the visualization of multi-dimensional data. The glyph can be located at an arbitrary position and it visualizes the local characteristics of several flow attributes.

In chapter 2, we discussed the visualization of the thickness of femoral cartilage. Since the femoral cartilage constitutes a curved structure, we concentrate on visualizing the thickness information by unfolding the cartilage. In this chapter we focus on the patellar cartilage, which is a flat structure when no lesions are present. Thus no deformations are necessary to represent the thickness in a reliable way. Moreover, given the current scan resolution, the patellar cartilage is thick enough for observing spatial variations of the T_2 times within the cartilage.

3.3   Graph of Profiles

A graph of profiles (see Figure 3.2) is the first indicator of irregularities in the structure of the T_2 map. Since the shape of a T_2 profile is dependent on several factors like the age or the physical proportions of the patient, a default T_2 profile cannot be determined. Moreover, chemical shift artifacts at the bone/cartilage surface introduce longer T_2 values at this boundary. The shape of the curve thus depends on the segmentation technique [68]. Therefore, the graph of profiles is crucial to provide a statistical reference for the radiologists. A set of uniformly distributed profiles is computed on the entire surface starting from the subchondral bone. Each profile is shown in the graph in order to give an overview of all profiles. Such a simultaneous representation of many profiles discriminates the ones with suspicious characteristics as outliers. During browsing the profiles with the Profile Flag, the currently investigated profile is emphasized in red, while the remaining profiles yield a statistical information on the shapes of all the other T_2 profiles. Figure 3.2 shows a graph of profiles of a healthy specimen.
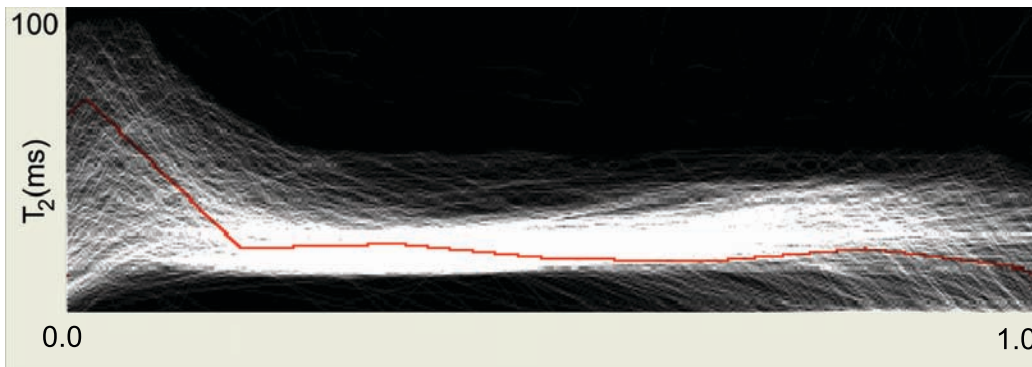
Figure 3.2: *Spatial variation in T_2 as a function of normalized distance from the subchondral bone (0.0) to the articular surface (1.0) of the patella. The selected profile is depicted in red.*

3.4 Profile Flag

So far, we have discussed the generation of the T_2 maps, which are investigated in a slice-by-slice manner in clinical practice. In this section we are presenting the Profile Flag for probing of the T_2 maps by browsing the reconstructed surface of the cartilage. The Profile Flag is a bulletin board pin-like interface for probing and annotating of underlying data. In order to visualize the corresponding profile, the Profile Flag is located on the surface of the cartilage. Since the T_2 profiles are defined along lines perpendicular to the subchondral bone interface, the Profile Flag is aligned with the normal vector of the surface at that position. During the investigation, one can drag the Profile Flag along the entire surface of the inspected object. Multiple Profile Flags can be stuck into the object in order to visualize multiple profiles or to emphasize the difference between two or more profiles. A Profile Flag consists of four components: the banner, the range selector, the needle and the cutting plane (see Figure 3.3). In the following the components of the Profile Flag and interactions therewith are discussed.

3.4.1 The Needle

The needle is located beneath the surface of the inspected object. It defines the position of the reference profile. Two types of needles can be defined: a needle with a fixed length and a needle with an adaptive length. The fixed length needle samples the underlying volume at equally spaced intervals starting from the subchondral bone (see Figure 3.4(a)). It yields the measured values in relation to the distance from the subchondral bone. In the investigation process of the cartilage, such a needle is designed for measuring the (absolute length) T_2 profiles. If a needle with an adaptive length is applied, the needle measures the normalized profile. It can

39
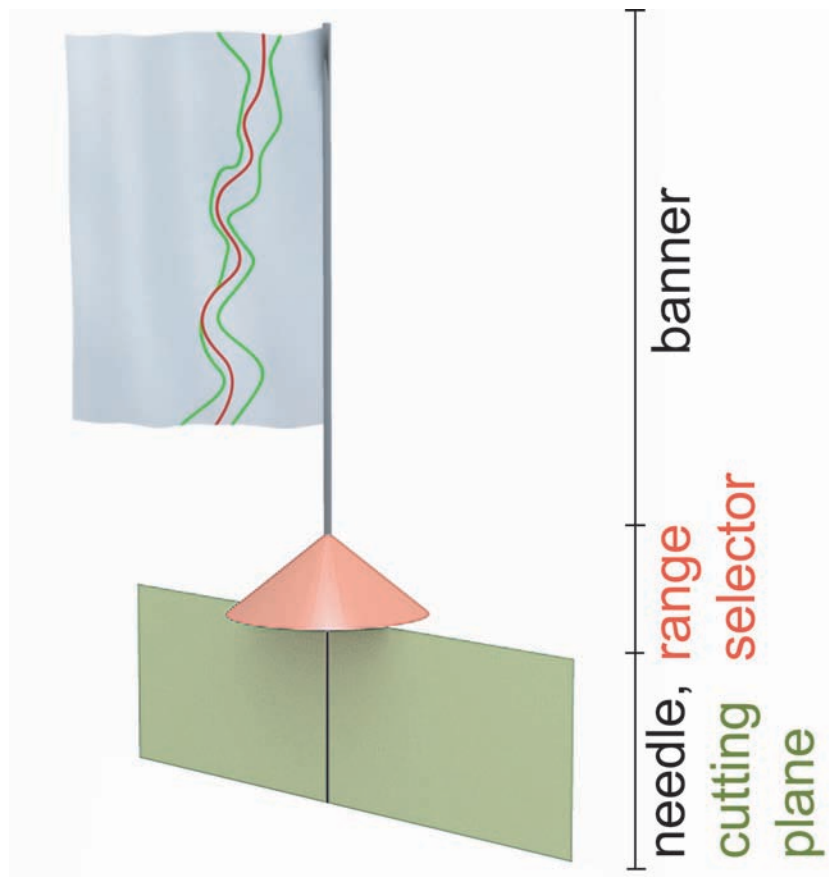
Figure 3.3: *Profile Flag: a 3D glyph for probing of profiles. The glyph is located on the surface of the investigated structure, perpendicular to its surface. It consists of the banner, the range selector, the needle, and the cutting plane.*

be considered as a needle scaled to the thickness of the cartilage at the currently investigated point (see Figure 3.4(b)).

3.4.2   The Range Selector

The range selector is a cone which enables the definition of the size of the investigated neighborhood. While the reference profile is defined by the position of the needle, the range selector determines the size of the interesting neighborhood through the radius R of the cone base-circle. All profiles located within this range are visualized according to the type of the banner (see section 3.4.3). If the radius is set to 0, only the reference profile will be visualized (see Figure 3.5).
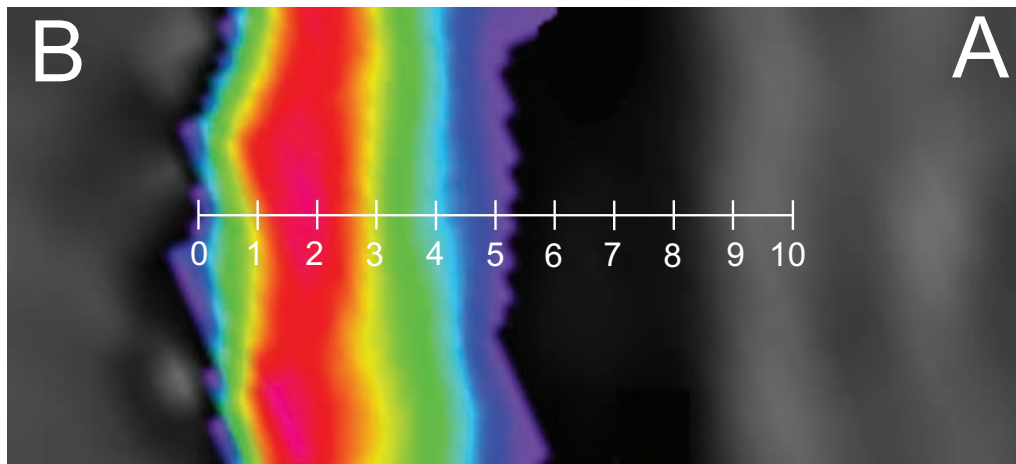
(a)
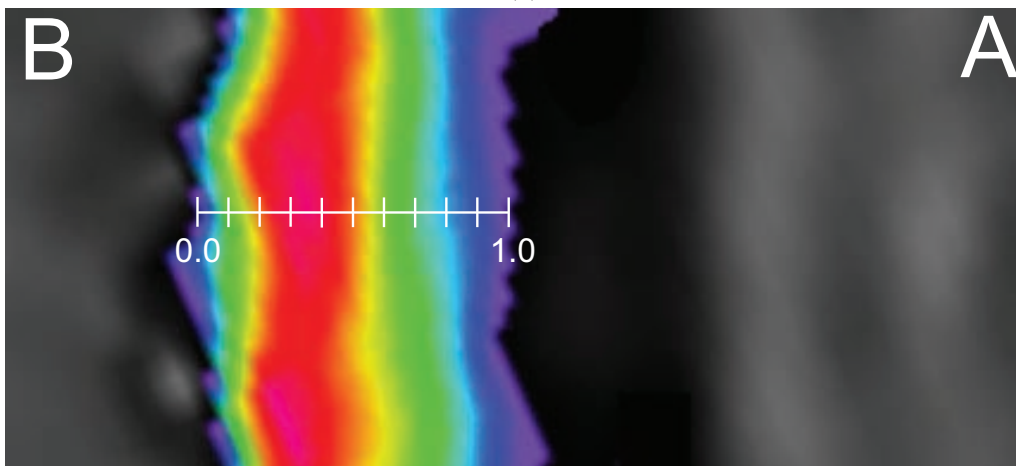
(b)

Figure 3.4: *Two types of needles: (a) needle with a fixed length is probing the values at regularly spaced intervals and (b) an adaptive needle is sampling the measured values along the normalized distance from the subchondral bone B to the articular surface A.*

3.4.3 The Banner

The banner represents the information defined by the position of the needle and the range defined by the range selector. For normalized profiles, the top of the banner corresponds to the subchondral surface, while the bottom of the banner corresponds to the articular surface (see Figure 3.6). The banner is always facing the camera. This avoids projective distortions and thus distortions of the visualized information. On the banner the profile information is shown in one of several ways:

41

(a) (b)
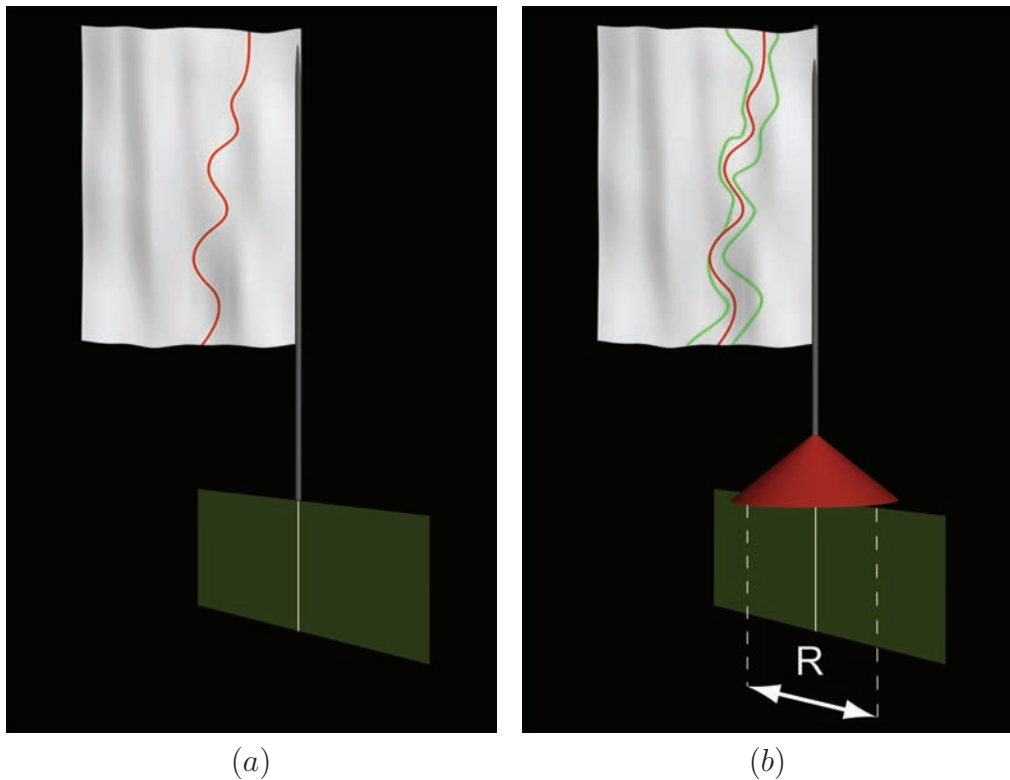
Figure 3.5: *Two setups of the range selector. If the radius R is set to 0 (a), only the reference profile is measured, setting $R > 0$ (b), all profiles within the neighborhood are visualized on the banner. The profile at the needle is shown in red. The green lines delimit all profiles in the neighborhood.*

- **single profile banner**: by setting the radius R to 0 only the reference profile at the needle is shown (see Figure 3.7(a)).

- **single averaged profile banner** $(R > 0)$: this type of banner averages all profiles within the radius R and shows only one averaged profile.

- **multiple profiles banner** $(R > 0)$: in addition to the reference profile, all profiles within radius R are taken into account. In order to avoid visual clutter by showing all profiles in the neighborhood, only the minimal and maximal values from all profiles are rendered in green (see Figure 3.7(b), (c)). The green lines are not existing profiles but enclosure lines of all profiles in the investigated neighborhood.

- The **deviation profile banner** illustrates the difference of profiles from a reference profile. The reference profile is straightened and coincides with the vertical axis (see Figure 3.7(d)). The other profiles undergo the same

Figure 3.6: *One slice of the T_2 map with one profile (left) and the corresponding banner (right). When measuring a normalized profile, the top of the banner (right) corresponds to the bone/cartilage interface B, while the bottom of the banner represents the articular surface A.*

transformation. Thus the deviations from the reference profile are easily perceived. A deviation profile can be used to show the profile varianc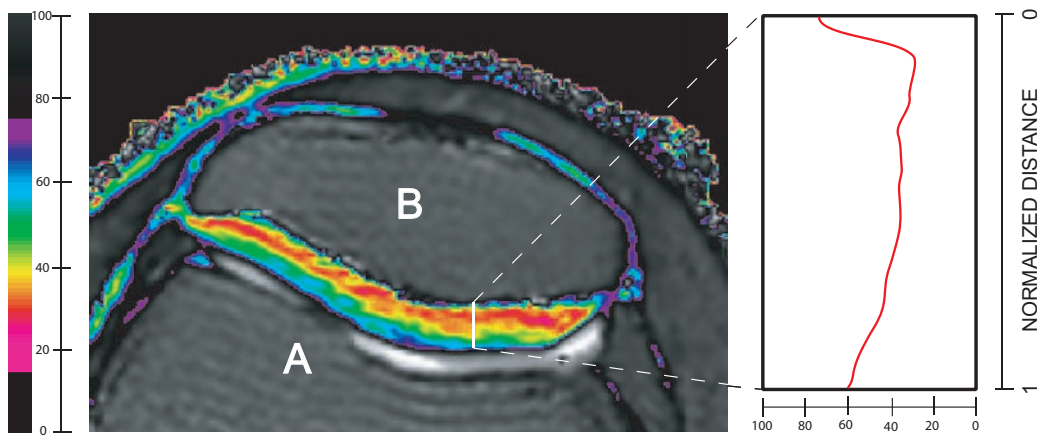e within a single neighborhood. Another possibility compares two different cartilage regions with two Profile Flags. The first Profile Flag defines the reference profile, e.g., in a healthy region. The second Profile Flag shows then the difference profiles in another (possibly suspicious) region (see Figure 3.7(e)).

These banner types are a small collection of conceivable definitions of a set of profiles. Further possibilities include occurrence-based profile displays and reference profiles with statistical annotations (mean, variance).

3.4.4 The Cutting Plane

The cutting-plane component of the Profile Flag is an extension of the multi-planar reconstruction, a tool which is usually applied for inspection of T_2 maps. Since we are primarily interested in those cross-sections of the data that include the reference profile, the needle should be included in the cutting plane. In order to investigate the entire neighborhood of the profile, the plane can be rotated by an arbitrary angle around the needle (see Figure 3.8). Notice that, when the cutting plane is shown, the needle is not rendered in order not to hide the reference profile at the cross-section.

Moreover, the interaction with the reconstructed surface of the cartilage can facilitate the initial setting of the position and rotation of the desired cutting plane.

43
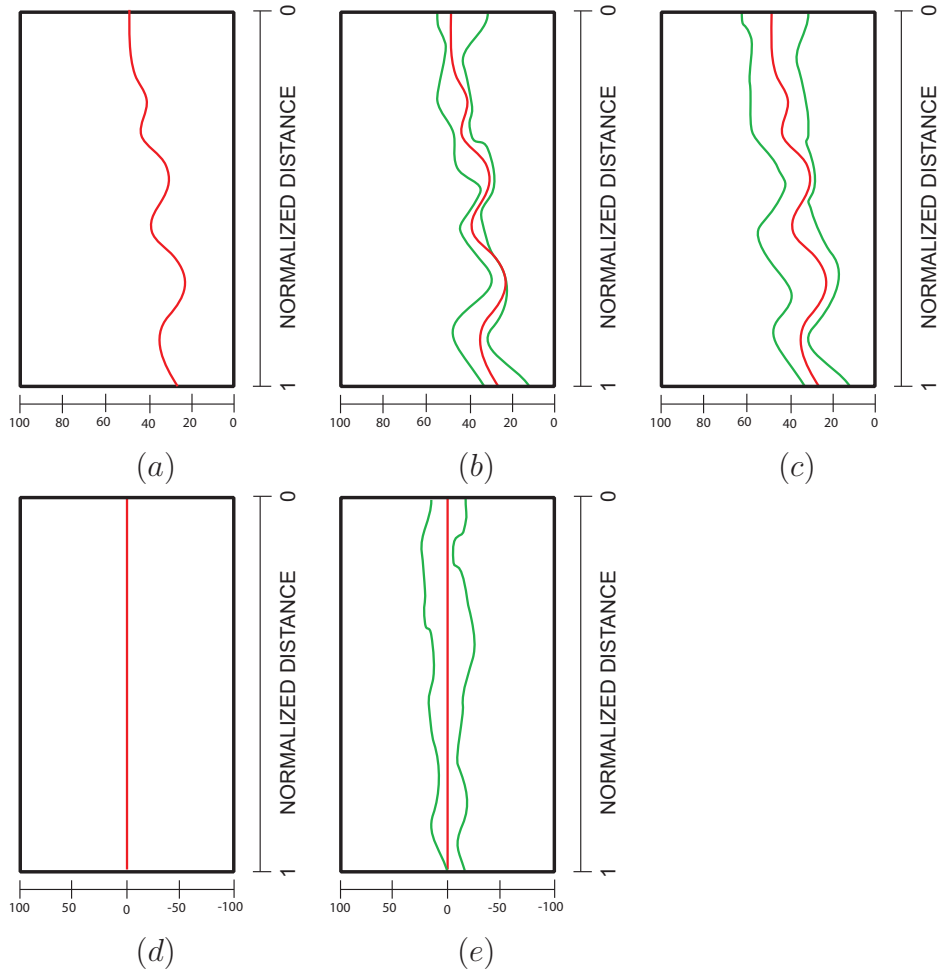
Figure 3.7: *According to the type of the banner, the profiles defined by the needle and the range selector are visualized: (a) single profile banner, (b) multiple profiles banner (radius = 1mm), (c) multiple profiles banner (radius = 3mm), (d) deviation profile banner (radius = 0mm), (e) deviation profile banner (radius = 1mm).*

Therefore, the cutting plane is defined by a point on the needle and a normal vector, independently from the rotation of the object. The normal vector of the plane has to be perpendicular to the direction vector of the needle. To choose the normal vector facing the camera, it should be located in the plane defined by the direction vector of the needle P and the viewing vector V. The normal vector can be calculated by $N = (V \times P) \times P$, where V is the viewing vector from the camera to the location of the profile and P is the direction vector of the needle.

The two modes for interaction with the cutting plane are:
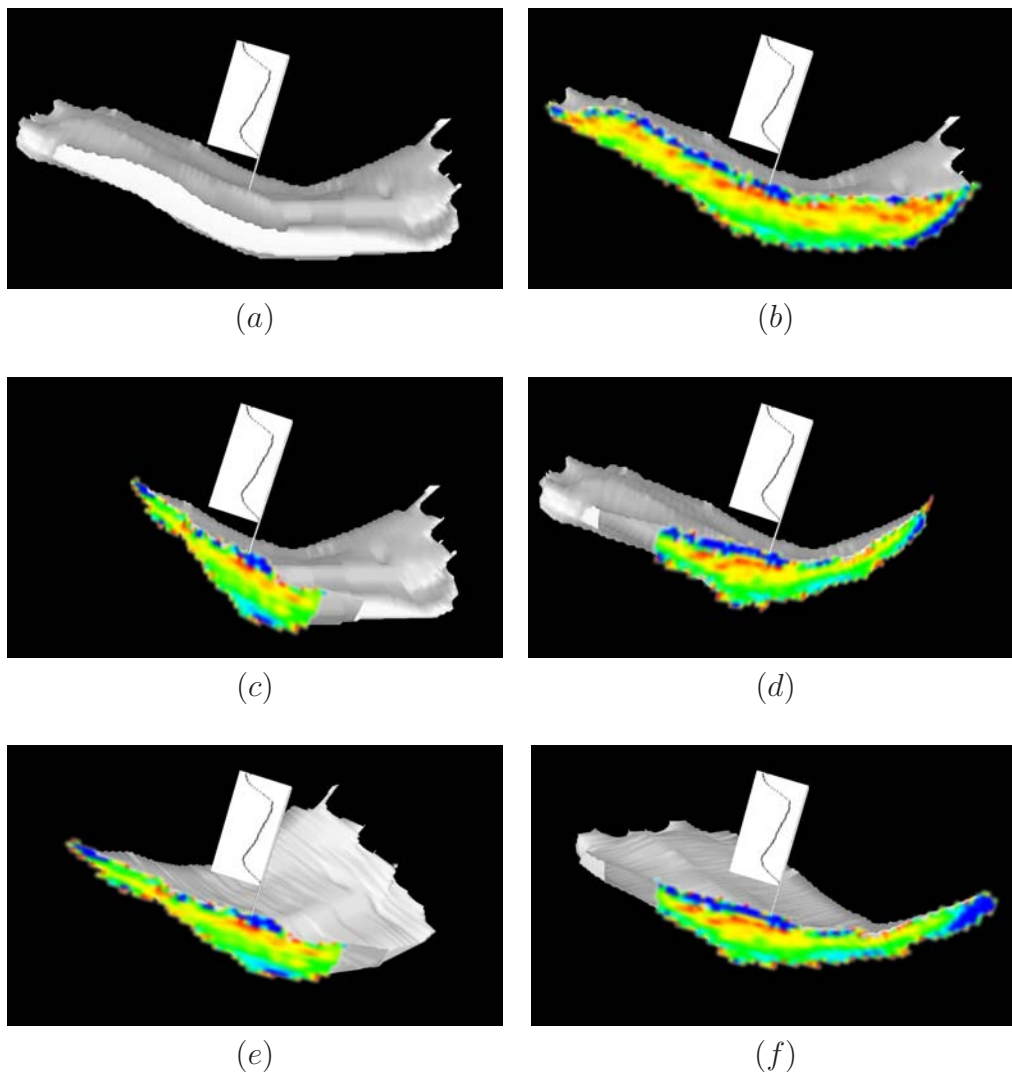
Figure 3.8: *The reconstructed surface (a) of the articular cartilage including one Profile Flag. The cutting plane (b) is generated by taking into account the viewing vector and the needle position of the observed profile. Figures (c) and (d) demonstrate the rotation of the cutting plane around the needle at $+40$ and -40 degrees, respectively. Notice the distortion of the resulting T_2 map caused by the rotation and projection. Figures (e) and (f) show the rotation of the reconstructed surface around the needle at $+40$ and -40 degrees, respectively. The cutting plane remains parallel to the image plane.*

- **rotation of the cutting plane around the needle**: This mode is convenient for rotation with small angles. The oblique position of the cutting plane produces projection distortions which grow with increasing rotation angle (see Figure 3.8(c) and (d)).

45

- **rotation of the object around the needle**: The second mode is designed for rotation with an arbitrary angle. The cutting plane remains parallel to the image plane and does not change its position in image space during the interaction. One can easily observe the entire neighborhood of the current profile. On the other side, a disorientation may occur while rotating the clipped reconstructed surface (see Figure 3.8(e) and (f)).

3.5 Results

In this chapter we shortly discuss three scenarios of data annotations with the previously described Profile Flag. Figure 3.9 shows two possibilities of annotating the quality of articular cartilage. Figure 3.9(a) contains two Profile Flags visualizing a healthy (left) and a suspicious profile (right). Moreover the left Profile Flag can be set as a reference Profile Flag (Figure 3.9(b)). Then, the right Profile Flag measures the deviations to the profile defined by the reference Profile Flag. Figure 3.10 visualizes also the profiles in the neighborhood of the reference profile. Notice, that while the reference Profile Flag visualizes the minimal and maximal T_2 values within the defined area, the right Profile Flag depicts the minimal and maximal deviation from the reference Profile Flag. An arbitrary number of Profile Flags can be stuck into the surface of the investigated object. Figure 3.11 shows an articular cartilage with three annotated profiles. The middle one defines the cutting plane, which shows a cross-section of the T_2 map including the profile defined by the reference profile.

3.6 Discussion

The basic concept of the Profile Flag offers many opportunities. Here we discuss some of the possible extensions and applications of the Profile Flag.

- **profile flag as an annotation tool**: By sticking one or more Profile Flags into the inspected structure, one can easily annotate regions of the object, which contain suspicious internal characteristics. In clinical practice, this step is crucial for transmitting the diagnosis from the inspecting radiologist to the orthopedist, who is performing the arthroscopy. This can be achieved in an efficient way by highlighting the damaged regions of the object in conjunction with the anatomical context.

- **automatic positioning of profile flags**: Additionally to browsing the profiles, one can think of an automatic positioning of the Profile Flags. This can be a pre-processing step before starting the investigation of the structure. In
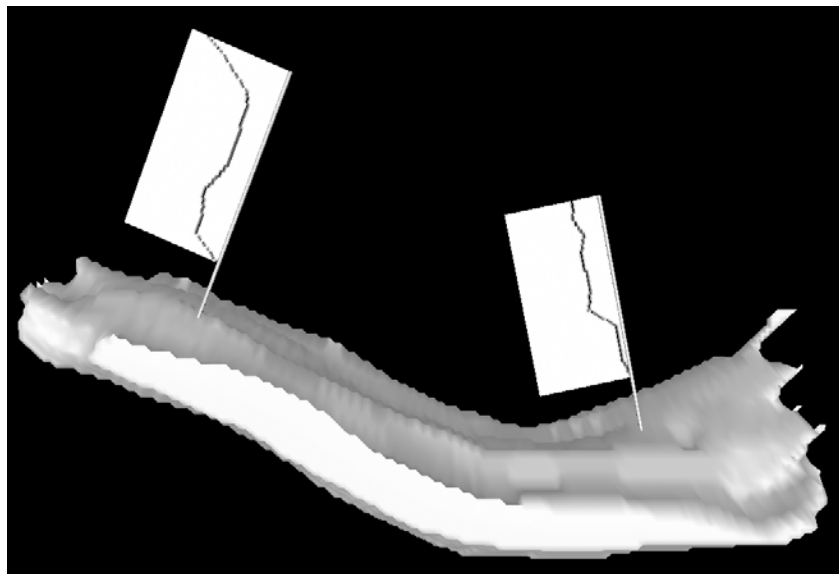
(a)
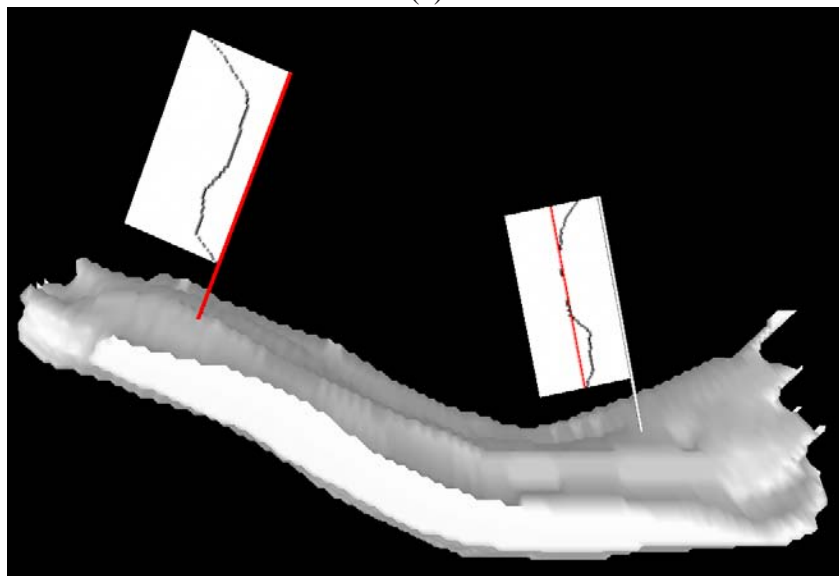
(b)

Figure 3.9: *A disruption (right Profile Flag) in the pattern of the T_2 map can be annotated in two ways. Figure (a) shows two Profile Flags, where the left one shows a healthy profile, while the right Profile Flag shows a suspicious profile. On the other hand, the left Profile Flag in Figure (b) is set as a reference Profile Flag. The right one shows the deviation of the probed profile from the reference Profile Flag.*

case of cartilage imaging, one profile, comprising a healthy behavior, can be determined. The following investigation of the cartilage would include the

47
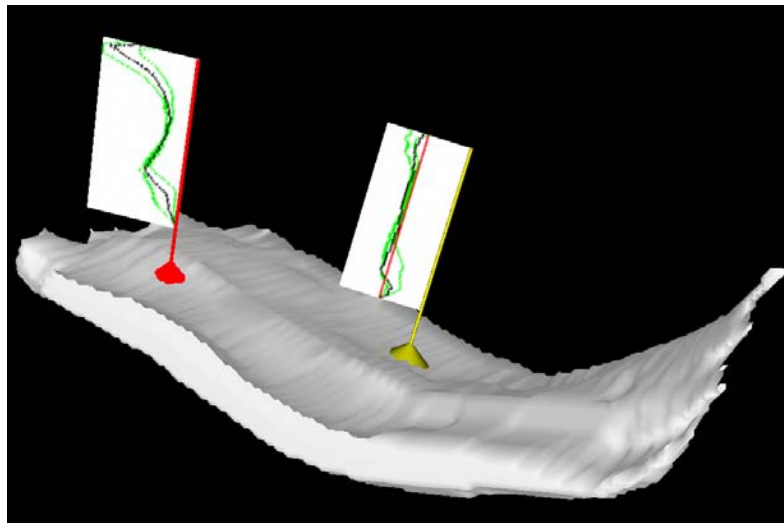
Figure 3.10: *The reference Profile Flag (red) is located at a position of a healthy profile. Additionally, the extent of the profiles within the selected range is shown. The right profile (yellow) is showing the deviations from the reference Profile Flag. Again, the neighborhood of the current profile is visualized.*
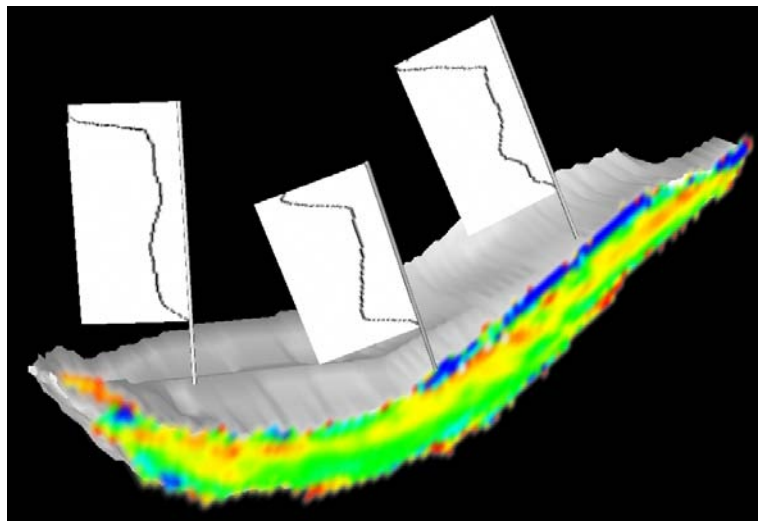
Figure 3.11: *A T_2 map annotated by three Profile Flags stuck into the reconstructed surface of the articular cartilage. A cutting plane is showing a cross-section of the T_2 map with respect to the Profile Flag in the middle.*

browsing of the cartilage with the deviation profiles, which show only the variation from the reference profile. This step would involve a sophisticated statistical analysis, since the T_2 profiles differ among the population. Several techniques of an automatic positioning of Profile Flags are discussed in

section 4.3.3.

- **seeding of profiles**: When inspecting an object with a curved surface, one can easily miss a profile with an important characteristic. This is particularly the case when using the Profile Flag for probing of profiles within a certain neighborhood. Thus, the density of the Profile Flags should be adapted to the curvature of the surface in order not to miss any area. A similar issue has been discussed by Vilanova et al. [77] for virtual colonoscopy.

- **selection of profiles**: The set of selected profiles can be defined by a certain condition. For instance, restricting the maximum deviation for the multiple profile banner at any position along the needle causes a reduction in the number of profiles to the ones, which fulfill this criterion. This involves a modification of the shape of the range selector by indicating only a subset of all previously selected profiles. Techniques for selection of profiles are discussed in section 4.3.2.

- **application areas**: In this chapter we demonstrate the use of Profile Flags for probing of T_2 maps. However the application of the tool is not limited to the investigation of knee cartilage. Other areas include visualization of 3D structures which have spatial or temporal curves associated to each 3D location. Examples include dense geologic data or time dependent series of dynamic contrast enhanced MRI for mammography (see section 4.4).

3.7 Conclusions

In this chapter we have presented the Profile Flag - a glyph for probing of underlying curve data. The Profile Flag consists of four components: the banner, the range selector, the needle and the cutting plane. It can be moved along the reconstructed surface of the cartilage by giving immediate feedback on the local characteristics of the underlying data. Since the essential information is rendered outside the investigated structure, there is no need to reduce the information about the shape or anatomy of the inspected object. Moreover, several regions of the object can be annotated, by using either the absolute or the relative representation of the measured quantity. We have presented the application of the Profile Flag in a medical environment for the investigation of knee cartilage. Besides observing the shape and the thickness of the cartilage, the radiologist can inspect the change in the quality of the cartilage by probing of the T_2 maps. The result of the inspection is the reconstructed surface of the object with annotated lesions, which can be easily interpreted by the orthopedist. The application of the Profile Flag is not restricted

to medical domains only. Other application areas include probing of curve data in structures, where the reduction of the context information is undesirable.

Chapter 4

Application-Oriented Extensions of Profile Flags

4.1 Introduction

In medical environments, many tools for visualization of volumetric data have been presented. These include volume rendering, multi-planar reformation, cutting planes, virtual endoscopy, etc. Most of the techniques try to classify the underlying data and enhance the essential information to be visualized. In this chapter, we present several extensions and an evaluation of Profile Flags (see chapter 3), a tool for probing of profile curves in volumetric data. We apply the extensions in two application scenarios where profiles play a crucial role: MR orthopedics and MRI mammography. While the orthopedic data contains profiles, which are arranged perpendicular to a surface, the mammographic data includes time-signal profiles with specific properties.

The chapter is structured as follows. Related work on data interaction and annotation is reviewed in section 4.2. The various extensions of the Profile Flags are described in detail in sections 4.3. In section 4.4, we discuss two application scenarios. Finally, we summarize and conclude the work in section 4.5.

4.2 Related Work

Default interaction and inspection tools in a medical workstation include cutting planes, multi-planar reformation and endoscopic navigation. Recently further new interaction tools have been developed. McGuffin et al. [47] presented an interactive tool for investigation of volumetric data based on different kinds of deformations and layerings of the objects. A tool for manipulation of molecular data has been presented by Huitema and van Liere [34]. It comprises various interaction capabilities including translation or measurement instruments. For medical purposes, a framework for the measurement of angles and distances has been presented by

Preim et al. [59]. Recently, annotation of volumetric structures has been widely discussed in the literature. For pre-segmented data, a feature can be annotated by a caption, which is either blended over the data [25], or located outside in a rectangular area [9]. De Leeuw and van Wijk [41] presented a glyph for the visualization of multi-dimensional flow data. Multiple local characteristics of flow attributes can be visualized at an arbitrary position within the data.

In chapter 3, we presented the basic concept of Profile Flags. It is a glyph for the interactive probing of profiles. By dragging the glyph along the surface of the probed object, one can browse data values along lines in the tissue beneath. The profile at the position of the Profile Flag is visualized. Subramanian et al. [72] presented a tool for classification of time-signal profiles for dynamic contrast enhanced magnetic resonance imaging (DCE-MRI) data. The user specifies a time-signal profile with shape characteristics he is interested in. The system classifies the entire space of time-signal profiles according to the similarity to the pre-defined profile. Unfortunately, this approach restricts the inspection of the data to profiles similar to the pre-defined shape. Another approach by Carotenuto et al. [12] computes False Color Maps from time-signal profiles. By classifying profiles into non-overlapping regions, different areas of the volume are shown in different colors, respectively. The results of the semi-automatic detection of the suspicious profiles are visualized by maximum intensity projection. Suspicious areas are additionally color coded. Kohle et al. [38] discussed color schemes for two clinical applications: inspection of acute stroke in human brain and detection of tumors in 4D DCE images. In order not to blend the classified color-coded data, different rendering techniques, e.g., stereoscopic view, and (local) maximum intensity projection, have been demonstrated. Recently, Coto et al. [16] presented a tool analyzing breast DCE-MRI volumes. The user is provided with a set of scatterplots for all pairs of consecutive time-steps. With interactive linking and brushing in the domain of the time-signal profiles, the volume can be categorized according to the properties of the profiles. The resulting classified data are visualized with importance-driven volume rendering [78].

4.3 Extensions of Profile Flags

The Profile Flag (see chapter 3) is a bulletin-board-pin-like glyph for probing and annotating of underlying profile data. It consists of four components: the banner, the range selector, the needle and the cutting plane (see Figure 3.3). We discussed the use of Profile Flags for measuring T_2 profiles. These are curves of varying values that are measured perpendicular to the surface of articular cartilage. The Profile Flag can be inserted on the surface of the inspected object and aligned with the normal vector of the surface in that position. For that purpose, the needle is

positioned beneath the surface of the probed object. It defines the location of the reference T_2 profile. Two types of needle can be selected: the fixed-length needle, which probes the data values along the distance from the subchondral bone, and a needle with adaptive length for measurement of normalized profiles.

The inspected profile is visualized on the banner. The top of the banner corresponds to the upper surface of the inspected object and the bottom of the banner corresponds to the bottom surface of the object. The measured values are depicted on the horizontal axis of the banner. The right side of the banner corresponds to the lowest (0.0) measured value, while the left side of the banner corresponds to the highest value. The cone-shaped range selector is located above the surface of the object. By increasing the range selector, additional profiles in the neighborhood of the reference profile can be visualized.

According to the settings of the range selector, several types of banners can be defined. A single-profile banner shows only the reference profile at the position of the needle. By setting the radius of the range selector to a value larger than zero, either a single averaged profile is shown, or the minimal and the maximal values from all profiles in the neighborhood of the reference profile are visualized. The deviation-profile banner illustrates the difference of profiles from a reference profile defined by another Profile Flag. Thus, the deviations from the reference profile are easily perceived. The cutting-plane component of the Profile Flag is an extension of multi-planar reformation, a tool which is usually applied for inspection of T_2 maps. Either the cutting plane can be rotated around the needle or the cutting plane is facing the camera and the inspected object is rotated around the needle. During investigation, one or more Profile Flags can be stuck into the inspected object. They are moved along the object's surface, while showing the underlying T_2 profiles. Multiple Profile Flags can be placed to emphasize differences between profiles at different spatial locations.

In this section, we describe several extensions of the Profile Flags according to the application and, thus, the type of measured underlying data. In section 4.3.1, we discuss possibilities for enhancement of the glyph by incorporating thickness information into the basic concept. In section 4.3.2, we show additional modi for selection of the inspected profiles. Automatic positioning of the Profile Flags is presented in section 4.3.3. In section 4.3.4 we show the extension of the Profile Flags for probing of time-varying volume data.

4.3.1 Thickness Visualization

When probing profile data, we are also interested in the thickness of the cartilage in addition to the profile itself. This can be achieved by measuring the absolute profiles, i.e., measuring the sampled values against the distance from the surface. However, this does not allow comparison of two profiles with different lengths.
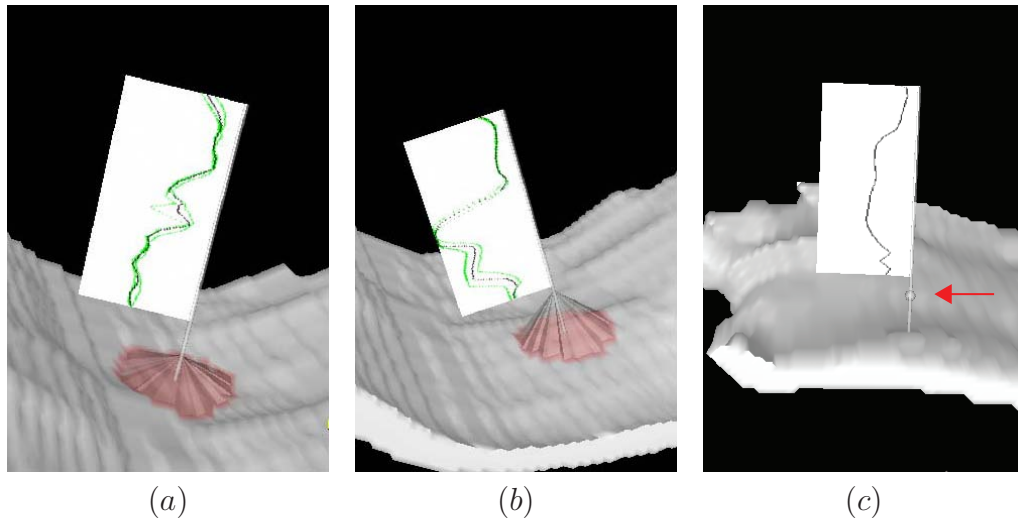
(a) (b) (c)

Figure 4.1: *Different approaches to visualize the thickness of the underlying tissue: (a) thin cartilage = low range selector, (b) thick cartilage = high range selector and (c) thickness illustrated by a spherical marker on the flagpole.*

Another possibility is to show a normalized profile and visualize the thickness in a different way. Extending the basic metaphor of the Profile Flag allows showing the thickness information in two ways. The first approach deals with changing the height of the range selector cone. As shown in Figure 4.1 (a), (b) the thickness of the underlying object corresponds to the height of the range selector. In order to represent the thickness and not to occlude the information rendered on the banner, the height of the range selector should be in the range between the surface of the probed object and the bottom of the banner. Knowing the range of the measured thickness values (t_{min}, t_{max}), the entire length of the flag pole can be exploited for the visualization of the thickness. The length of the flag pole corresponds to the distance between both ends of the flagpole, i.e., the surface of the object (h_{min}) and the bottom of the banner (h_{max}).

Then the height H of the range selector is:

$$H = h_{min} + \frac{(T - t_{min})(h_{max} - h_{min})}{(t_{max} - t_{min})}, \qquad (4.1)$$

where h_{max} is smaller or equal to the length of the flag pole from the surface of the object to the bottom of the banner and h_{min} is larger than or equal to 0. T is the thickness value at the current Profile Flag position. Another possibility to illustrate the thickness values is a spherical marker on the flag pole (see Figure 4.1 (c)). The new concept of thickness visualization enables browsing of profiles with multiple Profile Flags without the need of inserting the cutting plane at the current location.

54

Furthermore, one reference Profile Flag can be stuck at the position of a healthy profile. Areas with thickness differing from the reference profile can be easily located by browsing the underlying object with the help of a second Profile Flag.

4.3.2   Selection of Inspected Profiles

Up to now, the range selector has been an interface element which enables the selection of the visualized profiles. In chapter 3, just a conical range selector was used. The profiles of all surface positions covered by the base circle are simultaneously visualized on the banner. Extending the basic concept of the range selector enables also to indicate profiles with similar attributes. In the following we will call such a range selector a range indicator. We are not only interested in the spatial differences between profile locations, but also in the curve differences of the profiles themselves. Showing all the profiles around a Profile Flag where the profile difference is below a certain threshold generates range indicators with a polygonal base. This extension allows to illustrate the size and non-isotropic spread of a lesion. In this section, we discuss the spatial-difference as well as the curve-difference based specification of range indicators.

The selection of the set of profiles influences also the interaction with the cutting plane. For a Profile Flag showing a single profile, the cutting plane can be applied in order to show the T_2 map in the neighborhood of the Flag. When selecting multiple profiles, the cutting plane can be moved forward and backward along the plane normal within the range of the selected profiles (see Figure 4.2). This allows to inspect the entire set of selected profiles also in a slice-by-slice manner.

Spatial-difference range-indicator

In the basic concept, the range selector is positioned on the surface of the inspected surface. By changing the radius of the cone, all profiles located within the radius of the base circle are represented in the visualization. In addition to circular ranges now more general shapes, e.g., squares or arbitrary polygons are possible (see Figure 4.3 (a)). An example would be to show on the banner the weighted average of all the profiles covered by the range indicator. This performs a convolution based noise removal. The kernel is given by the shape and size of the range indicator.

Curve-difference range-indicator

The range selector can be modified to enclose only those profiles, which fulfill certain criteria. Starting from the reference profile, located at the position of the needle, a set of neighboring profiles can be selected by region growing on the
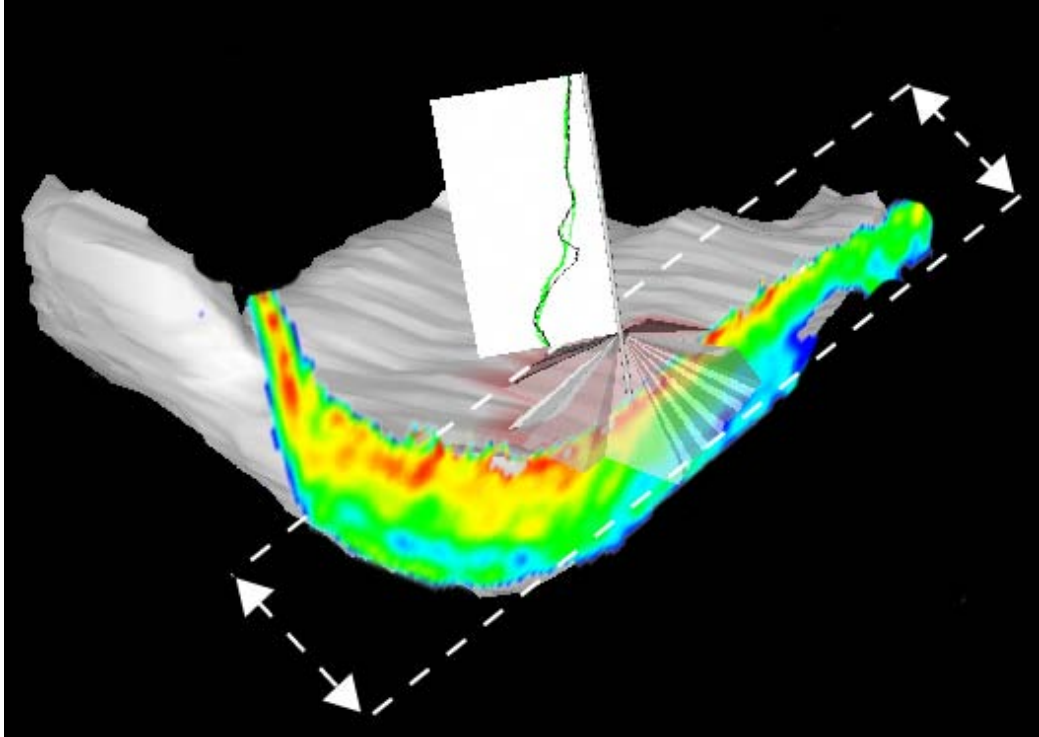
Figure 4.2: *The cutting plane can be moved along its normal within the range of selected locations.*

domain of profile curves. This guarantees that the result of the selection is a connected polygonal region whose profiles are "similar" to the reference profile.

The similarity criterion for profiles requires that a metric is defined on the profile curves. Let us assume that a profile curve C is given as a polyline consisting of $n + 1$ points C_i with value $V(C_i)$. The difference between two profiles C, D can be measured as the maximal point-wise difference $diff(C, D) = \max_{0 \leq i \leq n} | V(C_i) - V(D_i) |$. Another difference measure is the average point-wise difference: $diff(C, D) = \sum_{i=0}^{n} | V(C_i) - V(D_i) | / (n + 1)$. Another way of specifying a set of profiles is threshold based: $\{C \mid V(C_i) < T; \forall i \in (0, n)\}$. Additionally one can subdivide the probed object along the needle into $m + 1$ layers $\{L_0, L_m\}$. Then, defining a threshold for each layer, respectively, allows to detect profiles with suspicious characteristics with respect to their position along the needle (e.g., lesions near to the surface): $\{C \mid V(C_i) < T_j; \forall i \in (0, n), j \in (0, m), C_i \in L_j\}$.

A set of profiles is grown starting from the reference profile until the predefined threshold T or a difference threshold to the reference profile is exceeded. In general, using the range indicator, an arbitrary profile neighborhood can be defined by a combination of the spatial-difference and the curve-difference criteria. In order to compare two profiles with different lengths, one can apply the needle with adaptive
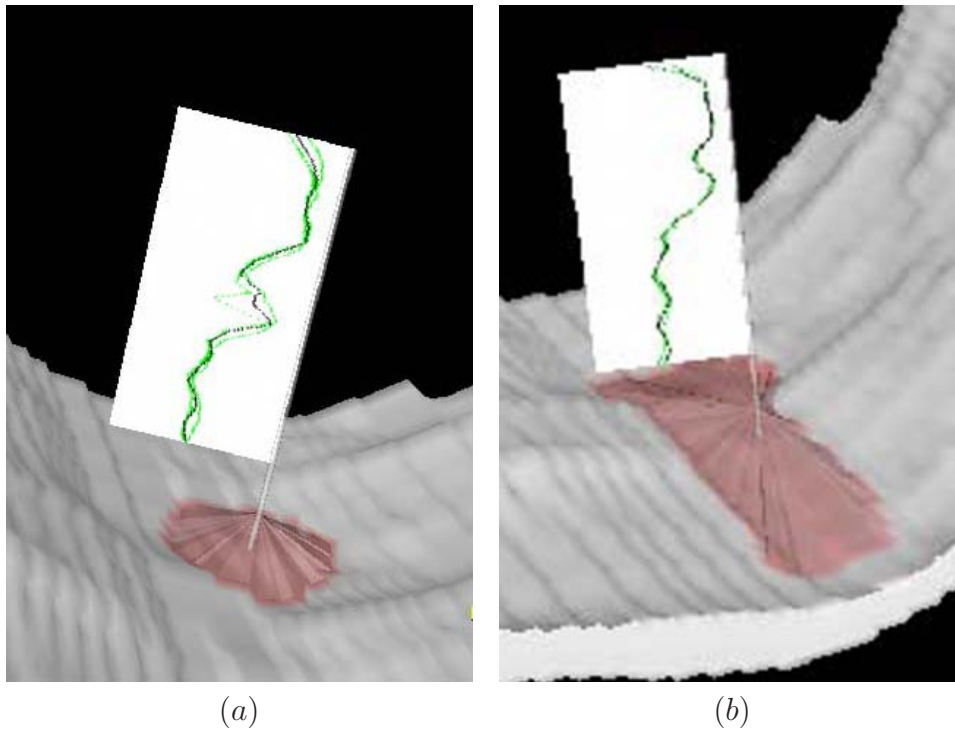
56

(a)　　　　　　　　　　　　　(b)

Figure 4.3: *Profile Flag showing selection of profiles according to a certain criteria: (a) spatial-difference, (b) curve-difference.*

length, which includes a fixed number of sampling positions along the needle irrespective of the profile length. Figure 4.3 (b) shows a Profile Flag representing a set of profiles with an average deviation smaller than a certain threshold.

4.3.3　Automatic Classification for Positioning of Profile Flags

An essential pre-processing step to the inspection of an object is the automatic positioning of the Profile Flags. In a medical environment we are usually interested in two types of profile data: a typical healthy profile and a suspicious profile significantly differing from the healthy one. With the help of Profile Flags, one or more suspicious profiles can be automatically depicted. Additionally, one Profile Flag can be used to depict a healthy profile as reference. The size of the suspicious area is visualized by an automatic selection of a set of profiles in the neighborhood of the detected profile. For the automatic positioning of the profiles, two types of classifications of the profiles can be used: model-based selection and statistics-based selection.

57

Model-based Selection

With a model-based selection, we assume to have a shape model of the measured profiles. This model can be constructed either from an empirical study on a large set of healthy data or from a mathematical model of the profile. By evaluating all profiles within the dataset, one can find the healthy profile using the metrics discussed in the previous section.

Statistics-based Selection

If just a small set of the inspected specimens is available or the specimens do strongly differ from each other, the model-based selection cannot be applied. In this case, a method can be based on a single specimen, assuming that the profiles in the healthy regions exhibit a similar shape. One can build a statistical model from the set of all available profiles within the data. By searching for a profile with the maximal or minimal deviation from the average model, the suspicious or healthy profiles can be defined. The advantage of this technique is that no model or database of healthy specimens is needed. A statistical-based selection mode is convenient for detecting relatively small features in the inspected data.

4.3.4   Probing of Time-Varying Volume Data

Our next modification of the original Profile Flag is concerned with time-varying 3D volumetric data. The profile information is then taken along the time axis. Previously, we probed the data along a line in 3D space, now we are profiling the temporal development at a specific 3D point location. When inspecting 3D time-varying data, where each spatial location corresponds to one profile, we need a different needle and range selector / range indicator (see Figure 4.4). For measuring time-signal profiles, the needle tip is extended in the simplest case to a spherical range selector which encloses the selected profiles. The set of needles which extent into the temporal dimension is illustrated by black dots. The size of the selection sphere can be modified by moving a marker along the flag pole. In the more general case the range selector can be a general polytope including all time-signal profiles similar to the reference profile in the center. The shape of the range selector determines either the spatial size of the neighborhood or the value of the threshold used for the selection of the set of profiles. When visualizing temporal data, the horizontal axis usually corresponds to the time-axis. Therefore for time-varying data the banner visualizes the time-steps along the horizontal axis, while the vertical axis shows the values for each measured time-step. Additionally, for sparse temporal data (i.e., just a few time steps given), vertical lines are included in order to facilitate reading off the values at particular time-steps.
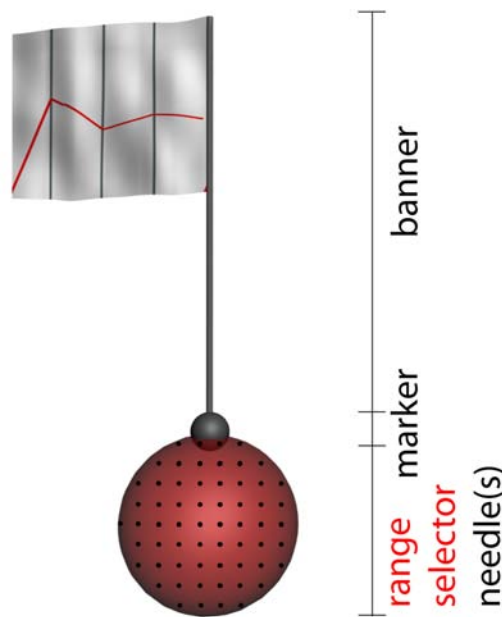
Figure 4.4: *Extension of the Profile Flags for measurement of time-signal profiles.*

4.4 Applications of Profile Flags

In this section we discuss two application areas of Profile Flags. In both cases the Profile Flag is guiding the inspecting radiologist to a suspicious profile through an automatic positioning of one or more glyphs. This reduces the time-consuming process of studying multiple volumetric sequences in a slice-by-slice manner. By dragging and repositioning the Profile Flag, one can browse the profiles in the neighborhood of the detected profile. Another Profile Flag can be stuck into the investigated tissue in order to give a reference to a healthy profile. Finally the annotated tissue can be rendered as a single image in contrast to rendering all slices with the suspicious profiles.

In section 4.4.1 we present an evaluation of inspecting knee-cartilage lesions. In section 4.4.2 we show the application of the Profile Flags for the detection of breast tumors.

4.4.1 Inspection of Knee-Cartilage Lesions

Twenty-nine semi-automatically pre-segmented specimens (7 healthy, 22 suspicious) have been investigated. The visualization of the data includes an automatic selection of suspicious profiles. The automatic selection of the most suspicious profile was performed by searching for the highest value in the T_2 map within
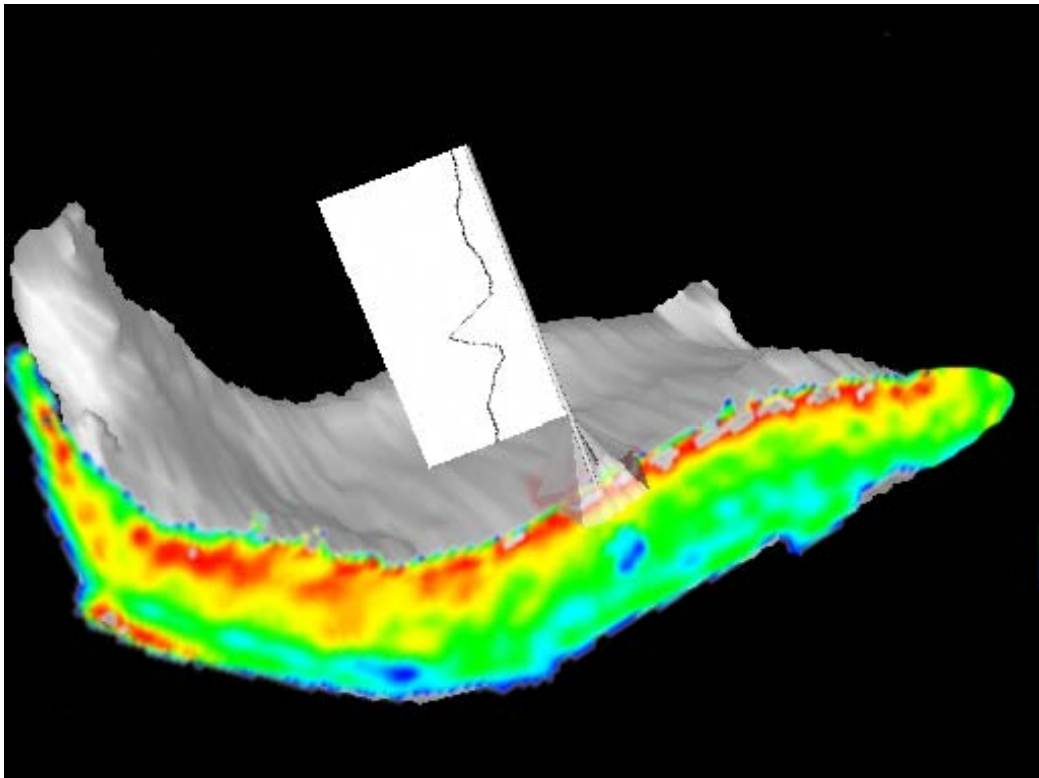
Figure 4.5: *Cartilage lesion annotated by a Profile Flag.*

the cartilage. The size of the lesion is shown by region growing on the domain of profile curves. In this example we used the average point-wise difference to determine the shape of the lesion. The size of the lesion is denoted by the size and shape of the range indicator. Additionally, the average thickness of the cartilage in the selected region determines the height of the range indicator. Figure 4.5 shows a cartilage with a rather large lesion in the medial part. The cutting plane can be moved within the suspicious region in order to allow studying the T_2 map in the selected area.

Evaluation and discussion

In order to assess the value of the proposed visualization techniques, we have asked the medical partners from Catharina Hospital in Eindhoven to fill out a questionnaire (see Appendix A). The questionnaire included over twenty figures with descriptions and open questions concerning the basic concept and the extensions of the Profile Flags. So far only two radiologists, who are experts on T_2 maps, have filled in the questionnaire. It is clear that a larger study is necessary for statistically

relevant conclusions. Here we give some qualitative findings that have emerged.

The evaluation has been performed by radiologists with good PC skills and above-average knowledge on medical workstations. At first glance, the concept of using Profile Flags seemed very interesting to the evaluators. Displaying the cutting plane with T_2 maps at suspicious areas is helpful and essential for the diagnosis. Omitting the needle when showing the clipping plane is preferable as the T_2 profile is not occluded at the needle position. The figures that did not contain the cutting plane with the T_2 map were ranked lower in explanatory power than those showing the cross-section. The best rated technique among all presented methods was the visualization of the lesion shape through the range indicator. According to the radiologists, it helps to suggest the shape of the underlying lesion. However, this visualization is neither sufficient for the final diagnosis of the exact shape of the lesion nor for conveying the complete information about the T_2 map. Insertion of the T_2 map at the position of the needle adds the missing information. The respondents have chosen an image showing a Profile Flag with a selected set of profiles and a cutting plane as the most valuable and diagnostically-relevant visualization (similar to Figure 4.2). This figure included a description of interaction with the cutting plane by moving it along its normal within the area of the range indicator. The next set of questions in the questionnaire dealt with the usability of rotating either the cutting plane or the object around the needle. No clear preferences were shown by the evaluators concerning the rotation of the cutting plane. This uncertainty might be due to low familiarity with object manipulations in 3D environments. The use of the deviation banner for showing the T_2 profiles as a difference from a healthy profile has been rated as just a possible extension. This might be due to the fact that so far clinical inspections are based on absolute T_2 values. The Profile Flags as a tool for annotation of damaged areas and for transferring the diagnosis to the orthopedists has been rated as very essential.

4.4.2   Inspection of Tumors in Breast DCE-MRI Data

Applying the previously described extensions, Profile Flags can be used for the exploration and the detection of tumors in breast DCE-MRI data. In dynamic contrast enhanced magnetic resonance imaging (DCE-MRI) mammography, the diagnosis of a tumor is usually based on the development of time-signal profiles. These are based on the flow of the contrast agent within the tissue. Before the acquisition of data, a contrast agent is introduced into the patient's body. This results in the increase of signal in the scanned tissue and simplifies the diagnosis of the disease. Several scans are acquired over a period of time. This process results in a set of volumes, one for each time-step. The classification of the behavior of the tissue can be determined by subtracting the pre-contrast volume from all post-contrast images. Since the acquired volumes are registered, one can generate time-signal
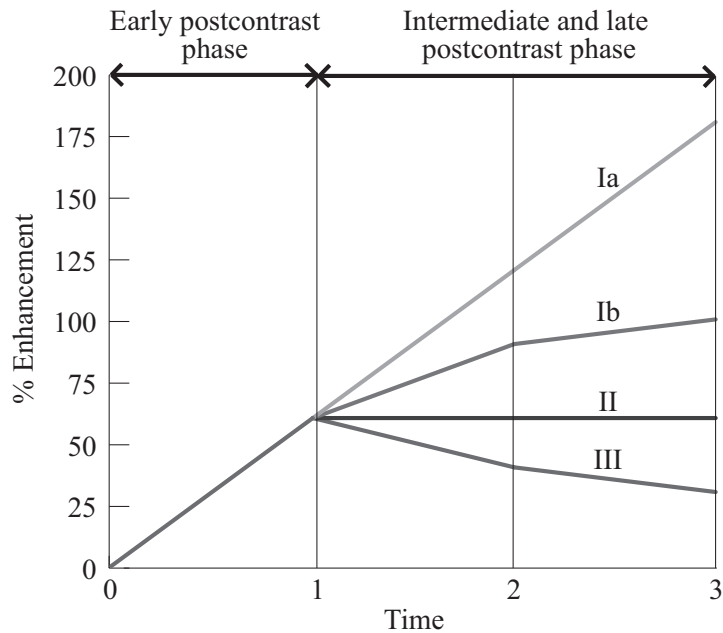
Figure 4.6: *Four types of time-signal profiles for DCE-MRI mammography (courtesy of Coto et al. [16]).*

profiles for each spatial location in the volume. Time-step 0 corresponds to the pre-contrast volume, while the following acquisition times correspond to the post-contrast volumes. The diagnosis from such time-varying data is based on the fact, that the breast tumor cells absorb and release the contrast agent in a different way than healthy breast cells. In cancerous breast regions newly formed blood vessels cause a faster inflow as well as outflow of contrast agent. Healthy regions are characterized by a low signal increase in the early post-contrast phase. Additionally three other types of time-signal profiles exist (see Figure 4.6). Persist profiles (type Ia, Ib) contain an increase of signal in the immediate and late post-contrast phase. Platau profiles (type II) show no change in the intensity in the intermediate and late post-contrast phases. The washout profiles (type III) contain a significant signal decrease in the intermediate and late post-contrast phases. According to the classification, cells with persist behavior indicate benign lesions, while the platau and washout profiles are with high probability malignant lesions [39].

In the clinical routine, the radiologist studies a set of time-series in a slice-by-slice manner. During the first step of the investigation, he defines one or multiple suspicious regions. The diagnosis continues with the detailed inspection of the previously selected regions by computing and studying the time-signal profiles within these regions. This is a time-consuming process, which involves a high level of concentration. The suspicious regions can be very small in comparison to
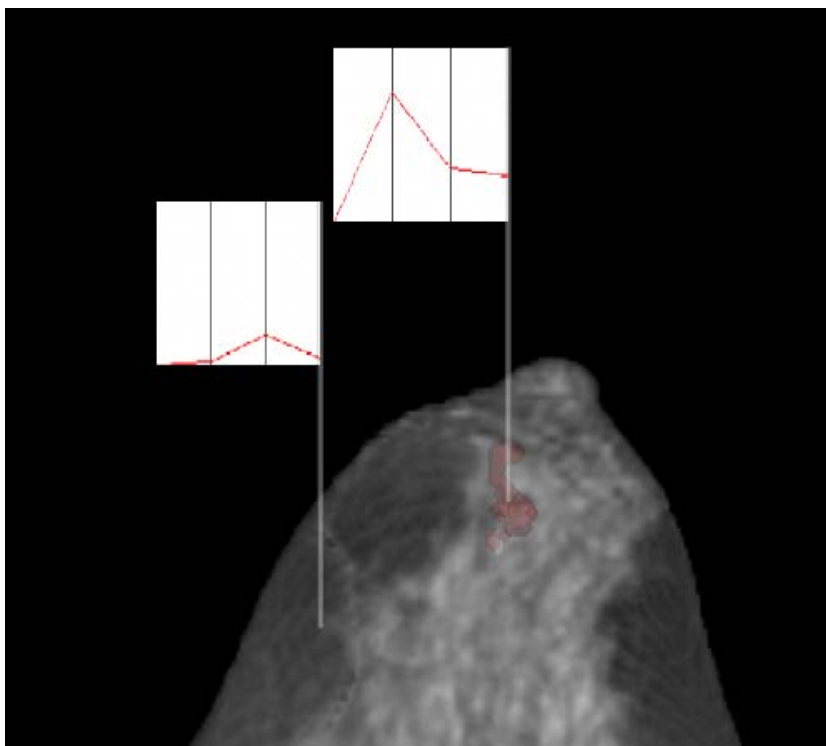
Figure 4.7: *Two time-signal profiles annotated by Profile Flags: a healthy profile (left) and a malignant profile (right).*

the spatial extent of the entire data.

Figure 4.7 shows a visualization of the cancerous nodes in a patient's body. Two Profile Flags have been automatically positioned in the dataset: the left one is showing a healthy time-signal profile, while the right Profile Flag visualizes a set of suspicious profiles. The cost function for the automatic detection of the selected set of time-signal profiles is based on the model for tumor classification by Kuhl et al. [39]. By dragging the Profile Flag over the 3D spatial domain, one can inspect the neighborhood of the automatically selected region.

4.5 Summary and Conclusions

In this chapter we have presented two applications of probing dense but not homogenous data using Profile Flags. Several extensions of the basic Profile Flag concept, have been discussed. They are essential for the effective use of the glyph in the context of specific application-oriented data. The extensions include selection of a set of profiles based on spatial as well as curve differences, automatic positioning of the Profile Flags, and adaptation for probing of time-varying volumetric

data. The extensions have been tested on MR data in orthopedics and DCE-MRI data in mammography. Further, the preliminary evaluation of the techniques by our clinical partners have been described and discussed. With the extensions presented the Profile Flag is suitable for effective probing and sparse annotation of spatial and temporal profile data.

Chapter 5

Summary and Conclusions

MRI is considered currently as the best noninvasive technique for the detection of cartilage defects. Therefore, a lot of attention has been paid to this technique in recent years [61, 60]. Benefits include low radiation exposure of patients, high quality images of soft tissue structures, and non-invasiveness. The major directions in the further development of MRI for cartilage inspection include long-term evaluation of cartilage volume, new fast pulse sequences with high spatial resolution and high signal-to-noise ratio, as well as accurate cartilage segmentation and intuitive visual representation for effective diagnosis. MRI has a high potential for detecting of early stages of cartilage degeneration.

Articular cartilage is a structure where the detection of slight thickness changes is crucial for early diagnosis. Development of faster and more reliable segmentation methods is a prerequisite for MRI to be widely used clinically. Segmentation is currently performed manually or semi-automatically. To achieve an accurate segmentation, sophisticated filtering is necessary due to high noise and global intensity variations in MRI data. Due to the complex structure of the collagen matrix, the mapping of acquired values to optical properties is essential. This allows to measure both quantitative and qualitative characteristics of the cartilage. Visualizing the change of the cartilage's thickness and its inner structure makes impossible to detect cartilage defects in an early stage. In this dissertation we have presented methods to visualize the thickness of femoral cartilage and the inner structure of patellar cartilage.

Since the femoral cartilage is very thin, the representation of thickness information by direct volume rendering is not sufficient. Therefore, our approach deals with unfolding of the tissue in a focus-and-context manner and with representing it as a height field. In order to preserve the thickness information, it is mapped to the unfolded surface after the transformation of the structure. We have demonstrated, that unfolding of structures with a relatively small extent in one dimension is essential to emphasize the information contained along that dimension. Moreover, the unfolded representation of the tissue allows to apply 2D geometrical operations

and visualization methods. Several approaches to perform operations on the height field have been proposed and discussed.

Besides the visualization of the thickness of the cartilage, T_2 maps give information about the cartilage quality. This information is essential for early diagnosis before the thinning of the cartilage starts. We have presented the Profile Flag - a glyph for probing and annotating of T_2 profiles in dense, but not homogenous cartilage data. The Profile Flag consists of four components: the banner, the range selector, the needle and the cutting plane. The interaction with the glyph includes dragging and moving it along the reconstructed surface of the cartilage. During the interaction, the Profile Flag gives a visual feedback about the local characteristics of the underlying T_2 profiles. It also enables annotation of the inspected cartilage in a single image.

Furthermore, we have presented several application-oriented extensions of Profile Flags. Two applications, where profiles play a crucial role, have been chosen to demonstrate the usability of the glyph. The first group of extensions includes several metrics for the selection of visualized profiles. They are based on both spatial and curve differences between multiple profiles. Another group of extensions deals with an automatic classification and positioning of the Profile Flags. This method is essential in the pre-processing stage in order to denote areas where the T_2 profiles differ significantly from a healthy T_2 profile. Another extension of the Profile Flags combines the information on the T_2 map with the information on the thickness of the underlying tissue. It has been shown that Profile Flags can be applied for the inspection of time-dependent data comprising temporal profiles. The proposed techniques and extensions have been evaluated by our clinical partners.

Bibliography

[1] E. J. Alexander, T. P. Andriacchi, and P. K. Lang. Functional imaging of the normal and arthritic knee. In *24th Annual Meeting of the American Society of Biomechanics*, pages 119–120, 2000.

[2] S. Angenent, S. Haker, A. Tannenbaum, and R. Kikinis. On the Laplace-Beltrami operator and brain surface flattening. *IEEE Transactions on Medical Imaging*, 18:700–711, 1999.

[3] G. A. Ateshian, L. J. Soslowsky, and V. C. Mow. Quantitation of articular surface topography and cartilage thickness in knee joints using stereophotogrammetry. *J. Biomechanics*, 24(8):761–776, 1991.

[4] M. A. G. Ballester, A. P. Zisserman, and M. Brady. Estimation of the partial volume effect in MRI. *Medical Image Analysis*, 6:389–405, 2002.

[5] E. Bayram, Y. Ge, and Ch. L. Wyatt. Confidence based anisotropic filtering of magnetic resonance images. *Med. Biol. Mag.*, 21(5):156–160, 2002.

[6] B. Bell, S. Feiner, and T. Höllerer. View management for virtual and augmented reality. In *Proceedings of the 14th annual ACM symposium on user interface software and technology*, pages 101–110, 2001.

[7] Ch. Bennis, J.-M. Vézien, and G. Iglésias. Piecewise surface flattening for non-distorted texture mapping. In *SIGGRAPH 1991*, pages 237–246, 1991.

[8] A. D. Brett, J. C. Waterton, S. Solloway, J. E. Foster, M. C. Keen, S. Gandy, B. J. Middleton, R. A. Maciewicz, I. Watt, P. A. Dieppe, and C. J. Taylor. The measurement of focal diurnal variation in the femoral articular cartilage of the knee. In *MICCAI*, pages 328–337, 1999.

[9] S. Bruckner and M. E. Gröller. VolumeShop: An interactive system for direct volume illustration. In *Proceedings of IEEE Visualization 2005*, pages 671–678, 2005.

[10] J. Canny. A computational approach to edge detection. *IEEE Trans. Pattern Anal. Mach. Intell.*, 8(6):679–698, 1986.

[11] S. K. Card, J. D. Mackinlay, and B. Shneiderman. *Readings in Information Visualization (Using Vision to Think)*. Morgan Kaufman Publishers, Inc., 1999.

[12] L. Carotenuto, M. Ercolani, R. Passariello, C. Catalano, F. Pediconi, and F. Venditti. Software tool for computer aided diagnosis of breast cancer in contrast enhanced MR sequences. In *EuroPACS-MIR 2004 in the Enlarged Europe*, pages 361–364, 2004.

[13] Z. A. Cohen, D. M. McCarthy, S. D. Kwak, P. Legrand, F. Fogarasi, E. J. Ciaccio, and G. A. Ateshian. Knee cartilage topography, thickness, and contrast areas from MRI: in-vitro calibration and in-vivo measurements. *Osteoarthritis and Cartilage*, 7:95–109, 1999.

[14] Z. A. Cohen, D. M. McCarthy, H. Roglic, J. H. Henry, W. G. Rodkey, J. R. Steadman, V. C. Mow, and G. A. Ateshian. Computer-aided planning of patellofemoral joint OA surgery: Developing physical models from patient MRI. In *MICCAI*, pages 9–21, 1998.

[15] Z. A. Cohen, V. C. Mow, J. H. Henry, W. N. Levine, and G. A. Ateshian. Templates of the cartilage layers of the patellofemoral joint and their use in the assessment of osteoarthritic cartilage. *Osteoarthritis and Cartilage*, 11(8):569–579, 2003.

[16] E. Coto, S. Grimm, S. Bruckner, M. E. Gröller, A. Kanitsar, and O. Rodriguez. MammoExplorer: An advanced CAD application for breast DCE-MRI. In *Proceedings of Vision, Modelling, and Visualization 2005*, pages 91–98, 2005.

[17] P. Danielsson. Euclidean distance mapping. *Computer Graphics and Image Processing*, 14:227–248, 1980.

[18] D. G. Disler, M. P. Recht, and T. R. McCauley. MR imaging of articular cartilage. *Skeletal Radiology*, 29:367–377, 2000.

[19] F. Eckstein, H. Sittek, S. Milz, E. Schulte, B. Kiefer, M. Reiser, and R. Putz. The potential of magnetic resonance imaging (MRI) for quantifying articular cartilage thickness - a methodological study. *Clinical Biomechanics*, 10:434–440, 1995.

[20] A. B. Ekoule, F. C. Peyrin, and C. L. Odet. A triangulation algorithm from arbitrary shaped multiple planar contours. *ACM Transactions on Graphics*, 10(2):182–199, 1991.

[21] S. C. Faber, F. Eckstein, S. Lukasz, R. Muhlbauer, J. Hohe, K.-H. Englmeier, and M. Reiser. Gender differences in knee joint cartilage thickness, volume and articular surface areas: assessment with quantitative three-dimensional MR imaging. *Skeletal Radiol.*, 30:144–150, 2001.

[22] A. Fan, W. Wells, J. Fisher, M. Çetin, S. Haker, R. Mulkern, C. Tempany, and A. S. Willsky. A unified variational approach to denoising and bias correction in MR. In *Information Processing in Medical Imaging (IPMI)*, pages 148–159, 2003.

[23] B. Fischl, M. I. Sereno, and A. M. Dale. Cortical surface-based analysis II: Inflation, flattening, and a surface-based coordinate system. *NeuroImage*, 9:195–207, 1999.

[24] M. S. Floater and K. Hormann. Surface parameterization: a tutorial and survey. In *Advances on Multiresolution in Geometric Modelling*, pages 157–186. Springer-Verlag, 2004.

[25] T. Goetzelmann, K. Ali, K. Hartmann, and Th. Strothotte. Adaptive labeling for illustrations. In *Proceedings of Pacific Graphics 2005*, pages 64–66, 2005.

[26] A. Guermazi, S. Zaim, B. Taouli, Y. Miaux, Ch. G. Peterfy, and H. K. Genant. MR findings in knee osteoarthritis. *European Radiology*, 13:1370–1386, 2003.

[27] S. C. Göhde, M. Goyen, M. Forsting, and J. F. Debatin. Prävention ohne Strahlen - eine Strategie zur umfassenden Früherkennung mittels Magnetresonanztomographie (MRT) (in German). *Der Radiologe*, 42(8):622–629, 2002.

[28] S. Haker, S. Angenent, A. Tannenbaum, and R. Kikinis. Nondistorting flattening maps and the 3D visualization of colon CT images. *IEEE Transactions on Biomedical Engineering*, 19(7):665–671, 2000.

[29] B. A. Hargreaves, G. E. Gold, C. F. Beaulieu, S. S. Vasanawala, D. G. Nishimura, and J. M. Pauly. Comparison of new sequences for high-resolution cartilage imaging. *Magnetic Resonance in Medicine*, 49(4):700–709, 2003.

[30] K. Hartmann, B. Preim, and Th. Strothotte. Describing abstraction in rendered images through figure captions. *Linköping Electronic Articles in Computer and Information Science*, 4(15), 1999.

[31] F. Heuer, M. Sommers, J. B. Reid III, and M. Bottlang. Estimation of cartilage thickness from joint surface scans: Comparative analysis of computational methods. In *ASME*, pages 569–570, 2001.

[32] J. Hohe, G. Ateshian, M. Reiser, K.-H. Englmeier, and F. Eckstein. Surface size, curvature analysis, and assesment of knee joint incongruity with MRI in vivo. *Magnetic Resonance in Medicine*, 47:554–561, 2002.

[33] J. P. Hornak. The basics of MRI, http://www.cis.rit.edu/htbooks/mri/, 2003.

[34] H. Huitema and R. van Liere. Interactive visualization of protein dynamics. In *Proceedings of IEEE Visualization 2000*, pages 465–468, 2000.

[35] H. Imhof, I.-M. Nöbauer-Huhmann, C. Krestan, A. Gahleitner, I. Sulzbacher, S. Marlovits, and S. Trattnig. MRI of the cartilage. *European Radiology*, 12:2781–2793, 2002.

[36] A. Kanitsar, D. Fleischmann, R. Wegenkittl, P. Felkel, and M. E. Gröller. CPR - Curved Planar Reformation. In *IEEE Visualization 2002*, pages 37–44, 2002.

[37] M. Kass, A. Witkin, and D. Terzopoulos. Snakes: Active contour models. *International Journal of Computer Vision*, 1(4):321–331, 1987.

[38] S. Kohle, B. Preim, J. Wiener, and H.-O. Peitgen. Exploration of time-varying data for medical diagnosis. In *Proceedings of Vision, Modelling, and Visualization 2002*, pages 131–138, 2002.

[39] Ch. K. Kuhl, P. Mielcareck, S. Klaschik, C. Leutner, E. Wardelmann, J. Gieseke, and H. H. Schild. Dynamic breast MR imaging: Are signal intensity time data useful for differential diagnosis of enhancing lesions? *Radiology*, 211(1):101–110, 1999.

[40] S. Lakare, D. Chen, L. Li, A. Kaufman, and J. Liang. Electronic colon cleansing using segmentation rays for virtual colonoscopy. In *SPIE*, pages 412–418, 2002.

[41] W. C. de Leeuw and J. J. van Wijk. A probe for local flow field visualization. In *Proceedings of IEEE Visualization 1993*, pages 39–45, 1993.

[42] B. Lévy and J.-L. Mallet. Non-distorted texture mapping for sheared triangulated meshes. In *SIGGRAPH 1998*, pages 343–352, 1998.

[43] S. Lobregt and M.A. Viergever. A discrete dynamic contour model. *IEEE Transactions on Medical Imaging*, 14(1):12–24, March 1995.

[44] J. A. Lynch, S. Zaim, J. Zhao, C. G. Peterfy, and H. K. Genant. Automating measurement of subtle changes in articular cartilage from MRI of the knee by combining 3D image registration and segmentation. In *SPIE*, pages 431–439, 2001.

[45] J. A. Lynch, S. Zaim, J. Zhao, A. Stork, Ch. G. Peterfy, and H. K. Genant. Cartilage segmentation of 3D MRI scans of the osteoarthritic knee combining user knowledge and active contours. In *SPIE*, pages 925–935, 2000.

[46] J. R. MacFall, S. J. Riederer, and H. Z. Wang. An analysis of noise propagation in computed T_2, pseudodensity and synthetic spin-echo images. *Medical Physics*, 13(3):285–292, 1986.

[47] M. J. McGuffin, L. Tancau, and R. Balakrishnan. Using deformations for browsing volumetric data. In *Proceedings of IEEE Visualization 2003*, pages 401–408, 2003.

[48] T. J. Mosher, Ch. M. Collins, H. E. Smith, L. E. Moser, R. T. Sivarajah, B. J. Dardzinski, and M. B. Smith. Effect of gender on in vivo cartilage magnetic resonance imaging T2 mapping. *J. Magn. Reson. Imaging*, 19:323–328, 2004.

[49] T. J. Mosher, B. J. Dardzinski, and M. B. Smith. Human articular cartilage: Influence of aging and early symptomatic degeneration on the spatial variation of T2 – preliminary findings at 3T. *Radiology*, 214:259–266, 2000.

[50] T. J. Mosher, H. Smith, B. J. Dardzinski, V. J. Schmithorst, and M. B. Smith. MR imaging and T2 mapping of femoral cartilage: in vivo determination of the magic angle effect. *American Journal of Roentgenology*, 177:665–669, 2001.

[51] O. J. Muensterer, F. Eckstein, D. Hahn, and R. Putz. Computer-aided three dimensional assessment of knee-joint cartilage with magnetic resonance imaging. *Clinical Biomechanics*, 11(5):260–266, 1996.

[52] J. C. Mullikin. The vector distance transform in two and three dimensions. *GMIP*, 54(6):526–535, November 1992.

[53] W. R. Nitz and P. Reimer. Contrast mechanisms in MR imaging. *European Radiology*, 9(6):1032–1046, 1999.

[54] R. E. Outerbridge. The ethiology of chondromalacia patellae. *J. Bone Joint Surg.*, 43(4):752–767, 1961.

[55] A. W. Paeth. Digital cartography for computer graphics. *Graphics Gems*, pages 307–320, 1990.

[56] G. J. M. Parker, J. A. Schnabel, and G. J. Barker. Nonlinear smoothing of MR images using approximate entropy - a local measure of signal intensity irregularity. *Information Processing in Medical Imaging*, 1613:484–489, 1999.

[57] M. P. Persoon, I. Serlie, F. H. Post, R. Truyen, and F. M. Vos. Visualization of nosiy and biased volume data using first and second order derivative techniques. In *IEEE Visualization*, pages 379–386, 2003.

[58] C. dan Pirnog. Articular cartilage segmentation and tracking in sequential MR images of the knee. *ETH Zürich*, 2005.

[59] B. Preim, Ch. Tietjen, W. Spindler, and H.-O. Peitgen. Integration of measurement tools in medical 3D visualizations. In *Proceedings of IEEE Visualization 2002*, pages 21–28, 2002.

[60] M. P. Recht, D. W. Goodwin, C. S. Winalski, and L. M. White. MRI of articular cartilage: Revisiting current status and future directions. *American Journal of Roentgenology*, 184(4):899–914, 2005.

[61] M. P. Recht and D. Resnick. MR imaging of articular cartilage: Current status and future directions. *American Journal of Roentgenology*, 163:283–290, 1994.

[62] R. H. van der Rijt, H. van den Bosch, A. Knowles, J. H. Kortman, and J. H. Wondergem. High resolution quantitative imaging of patellar cartilage defects at 1.5T. *Proc. Intl. Soc. Mag. Reson. Med.*, 11:442, 2003.

[63] P. Rösch, T. Netsch, M. Quist, and J. Weese. 3D respiratory motion compensation by template propagation. In *MICCAI*, pages 649–646, 2002.

[64] P. V. Sander, J. Snyder, S. Gortler, and H. Hoppe. Texture mapping progressive meshes. In *SIGGRAPH 2001*, pages 409–416, 2001.

[65] R. Satherley and M. W. Jones. Vector-city vector distance transform. *Computer Vision and Image Understanding*, 82(3):238–254(17), 2001.

[66] M. Schnier. Validierung dreidimensionaler MRT-basierter Knorpelvolumen und -dickenmessungen mit der CT-arthrographie (in German). *LMU Munich*, 2002.

[67] H. Shahriaree. Chondromalacia. *Contemp. Orthop.*, 11:27–39, 1985.

[68] H. E. Smith, T. J. Mosher, B. J. Dardzinski, B. G. Collins, Ch. M. Collins, Q. X. Yang, V. J. Schmithorst, and M. B. Smith. Spatial variation in cartilage T2 of the knee. *J Magn Reson Imaging*, 14:50–55, 2001.

[69] S. Solloway, C. Hutchinson, J. Waterton, and C. Taylor. The use of active shape models for making thickness measurements of articular cartilage from MR images. *Magn Reson Med*, 37(6):943–952, 1997.

[70] S. Solloway, Ch. J. Taylor, Ch. E. Hutchinson, and J. C. Waterton. Quantification of articular cartilage from MR images using active shape models. *ECCV*, 2:400–41, 1996.

[71] O. Sorkine, D. Cohen-Or, R. Goldenthal, and D. Lischinski. Bounded-distortion piecewise mesh parameterization. In *IEEE Visualization 2002*, pages 355–362, 2002.

[72] K. Subramanian, J. Brockway, and W. Carruthers. Interactive detection and visualization of breast lesions from dynamic contrast enhanced MRI volumes. *Computerized Medical Imaging and Graphics*, 28(8):435–444, 2004.

[73] Z. Szalavári and M. Gervautz. The personal interaction panel - a two-handed interface for augmented reality. *Computer Graphics Forum*, 16(3):335–346, 1997.

[74] S. Trattnig, G. Kontaxis, M. Breitenseher, Ch. Czerny, Th. Rand, K. Turetschek, M. Barth, and H. Imhof. MRT auf Niederfeldtomographen (0,2 tesla) (in German). *Radiologe*, 37:773–777, 1997.

[75] K. L. Verstraete, F. Almqvist, P Verdonk, G. Vanderschueren, W. Huysse, R. Verdonk, and G. Verbrugge. Magnetic resonance imaging of cartilage and cartilage repair. *Clinical Radiology*, 59(8):674–689, 2004.

[76] A. Vilanova Bartrolí, R. Wegenkittl, A. König, and E. Gröller. Nonlinear virtual colon unfolding. In *IEEE Visualization 2001*, pages 411–418, 2002.

[77] A. Vilanova Bartrolí, R. Wegenkittl, A. König, E. Gröller, and E. Sorantin. Virtual colon flattening. In *VisSym 2001 Joint Eurographics - IEEE TCVG Symposium on Visualization*, pages 127–136, 2001.

[78] I. Viola, A. Kanitsar, and M. E. Gröller. Importance-driven feature enhancement in volume visualization. *IEEE Transactions on Visualization and Computer Graphics*, 11(4):408–418, 2005.

73

[79] U. Vovk, F. Pernus, and B. Likar. Retrospective correction of MR intensity inhomogeneity via regularised feature condensing. In *8th Computer Vision Winter Workshop (CVWW)*, pages 165–168, 2003.

[80] J. Weese, P. Röche, T. Netsch, T. Blaffert, and M. Quist. Grayvalue based registration of CT and MR images by maximization of local correlation. In *Medical Imaging Computing and Computer-Assisted Intervention – MICCAI 1999*, pages 656–663, 1999.

[81] T. G. Williams, Ch. J. Taylor, Z. Gao, and J. C. Waterton. Corresponding articular cartilage thickness measurements in the knee joint by modelling the underlying bone. In *IPMI*, volume 2732, pages 126–135, 2003.

[82] A. E. Wluka, S. Stuckey, J. Snaddon, and F. Cicuttini. The determinants of change in tibial cartilage volume in osteoarthritic knees. *Arthritis&Rheumatism*, 46(8):2065–2072, 2002.

Appendix A

Questionnaire

Dear Ladies and Gentlemen,

at the Technical University of Vienna, we are working on 3D visualization techniques for computer aided diagnostics of knee cartilage. In order to get a feedback from you as a potential user, we would like to kindly ask you to help us to assess the value of our techniques. In the following we present several images concerning the inspection of T_2 maps. Please rate your preferences for every question from 1 to 5. In case of any questions or if you are missing something in this form, please let us know or note your comments in the specific question or in the question 22. Please answer the questions in the order from the first one to the last one. At the end of the questionnaire, we will ask you to choose an image, which is to your opinion the most useful for diagnostic purposes.

1. Name:

2. Please rate your PC skills:

1-Very good	2-Good	3-Average	4-Basic	5-No experience

3. How do you rate your knowledge on 3D medical applications:

1-Very good	2-Good	3-Average	4-Basic	5-No experience

Background
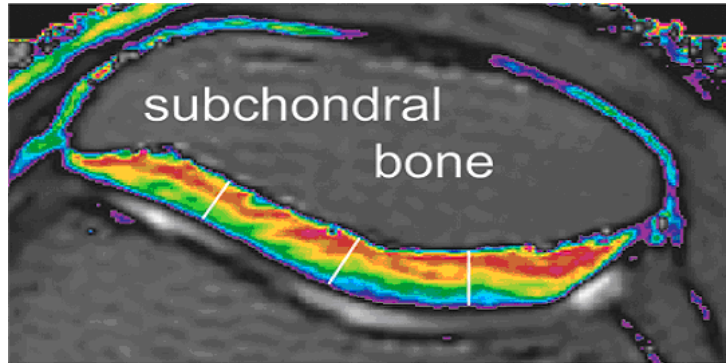
For the validation of the quality of the cartilage by means of disruptions in the T_2 map, so called T_2 profiles can be calculated. A T_2 profile is the curve of varying T_2 values along a line that is perpendicular to the subchondral bone and ends at the surface of the cartilage. For healthy cartilage, the profiles have a typical characteristic shape. For degenerated cartilage, there is a significant deviation from that shape. The figure above shows three locations where T_2 profiles are measured.
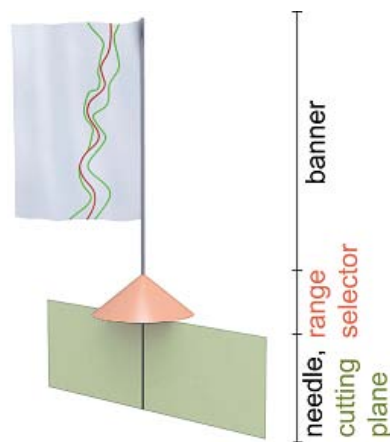
The Profile Flag is a tool for probing and annotating cartilage data. It comprises a bulletin-board pin-like shape with a small flag on top of it. While moving the glyph along the surface of the cartilage, the T_2 values are measured along the pin's needle and in its close neighborhood. In this representation the previously color-coded T_2 map is shown as a graph on the banner. The top of the banner corresponds to the bone-cartilage interface, while the bottom of the banner corresponds to the articular surface. A short movie demonstrating the interaction with the tool can be found under the following link: www.cg.tuwien.ac.at/research/vis/comrade/visualization2005/visualization2005.avi

76

Questions
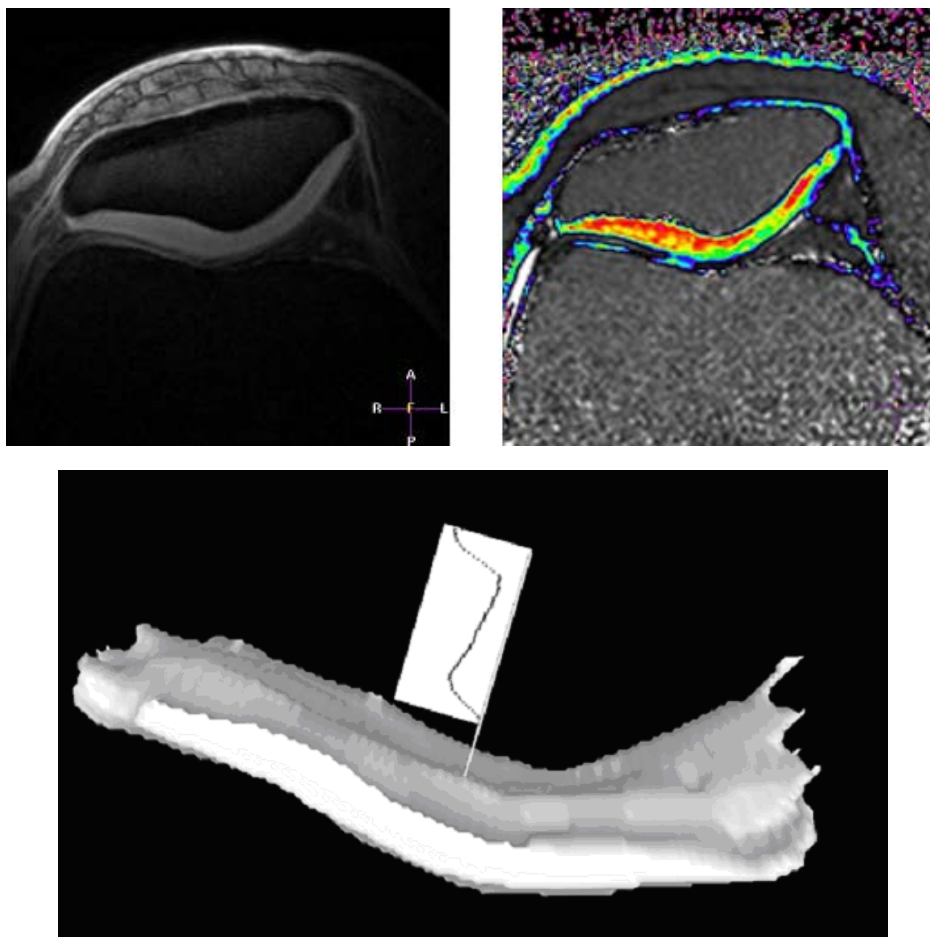
Inspection of the T_2 maps can be performed on two parallel screens by inspecting the entire stack of slices one by one. One possibility is to inspect the anatomic image (top left) for the changes in the thickness and the T_2 map (top right) for changes in the quality of the cartilage by means of disruptions in the T_2 map. Another possibility is to look at the surface of the cartilage (bottom image). By moving the Profile Flag along the surface, one can see the underlying T_2 profiles.
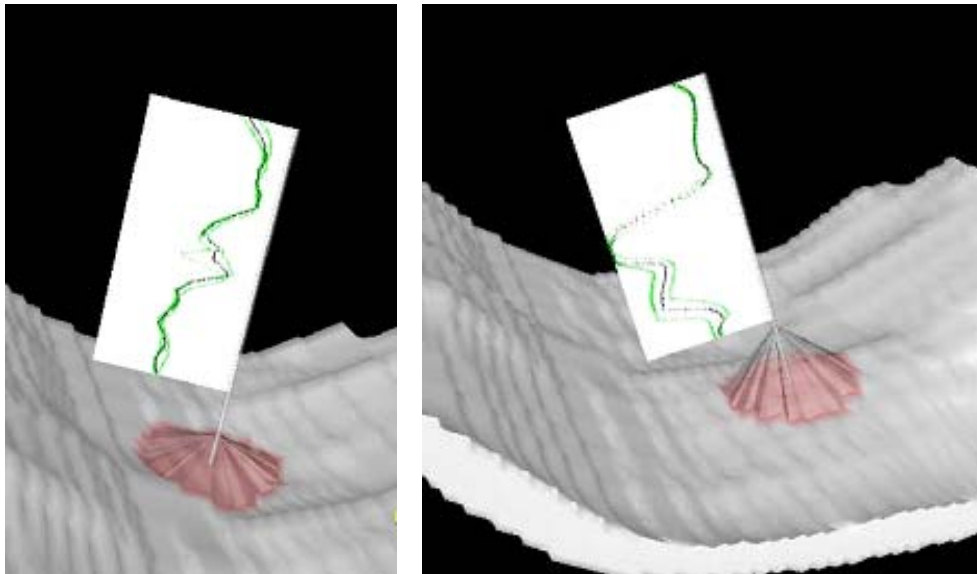
4. The Profile Flags concept sounds interesting:

1-I fully agree	2-I partially agree	3-I am not sure	4-I partially disagree	5-I strongly disagree	6- It is unclear to me
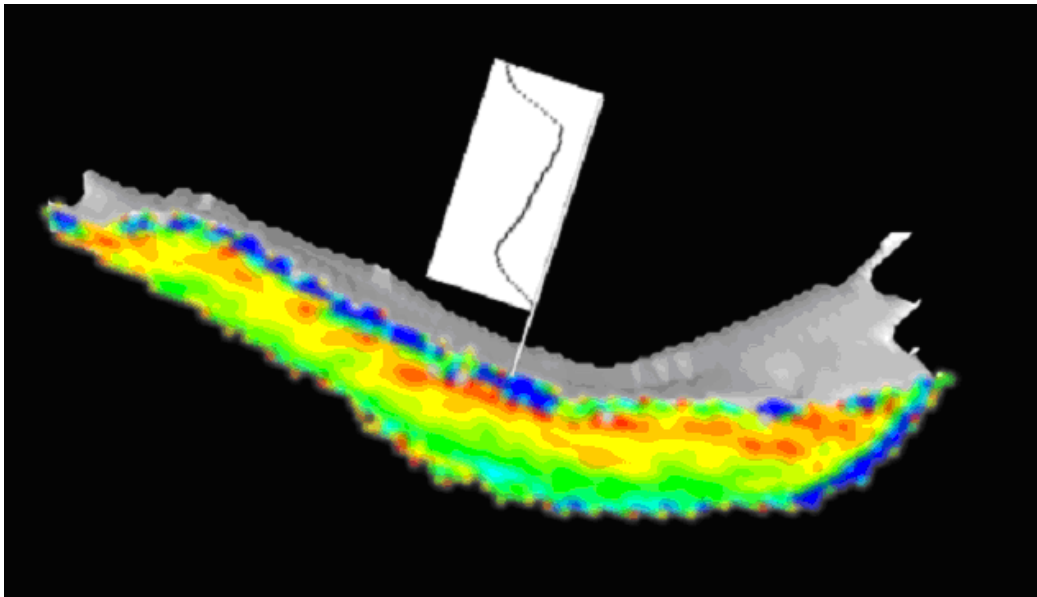
The user can cut and remove the cartilage at the position of the Profile Flag in order to see the entire T_2 map in the neighborhood of the measured T_2 profile.

5. Visualization of the entire plane with T_2 map is helpful:

1-I fully agree	2-I partially agree	3-I am not sure	4-I partially disagree	5-I strongly disagree	6- It is unclear to me

6. When showing the clipping plane, the needle (located beneath the surface) is not shown in order not to occlude the measured T_2 profile. This is useful:
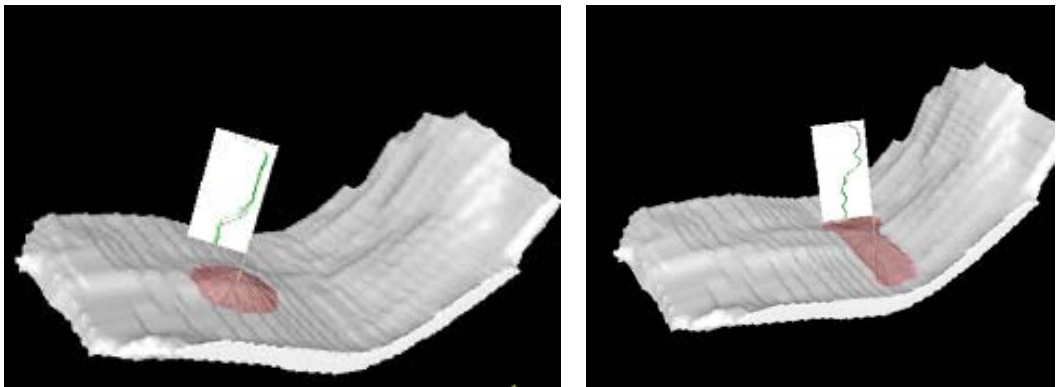
1-I fully agree	2-I partially agree	3-I am not sure	4-I partially disagree	5-I strongly disagree	6- It is unclear to me
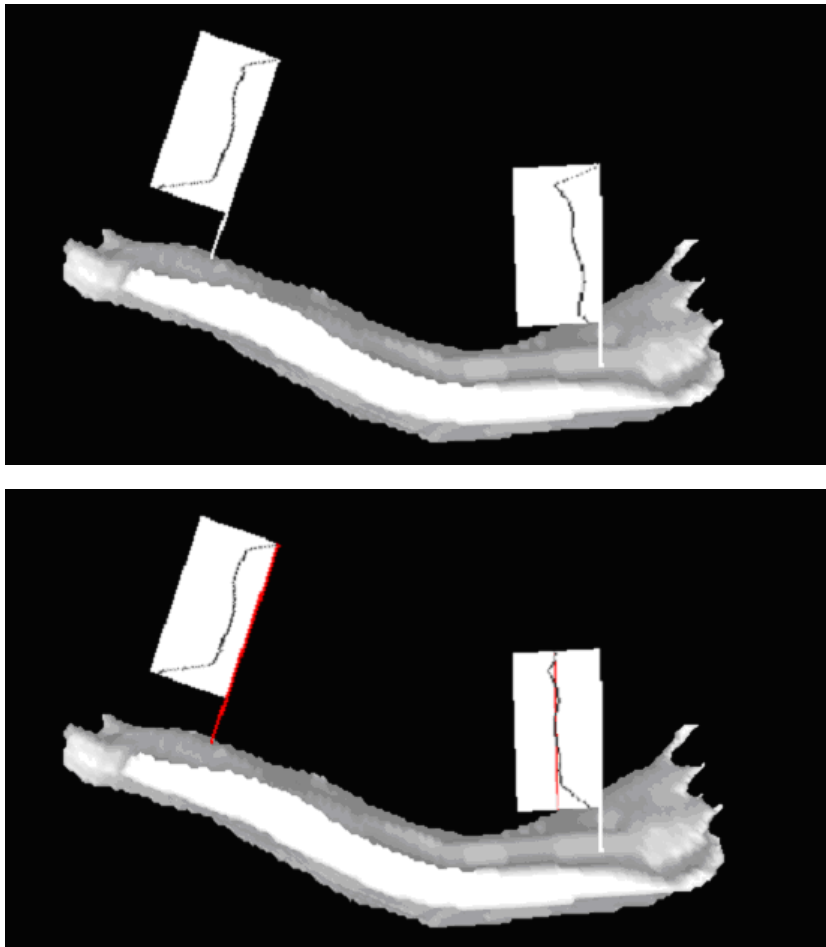
Two profile flags stuck into the surface of the patellar cartilage. The left Profile Flag shows a healthy T_2 profile, while the right one points to a degenerated area of the cartilage. The upper image shows two T_2 profiles, while at the bottom image, the right profile flags shows just the deviation from the healthy profile, i.e., if it is aligned with the red vertical line, it is a healthy profile as well.

7. Is It easier to differentiate between healthy and degenerated profile by showing the deviation profile?

1-I fully agree	2-I partially agree	3-I am not sure	4-I partially disagree	5-I strongly disagree	6- It is unclear to me

Two Profile Flags are annotating a T_2 profile. The thickness of the cartilage at a certain position is visualized by the height of the range selector (the red cone).

8. Does such visualization give me clear information about the thickness?

1-I fully agree	2-I partially agree	3-I am not sure	4-I partially disagree	5-I strongly disagree	6- It is unclear to me

Two Profile Flags annotating a lesion. The shape of the underlying lesion is visualized by the shape of the red range selector (it is marking all T_2 profiles with suspicious characteristics).

9. Can you imagine the shape and the size of the lesion?

1-I fully agree	2-I partially agree	3-I am not sure	4-I partially disagree	5-I strongly disagree	6- It is unclear to me

10. Is this information sufficient for me or do I need to see the complete shape of the lesion?

1-Sufficient	2-Rather suficient	3-I am not sure	4-Rather not sufficient	5-Not sufficient	6- It is unclear to me
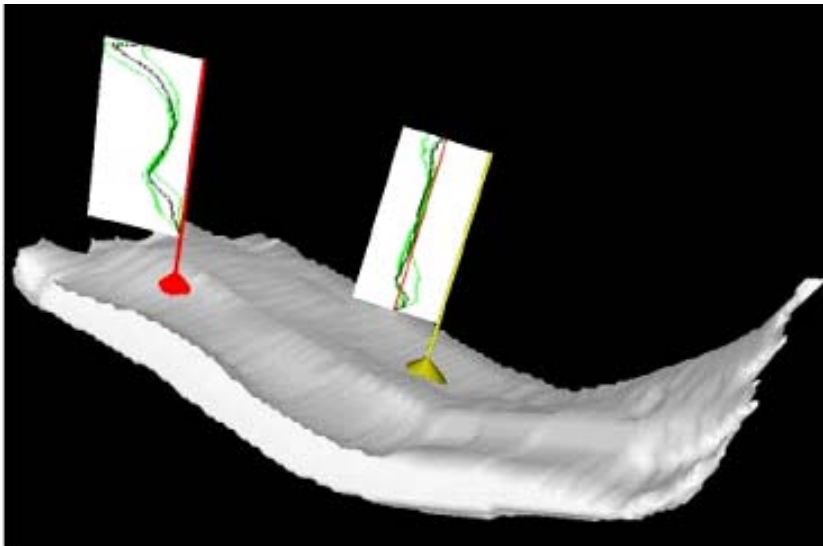
An example of a final annotation of the cartilage inspection.

11. Does such representation give me a complete information about the T_2 map?

1-Yes	2-Rather yes	3-I am not sure	4-Rather no	5-No	6- It is unclear to me

12. Annotations with Profile Flags could be useful for transferring the diagnosis to the orthopedist instead of printing slices with suspicious areas.

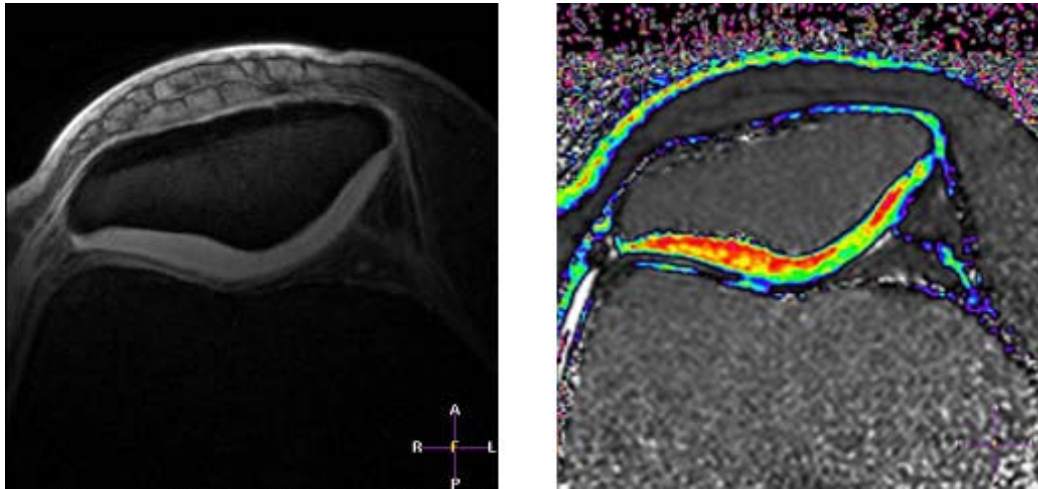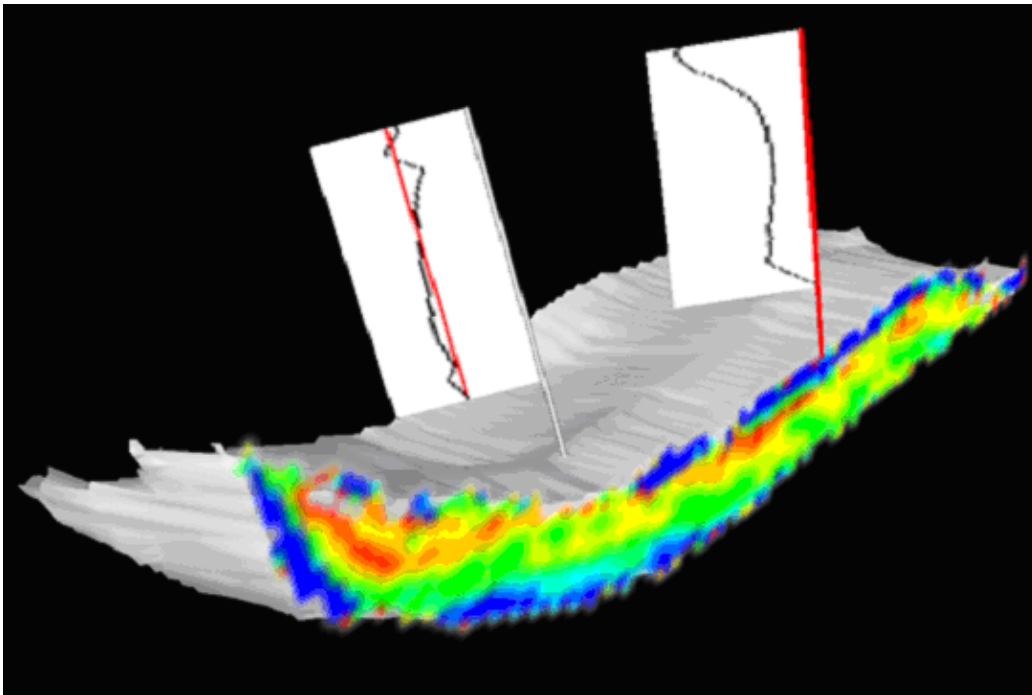| 1-I fully agree	2-I partially agree	3-I am not sure	4-I partially disagree	5-I strongly disagree	6- It is unclear to me

Figure A.9: *Cartilage annotated with three Profile Flags and one slice of the T_2 map.*

13. Do I need that amount of information to show the degenerated T_2 profile?

| 1-Yes	2-Rather yes	3-I am not sure	4-Rather no	5-No	6- It is unclear to me

14. Can I see a healthy profile with the entire slice of the T_2 map and a second profile, which slightly differs from the first one?

1-Yes	2-Rather yes	3-I am not sure	4-Rather no	5-No	6- It is unclear to me

15. Do I have sufficient information about the quality of the cartilage?

| 1-Yes	2-Rather yes	3-I am not sure	4-Rather no	5-No	6- It is unclear to me
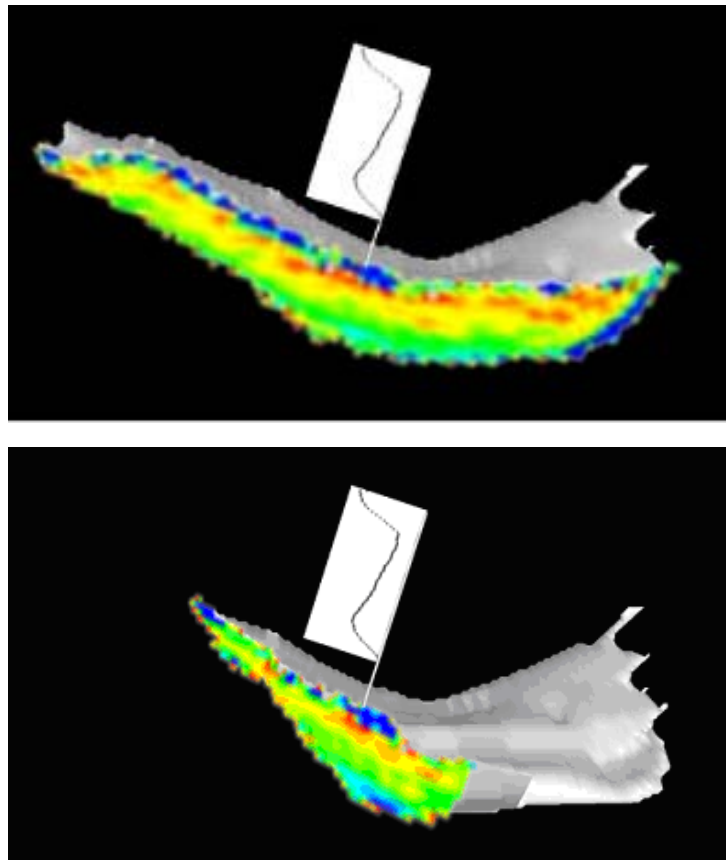
The plane showing the T_2 map can be rotated along the needle of the Profile Flag.

16. It is useful to see the the entire T_2 map in the neighborhood of the measured profile?

1-I fully agree	2-I partially agree	3-I am not sure	4-I partially disagree	5-I strongly disagree	6- It is unclear to me

17. If I rotate the plane, is it disturbing that I cannot see the T_2 map properly, since it is not directly facing the viewer?
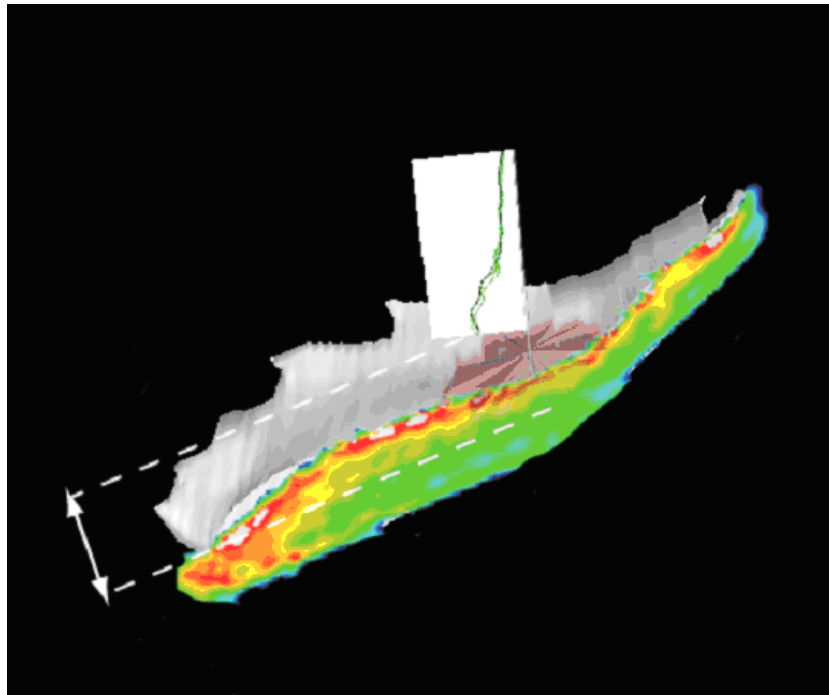
1-I fully agree	2-I partially agree	3-I am not sure	4-I partially disagree	5-I strongly disagree	6- It is unclear to me
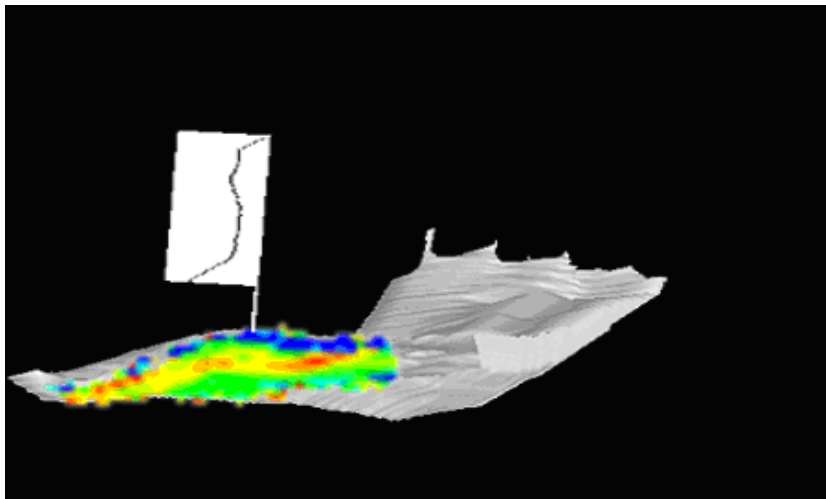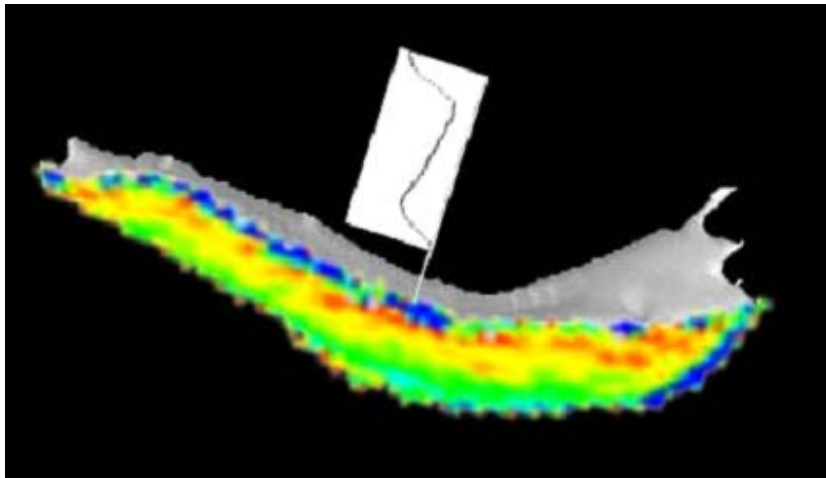
Additionaly, the entire cartilage can be rotated around the profile. In this case entire plane showing the T_2 map is always visible (it is allways facing the user).

18. I prefer the previous method, where I do not rotate the surface, because by rotating the cartilage I am disoriented.

1-I fully agree	2-I partially agree	3-I am not sure	4-I partially disagree	5-I strongly disagree	6- It is unclear to me

When annotating a profile with the plane showing the slice of the T_2 map, the plane can be moved forwards and backwards within the range defined by the Profile Flag.

19. This interaction helps me to inspect the exact shape of the annotated lesion.

1-I fully agree	2-I partially agree	3-I am not sure	4-I partially disagree	5-I strongly disagree	6- It is unclear to me

20. I prefer to have the possibility to move the plane along the entire cartilage in order to inspect the entire cartilage.

1-I fully agree	2-I partially agree	3-I am not sure	4-I partially disagree	5-I strongly disagree	6- It is unclear to me

21. Please select the most valuable image from the entire form (1-20):

22. Other remarks:

Thank you for taking your time and please send this document to
mlejnek@cg.tuwien.ac.at.
Best regards,
Matej Mlejnek
Institute of Computer Graphics and Algorithms
Vienna University of Technology

Appendix B

Curriculum Vitae

Personal data

Matej Mlejnek
born on March 21th, 1977, in Bratislava, Slovakia.

Address:
Gaullachergasse 33/35, 1160 Vienna, Austria
Phone: +43 660 6537639
eMail: mio@cg.tuwien.ac.at

Education

06/2003 -	Ph.D. student in Computer Science
	(Medical Visualization for Orthopedic Applications)
	Vienna University of Technology, Austria
10/1997 - 06/2003	Study of Computer Science (Dipl.Ing.)
	Vienna University of Technology, Austria
10/1995–06/1999	Study of Computer Science (B.Sc.)
	Slovak Technical University, Bratislava, Slovakia
09/1992–06/1995	High school
	Gymnasium Vazovova, Bratislava, Slovakia
09/1983–06/1992	Elementary school
	Drieňová, Bratislava, Slovakia

Work experience

06/2003–	Research Associate
	Project management of the COMRADE project
	Vienna University of Technology, Austria
10/2001–01/2004	Teaching assistant
	Vienna University of Technology, Austria
02/2000–02/2002	Programming internships
	Siemens AG, Vienna, Austria.

Publications

M. Mlejnek, Pierre Ermes, Anna Vilanova, Rob van der Rijt,
Harrie van den Bosch, Frans Gerritsen, and M. E. Gröller
Application-oriented Extensions of Profile Flags
In *Proceedings of EuroVis 2006*, pages 339–346

M. Mlejnek, Pierre Ermes, Anna Vilanova, Rob van der Rijt,
Harrie van den Bosch, Frans Gerritsen, and M. E. Gröller
Profile Flags: a Novel Metaphor for Probing of T_2 Maps
In *Proceedings of IEEE Visualization 2005*, pages 599–606

M. Mlejnek, Anna Vilanova, and M. E. Gröller
Interactive Thickness Visualization of Articular Cartilage.
In *Proceedings of IEEE Visualization 2004*, pages 521–527

H. Hauser and **M. Mlejnek**
Interactive Volume Visualization of Complex Flow Semantics
In *Proceedings of Vision, Modeling and Visualization 2003*, pages 191–198

M. Mlejnek
Modelling the Visualization Mapping for Volumetric Flow Visualization
M.Sc. Thesis, Vienna University of Technology 2003

L. Neumann, B. Csébfalvi, I. Viola, **M. Mlejnek**, and M. E. Gröller
Feature-Preserving Volume Filtering
In *Data Visualization 2002*, pages 105–114

Patent applications

M. Mlejnek, Anna Vilanova, and M. E. Gröller
Visualization of Flattened Structures
Philips patent application PHNL041338US-P

M. Mlejnek, Anna Vilanova, and M. E. Gröller
Profile Flags; Annotation and Interactive Probing of Medical Images
Philips patent application (submitted)

Professional Activities
  » Reviewer for the following conferences:
    Eurographics, IEEE Visualization, Eurographics / IEEE VGTC Symposium
    on Visualization (VisSym/EuroVis), Vision, Modeling, and Visualization
    (VMV), Simulation and Visualization (SimVis), International Workshop on
    Volume Graphics (VG), International Conference on Computer Graphics
    Theory and Applications (GRAPP), Conference on Computer Graphics and
    Interactive Techniques (SIBGRAPI), Brazilian Symposium on Computer
    Graphics and Image Processing (GRAPHITE)

Teaching (since 10/2003)
  » Vienna University of Technology, Austria:
    › Grundlagen wissenschaftlichen Arbeitens [proseminar] ("Basics of
      Scientific Working")
    › Visualisierung [exercise] ("Visualization")
    › Informationsvisualisierung [exercise] ("Information Visualization")
    › supervision of Master theses and practicums
  » University of Bergen, Norway:
    › Topics in Visualization: Scientific and Information Visualization [ex-
      ercise]

Programming skills
C++, java, OpenGL, SQL, Visual Basic, MATLAB

Languages
Slovak (mother-tongue), Czech (father-tongue), German (fluently), English (flu-
ently), Russian (passive)

Hobbies
music, sport, visualization

May 2006